Empirical model in the characterization of High Frequency propagation in the Arctic region

by

Racheal Athieno

BSc. with Education, Mbarara University, 2007
BSc(Honors) in Astrophysics and Space Science, University of Cape Town, 2009
MSc., Rhodes University, 2011

A DISSERTATION SUBMITTED IN PARTIAL FULFILLMENT OF THE REQUIREMENTS FOR THE DEGREE OF

Doctor of Philosophy

In the Graduate Academic Unit of Physics

Supervisor:	P. T. Jayachandran, PhD Physics
Examining Board:	Abdelhaq Hamza, PhD, UNB Physics
	Igor Mastikhin, PhD, UNB Physics
	Bruce Colpitts, PhD, UNB Electrical Engineering
External Examiner:	Mike Warrington, PhD, University of Leicester

This dissertation is accepted

Dean of Graduate Studies

THE UNIVERSITY OF NEW BRUNSWICK

April, 2017

Abstract

The use of high frequency (HF) communication at high latitudes still forms the backbone of many systems, owing to the fact that there are few alternatives to HF radio for the merchant and fishing fleets, military forces (land, sea and air) and for the civil aviation industry for these latitudes. HF communication uses the ionosphere as a medium of propagation, but its variable nature can be a disadvantage to both the radio operators and users. The choice of a suitable usable frequency is thus dependent on the ability to predict the conditions of the ionosphere. Thus, HF propagation predictions can be inferred from the predicted conditions of the ionosphere. In fact, in most cases, the predictions of ionospheric conditions and HF propagation are often assumed to be identical. Hence, the need to develop ionospheric model(s) suitable for high latitudes to enable a relatively smooth operation of ionospheric-dependent radio communication.

Most of the available models, particularly the empirical ones were developed with little data at high latitudes. Data availability has improved over the

years due to technological advancement and continued research. For instance, the Canadian High Arctic Ionospheric Network (CHAIN) provides a wealth of data for the polar and auroral regions. Using CHAIN data, the performance of the Voice of America Coverage Analysis Program (VOACAP), Ionospheric Communication Enhanced Profile Analysis and Circuit (ICEPAC) and the recommendation 533 (REC533) propagation models was evaluated and some inconsistences were identified for each of the models. An additional study of ionospheric variability in the arctic region revealed that the currently available International Telecommunication Union Recommendation (ITU-R) variability factors demonstrate notable differences from observations during the winter and equinoxes. A model for the critical frequency of the F2 layer was developed using both CHAIN and Space Physics Interactive Data Resource (SPIDR) data. The model results show an improvement compared to the available baseline International Reference Ionosphere (IRI) model.

Dedication

Dedicated to my husband, Godfrey Kayizzi, and our son, Anderson Dante Kayizzi

Acknowledgements

I wish to extend my sincere gratitude to my supervisor, Prof. P. T. Jayachandran, for his guidance, motivation, patience and continued support throughout the entire period of this study. He has given me an opportunity to grow as a researcher by allowing me to publish papers, attend and participate in conferences, summer schools and seminars. Sincere gratitude to Prof. Abdelhaq Hamza and Prof. William Ward for the positive criticism and advice during the departmental seminars. Thanks to Richard Chadwick and Todd Kelly for their technical support, and to David Themens for his suggestions and valuable ideas. Thanks to the CHAIN members, and all the graduate students in the Physics department for the support, useful ideas, advice, and providing a conducive, positive environment for my research.

"Of all the gifts that life has to offer, a loving mother is the greatest of them all..." Special thanks to my mother, for the sacrifices she made for me, the love, support, encouragement. *To my dad, "you left us quite early, but I believe you are watching, and are very proud of your girl".* Thanks

to my brothers; Francis Ddembe, Aaron Waiswa and Godfrey Okello, in no particular order, and my sister Miriam Babirye for the support, love, care, and for being by my side all through my study time. May the Almighty God bless you all. *To my beloved husband, "its been a tough ride yet you have chosen to stick with me through it all."* I am very grateful for the love, care, financial and moral support, and for believing in me. *To my little boy, "the smiles, the love and the hugs from you are priceless. May God give me a chance to watch you grow into a responsible man."*

I am grateful for the financial support provided by the Natural Sciences and Engineering Research Council of Canada (NSERC). Infrastructure funding for CHAIN was provided by the Canada Foundation for Innovation and the New Brunswick Innovation Foundation. CHAIN operation is conducted in collaboration with the Canadian Space Agency. Science funding is provided by the Natural Sciences and Engineering Research Council of Canada.

And finally, Glory be to the Almighty God for His everlasting love, provision and for this far He has brought me, and (through the eyes of faith) the bright future ahead.

Table of Contents

List of Tables

List of Figures

Chapter 1

Introduction and Thesis Overview

1.1 Introduction

The characterisation of high frequency (HF) propagation plays an important role in a number of HF communication applications such as influencing the choice of frequencies for shortwave broadcasters, and providing a practical guide to radio navigation and radar system operators. HF propagation involves transmission and reception of radio signals within a frequency range of $2 - 30$ MHz. Sky wave propagation, one of the modes of HF propagation and our interest in this study, is the propagation of radio signals from one point to another after reflection by the ionosphere (Seybold, 2005).

The ionosphere is an ionised part of the atmosphere that lies between altitudes of about 50 km and 1000 km. It is formed when solar radiation interacts with the atoms and molecules in the neutral atmosphere by a process known as photoionisation. The ionosphere experiences both regular and irregular variations, as a consequence of its position in relation to the sun and the magnetosphere. Its ever-changing structure makes HF propagation and its applications vulnerable.

Space weather is one of the substantial contributors to ionospheric effects. It is a result of the sun's behaviour, the nature of Earth's atmosphere and geomagnetic field and our location in the solar system. It provides a description of the conditions in space that affect the Earth and its technological systems (Goodman, 2005). The magnitude of the effects depends upon the structure of the ionosphere and the frequency of the radio wave.

The effect of the ionosphere on HF propagation is studied mainly by sounding techniques, which use a system of synchronised transmitters and receivers to provide the required data. The techniques include vertical radio sounding (bottomside or topside), backscatter, incoherent scatter sounding, riometers, low frequency and very low frequency receivers (Sizun, 2005). The vertical or oblique bottomside sounding method uses radio systems located on the Earth's surface. The radio signals are transmitted at various frequencies and the reflected echo is received after a time delay. The virtual reflection height

is determined by the delay which corresponds to the radio wave propagation time (Sizun, 2005). The ionosonde, from which the data used in this study has been obtained, is one such instrument that uses this sounding technique. The reflected echo is processed to obtain the required ionospheric characteristics such as the critical frequency of the F2 layer (foF2) and the maximum usable frequency (MUF) for a given communication circuit (Davies, 1989).

There is no 'cure' to the unstable nature of the ionosphere but its impact on HF systems can be prevented or limited by developing ionospheric and HF prediction models that can predict the changes in the ionosphere and propagation conditions (Rush, 1986). A number of models have been developed with remarkable success except for the high latitude region that has had a challenge of data scarcity and the complex nature of its ionosphere. Data availability is very important in developing reliable and fairly accurate empirical models. With the installation of ground- and space-based instruments, coupled with technological advancements in data processing at the high latitudes, it is necessary to develop ionospheric model(s) suitable for the region to enable a relatively smooth operation of ionospheric-dependent radio communication. Examples of the available models, which have also been considered in this work, are the Voice of America Coverage Analysis Program (VOACAP), Ionospheric Communication Enhanced Profile Analysis and Circuit (ICEPAC) and the Recommendation 533 (REC533) propagation models.

The performance of these models was evaluated using data from observations, as a first step towards establishing suitable models for the high latitudes. The data was obtained from the Space Physics Interactive Data Resource, SPIDR (nolonger available) and the Canadian High Arctic Ionospheric Network (CHAIN) (Jayachandran *et al.*, 2009). SPIDR was a standard archive for different solar-terrestrial data obtained from a variety of instruments. The data was obtained from ionosondes at different ionospheric stations around the world. CHAIN is an array of ground-based radio instruments deployed and operated by the University of New Brunswick. The instruments include Global Positioning System (GPS) receivers and Canadian Advanced Digital Ionosonde (CADI)s at the following locations; Eureka (79.99° N, 274.10° E), Resolute (74.75° N, 265.00° E), Pond Inlet (72.69° N, 282.04° E), Cambridge Bay (69.12° N, 254.97° E), Hall Beach (68.78° N, 278.74° E) and Iqaluit (63.73° N, 2291.46° E). Data used in this work was obtained from the Resolute and Pond Inlet CADIs. Data from these sources was used to evaluate the performance of the currently available models, and attempts were made to provide solutions to the identified challenges.

Specifically, the performance of VOACAP, ICEPAC and REC533 propagation models were evaluated by a comparison between the CADI-measured and predicted MUF. Each of the models had strong and weak points during the different hours, seasons and solar cycles. Despite the fact that it is hard (but not necessarily impossible) to obtain an all round perfect model,

hourly, diurnal, seasonal and solar cycle variation prediction consistence is key to the smooth operation of ionospheric-dependent radio communication. This study identified two key specifications that could improve the performance of the studied models, namely, variability and a reliable ionospheric model. The variability of MUF at five high latitude stations over a period of three solar cycles was analysed, towards establishing a suitable index for ionospheric variability. The observations were compared to the only available global variability factors provided by the International Telecommunication Union Recommendation (ITU-R). The ITU-R factors seem to significantly deviate from the observations during the winter and equinoxes, an implication that there is a need to re-establish variabilty indices or factors that can nearly reproduce the high variability observed during these months. If such a study is to be done at the high latitudes, it requires a fairly consistent amount of observations over 3 solar cycles, which are not yet available but can be obtained with time. Also, an foF2 model was developed for Resolute and the results were compared to the predictions made by the International Reference Ionosphere (IRI), the available globally recognised ionospheric model. The single station model results are promising and with the suggestions and recommendations for future work, it could be modified to a regional and global model.

1.2 Thesis Overview

This thesis consists of seven chapters. Chapter 1 includes an introduction about the topic and thesis overview. HF propagation, the ionosphere, and modeling have been briefly introduced. Chapter 2 covers the theoretical background, which includes some details about the ionosphere and HF propagation and modeling. The structure of the ionosphere and its role in radio communication have been described. A brief description of the instrument used in the study and the data analysis technique is covered in Chapter 3. The data used in this thesis was obtained from the ionosonde. The Neural Network (NN) technique that has been used in modeling has also been discussed in the same chapter. Chapter 4 includes a comparison between CADI-derived MUF and VOACAP, ICEPAC, REC533 predictions, and also discusses the performance of each of the models. Chapter 5 presents results of a study of MUF variability in the arctic region. The ionospheric variability at five ionospheric stations, chosen due to the fact that data was available for observations spanning over three solar cycles, was analysed. The stations include; Resolute (74.75° N, 265.10° E), Dikson (73.50° N, 80.40° E), Norilsk (69.40° N, 88.10° E), Loparskaya (68.00° N, 33.00° E), and Sodankyla (67.40° N, 26.60° E). A comparison of the observations with the ITU-R variability factors for summer, winter, and equinoxes during low, moderate and high solar activity has been discussed in this Chapter. Chapter 6 includes results of a NN foF2 model that has been developed using both SPIDR and

CADI data for Resolute. The NN model predictions have been compared to CADI foF2 observations and IRI-modeled values, as a means of evaluating it. Chapter 7 contains concluding remarks and recommendations for future work.

Chapter 2

Theoretical Background

2.1 The ionosphere

2.1.1 Introduction

The ionosphere is a region of the Earth's atmosphere that, by generally accepted convention, extends from altitudes of about 50 km to 1000 km. It is mainly formed by photoionisation, a process in which solar radiation strips electrons from the atoms and molecules in the neutral atmosphere forming positively charged ions and electrons. Figure 2.1 illustrates the midlatitude daytime ion concentration profiles as a function of height. Nitrogen (N_2) and Oxygen (O_2) molecules are the dominant species in the lower atmosphere, in addition to minor species such as water vapor, Carbon dioxide and Nitric Oxide. The molecular constituents are, however, dissociated into atomic components, by incoming solar extreme ultraviolet (EUV) radiation in the

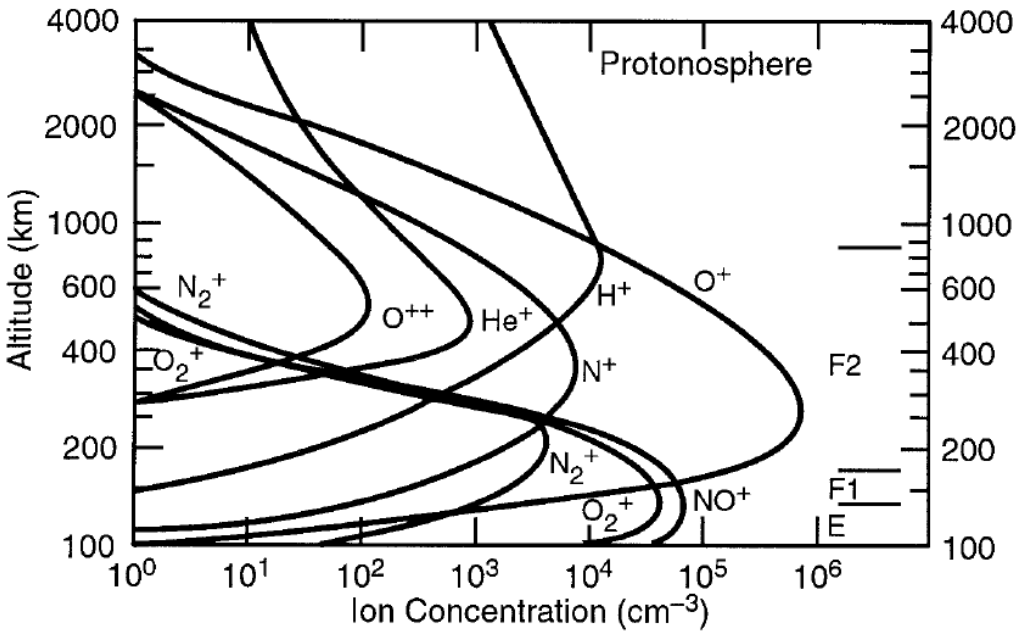

Figure 2.1: Typical midlatitude daytime ion concentration profiles as a function of height. Adopted from Goodman (2005).

upper atmosphere. The photoionisation process can be illustrated mathematically (Rishbeth and Garriot, 1969) as

$$A + h\nu \longrightarrow A^+ + e^- \tag{2.1}$$

where A is the neutral atom or molecule and $h\nu$ is the photon flux. The fact that photoionisation is dependent on the sun implies that it is a daytime phenomenon, and it is greatest around local noon. As the night wears on, the electrons and ions recombine to produce neutral atoms, a process known as recombination, the main process of electron depletion in the higher

ionosphere. There are two forms of recombination: radiative recombination, in which electrons and ions combine directly to form neutral ions, and dissociative recombination, which involves the interaction of positive ions with neutral molecules, forming a neutral atom and a positive molecule. Then the positive molecule recombines with electrons forming two neutral atoms (McNamara, 1990). Electron depletion in the lower ionosphere especially in the D region is by attachment, a process in which electrons are attached to neutral atoms, forming negatively charged ions.

Radiative recombination:

$$X^+ + e^- \longrightarrow X + h\nu \tag{2.2}$$

Dissociative recombination:

$$X^+ + Y_2 \longrightarrow YX^+ + Y \Rightarrow YX^+ + e^- \longrightarrow Y + X \tag{2.3}$$

Attachment:

$$XY^+ + e^- \longrightarrow XY^- \tag{2.4}$$

Both recombination and attachment occur at all times at the different altitudes in the ionosphere, and the rate of electron depletion is dependent on the number of neutral molecules at the altitude of interest.

The ionosphere is made up of the lower (between 50 km and 90 km),

the bottomside (between 90 km and about 400 km) and the topside regions (between 400 km and 1 000 km). The lower and bottomside ionosphere is further divided into three layers that vary in electron density and altitude, namely: the D, E, and F layers. Depending on the levels of ionisation, the F region is divided into the F1 and F2 layers. Daytime and nighttime electron density profiles for a typical midlatitude station at solar minimum and maximum are presented in figure 2.2. All the layers are present during daytime as a result of photoionisation while the D and F1 layers disappear at night mainly by the process of recombination, and the E layer gets weaker. Although its intensity decreases, the F2 layer persists throughout the night. The notable differences between the electron density profiles during low and high solar activity are evidence that the ionosphere owes its existence to the sun. For each of these layers, there exists a critical frequency which corresponds to the peak electron density of that particular layer. The critical frequency, f, is related to the electron density, N_e (Davies, 1989; McNamara, 1990) by

$$N_e(m^{-3}) = 1.24 \times 10^{10} f(MHz)^2 \tag{2.5}$$

2.1.2 Ionospheric layers

2.1.2.1 The D layer

The D layer is the lowest part of the ionosphere that falls between an altitude range of $\sim$ 70 - 90 km, and is characterised by much denser neutral atmo-

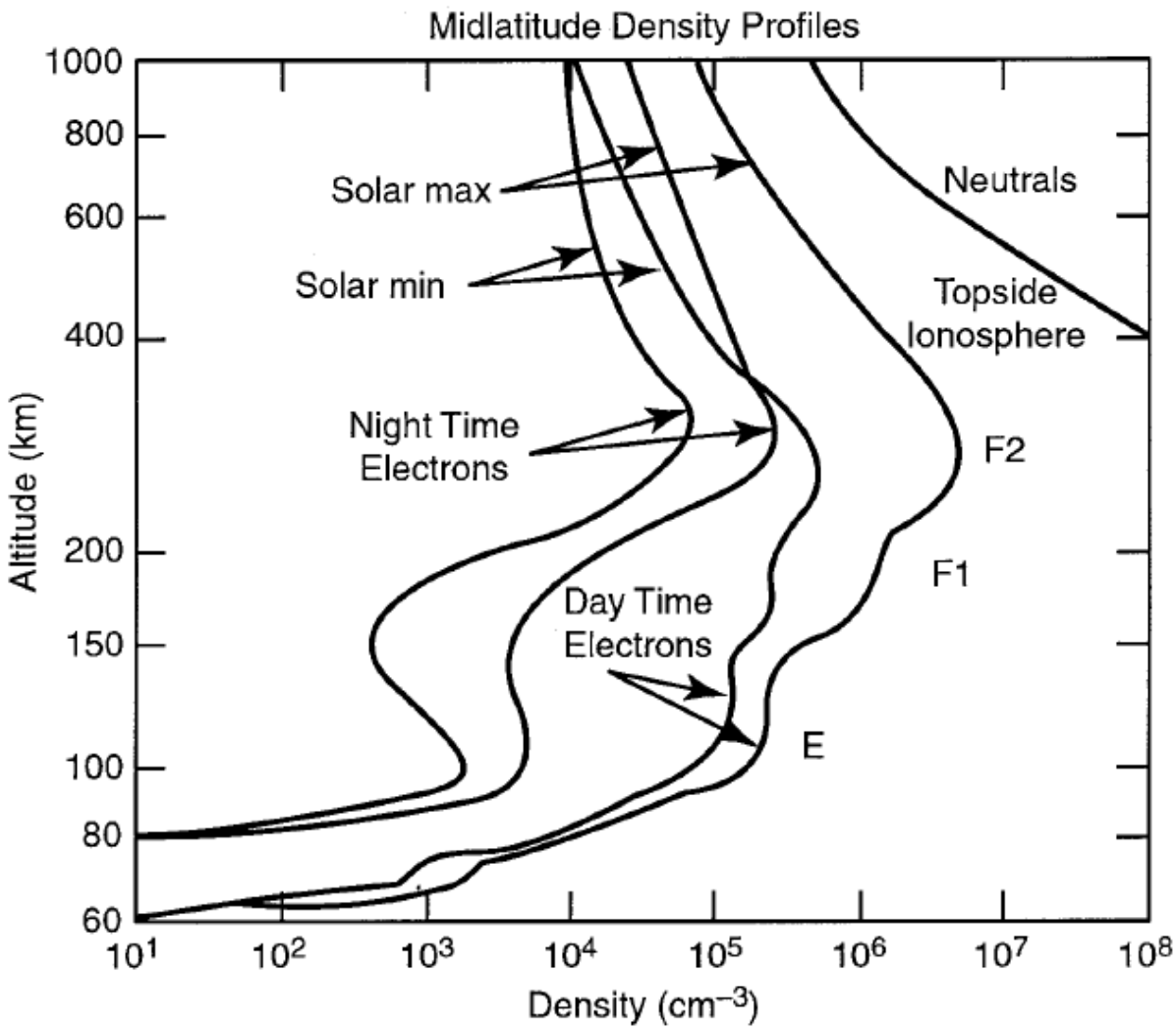

Figure 2.2: Typical daytime and nighttime ionosphere during solar minimum and maximum. Adopted from Goodman (2005).

sphere compared to the other layers above it. Its lower boundary, however, is usually set at 50 km to account for the galactic cosmic ray contribution to ion production, in the region that lies between the altitude range of 50

- 70 km, also known as the C layer (Goodman, 2005). Cosmic rays are mainly high energy protons (> 1 Mev) of solar origin which interact with the neutral atmosphere. The rays penetrate the F and E layers with less attenuation but interact more strongly with dense atmosphere in the D region. Ion production in the upper D layer is mostly due to Lyman-α ionisation of Nitric Oxide (NO) while that at lower levels is due to galactic cosmic rays (McNamara, 1990; Goodman, 2005). There is an additional contribution to ionisation by the EUV spectrum which interacts with molecular Oxygen (O_2) and Nitrogen (N_2). The other source of ionisation is hard X-rays that ionise all constituents in the D region with the greatest impact being on the major constituents, O_2 and N_2. It is important to note that the contribution of each of these sources is dependent on solar activity, time of day and latitude (Hunsucker and Hargreaves, 2003). As mentioned earlier, electron loss in the D region is by attachment of electrons to neutral molecules, forming negatively charged ions. One common example is the three body reaction that involves the attachment of an electron to O_2 in the presence of one other molecule, Z, forming O_2^-. The role of the other molecule is to get rid of extra kinetic energy from the reactants in order to conserve energy. The electron may be detatched from molecular Oxygen by a photon due to its low electron affinity.

Attachment:

$$e^- + O_2 + Z \longrightarrow O_2^- + Z \tag{2.6}$$

Detatchment:

$$O_2^- + h\nu \longrightarrow O_2 + e^- \tag{2.7}$$

and/ or

$$O_2^- + O \longrightarrow O_3 + e^- \tag{2.8}$$

This layer is known for its importance in the characterisation of absorption losses for short wave systems and its ability to reflect very low frequency (VLF) and low frequency (LF) waves (Goodman, 2005). For instance, the determination of the lowest usable frequency (LUF) for long distance communication is based primarily on the D-region absorption. During solar flares, the D layer experiences additional ionisation caused by highly energetic solar protons, and the impact is sometimes so strong that all high frequency (HF) radio waves may be absorbed, leading to a radio blackout.

2.1.2.2 The E region

The E layer is a part of the ionosphere that lies between altitudes of 90 - 120 km above the surface of the Earth. This layer owes its daytime existence to the photoionisation of molecular (O_2) and atomic (O) oxygen, while night-time ion production is due to electron and meteor bombardment. During daytime, the E layer is able to reflect HF radio waves of up to 20 MHz at oblique transmission (McNamara, 1990; Goodman, 2005). It is known to exhibit an anomaly, commonly called sporadic E (Es). The direct impact of solar radiation to the Es is small, compared to the other layers. The Es

layer can be viewed as a suspension of plasma clouds or an unpredictable region of high electron density within the E layer. The occurrence of the Es layer is linked to thunderstorms, meteor showers, solar activity, and geomagnetic activity (Whitehead, 1989). HF radio waves aimed at the F layer can sometimes be reflected by the Es layer especially if the critical frequency of the former is less than that of the latter. Also, irregular signal transmission and fading can result from the partial reflection of the radio waves by the Es and F layers (Davies, 1989). At low and mid-latitudes, sporadic E is known to occur during the day and in summer, while at the high latitudes, it is a nightime phenomenon.

2.1.2.3 The F region

The F layer lies between approximately 120 - 400 km. Electron and ion production is due to the photoionisation of atomic oxygen (O) by Lyman continuum or emission lines of Helium (He) (McNamara, 1990). This layer is further divided into the F1 and F2 layers, especially during daytime, and in summer. The F1 layer ranges from 120 - 200, and is prevalent during daytime, the summer and periods of low solar activity. The F1 and F2 layers usually merge during nightime and during high solar activity due to the absence of photoionisation, and the significant increment in the F layer electron density, respectively. The F2 layer ranges from about 200 - 400, and is able to support HF propagation due to its persistence throughout the day, and also reflects the highest frequencies in the HF range (Baumjohann

and Treumann, 1997; McNamara, 1990). Electron depletion in the F2 layer is by dissociative recombination of the Oxygen ion (O^+) (Hunsucker and Hargreaves, 2003),

$$O^+ + N_2 \longrightarrow NO^+ + N \Rightarrow NO^+ + e^- \longrightarrow N + O \tag{2.9}$$

One of the common occurrences in the F region, that is also a shortcoming to HF communication is the spread F phenomenon. It is associated with diffusion of the F region caused by radio wave scattering, travelling ionospheric disturbances (TIDs) and reflection from ionospheric plasma irregularities. The radio wave signal received is a superposition of transmitted waves reflected from different ionospheric heights at slightly different times. Spread F is known to be a nighttime phenomenon around the equinoxes at low latitudes, while at high latitudes, it is most likely to occur at night and in winter. Spread F can be either frequency spread, which refers to diffuseness near the critical frequency of the F2 layer, or range spread, which refers to diffuseness near the peak height of the F2 layer (Davies, 1989).

2.1.3 Regular ionospheric variations

Variations in the ionosphere occur at different timescales, ranging from minutes to years, and are mainly attributed to solar and geomagnetic activity. However, various studies have linked disturbances in the upper ionosphere to the propagation of atmospheric waves, such as gravity, tidal and plan-

etary waves, from the lower to the upper atmosphere (Chum *et al.*, 2011; Laštovička, 2006; Sindelarova *et al.*, 2012). Variations linked to solar activity are associated with solar EUV radiation and X-ray flux which are known to ionise the neutral atmosphere, whereas the disturbances, such as geomagnetic storms, due to geomagnetic activity are associated with the solar wind-magnetosphere-ionosphere coupling. Particle precipitation and plasma transport are additional causes of ionospheric variability at the high latitudes (Hunsucker and Hargreaves, 2003; Ruohoniemi and Greenwald, 2005; Kelley, 2009).

2.1.3.1 Diurnal variations

The ionosphere is known to vary with time of day, mainly because of the influence of the sun to the photionisation process. As a result the electron density increases and reaches a maximum around local noon and decreases towards the night, and consequently, the D layer disappears, the F1 layer merges with the F2 layer, while the E layer becomes much weaker. Nighttime HF communication is mainly via the F2 layer because it is able to survive throughout the night because of the decrease in the recombination rate with increasing height. The diurnal variation of the ionosphere is generally controlled by the photoionisation, recombination and transport (at high latitudes) processes (McNamara, 1990).

2.1.3.2 Solar activity variations

The fact that it owes its existence to the sun implies that solar activities such as flares, coronal ejections, in turn affect the ionosphere and ionospheric-dependent communication. During the 11-year solar cycle, the ionosphere experiences periods of low and high solar activity, causing variations in the electron density. The knowledge of the variation of relevant ionospheric and HF propagation parameters with solar activity is vital so as to ensure uninterrupted services to the respective users. For example, an increase in solar activity translates into high electron density which in turn allows the use of higher frequencies. The 10.7 cm solar radio flux (F10.7) and the sunspot number (SSN) are the most commonly used indices in quantifying solar activity (McNamara, 1990; Goodman, 2005).

2.1.3.3 Seasonal variation

Changes in seasons have an impact on the variations of the electron density in the different layers of the ionosphere. The D, E and F1 layer electron densities are greater in summer than winter owing to the position of the sun. However, the F2 region electron density variation is more complicated compared to the other layers; for instance, the anomalous behaviour of the winter noon peak electron density being greater than the summer values. Increased electron densities are observed during the equinoxes due to the fact that the sun is directly overhead at this time of the year (McNamara, 1990; Millward *et al.*, 1996).

2.1.4 Irregular ionospheric variations

Irregular ionospheric variations are unpredictable and have a great impact on HF propagation. The common irregular variations include sporadic E, spread F and ionospheric storms. The sporadic E and spread F have been briefly described in subsection 2.1.2.

2.1.4.1 Ionospheric storms

Ionospheric storms are associated with a number of phenomena, including solar activity and geomagnetic, auroral and magnetospheric storms. Ionospheric storms are known to affect ionospheric characteristics such as the electron density or the height of the F2 layer. They can cause an increase in the virtual height of the F2 layer and a decrease in the maximum electron density which may interrupt radio communication. In most cases, the lower layers are affected when the disturbance is great. These storms may affect human technology e.g. cause outages in electric power systems and increase of atmospheric drag on satellites (Davies, 1989; Sizun, 2005).

2.2 The high latitude ionosphere

The high latitude ionosphere is connected to the outer part of the magnetosphere by the geomagnetic field lines, a path that directs energetic particles to the Earth. For example, particles energised in the magnetosphere or originating from the sun cause substantial ionisation in the polar ionosphere.

This makes the high latitude ionosphere vulnerable to the dynamics of the magnetosphere and the changes in the solar wind flow. The solar wind can be viewed as the solar activity-Earth medium of communication, and the magnetosphere is the outermost region where the motion of particles or plasma distribution of the Earth is controlled by the geomagnetic field (Cannon, 1989; Hunsucker and Hargreaves, 2003).

The high latitude ionosphere is divided into three regions, namely, the auroral oval, the polar cap and the F-region trough. The auroral oval is well known for the luminous feature, the aurora, which is attributed to particle precipation in the E-region. It is one of the essential geophysical boundaries, as it marks the separation between open and closed field lines. The auroral oval is characterised by a continuous influx of energetic particles from closed magnetospheric field lines, responsible for several phenomena including geomagnetic disturbances and enhancements in the electron density. It forms a ring around the earth's magnetic pole, enclosing the polar cap (Watson, 2015). Experiments have shown that as geomagnetic activity and particle precipitation increases, the auroral oval undergoes both equatorward and poleward expansion.

The regions, in both hemispheres, poleward of the auroral oval are known as the polar caps, and they provide a connection between the geomagnetic field lines and the Interplanatary Magnetic Field (IMF), and thus, the sun. For this reason, the polar ionosphere, specifically the F region is characterised by drammatic features such as patches and sun-aligned arcs, associated with

particle precipitation and transport of plasma from the sunlit ionosphere by $E \times B$ convection. Sun-aligned arcs are described by a substantial decrease in the electron density during winter. They occur during periods of northward directed IMF, and are associated with low geomagnetic activity, while patches are generally enhancements above background electron density, observed to occur more frequently in winter than in summer. They are not formed locally but are rather transported from the source on the sunlit side to the observation point by polar convection, and appear to be stronger during high solar activity. Particularly, patch formation occurs on the dayside of the auroral oval when the IMF is directed southwards and convects anti-sunward across the polar cap, towards the nightside of the auroral oval, and occurs during high geomagnetic activity. The low rate of recombination in the F region allows the patches to drift from the source, and traverse the polar cap without considerable depletion (Hunsucker and Hargreaves, 2003). The F region trough is usually defined as an observation of plasma density depletion at the F-region heights, stretching from latitudes around 55° - 75°. This phenomenon is sometimes described as the main, mid-latitude, high-latitude, day- side and nightside troughs. The difference between the mid-latitude and high-latitude trough is associated to its location relative to the auroal oval. The former being equatorward of the auroral oval, while the latter occurs poleward of the oval (Rodger *et al.*, 1992). However, other studies suggest that the different forms of the trough are just a manifestation of the same phenomenon, and can thus be generally considered as the F-region

trough. The phenomenon is linked to simultaneous effects of precipitation, plasma convection, heating and neutral winds (Voiculescu *et al.*, 2006, and references therein). Care should be taken while selecting frequencies for HF communication for paths along the trough, otherwise, if not absorbed, the radio signal may be reflected off the great circle path (Stocker *et al.*, 2013).

2.3 HF propagation and the ionosphere

The ionosphere is important for radio communication because of its natural ability to reflect radio waves (McNamara, 1990). Radio wave propagation is described by the Appleton-Hartree equation which after neglecting collisions is simplified (Rishbeth and Garriot, 1969; Davies, 1989) as,

$$n^2 = 1 - \frac{X(1-X)}{(1-X) - \frac{1}{2}Y_T^2 \pm \{\frac{1}{4}Y_T^4 + (1-X)^2 Y_L^2\}^{\frac{1}{2}}} \tag{2.10}$$

where

$$X = \frac{\omega_p^2}{\omega^2}, \;\; Y = \frac{\omega_g}{\omega}, \;\; Y_L = Y cos\theta, \;\; Y_T = Y sin\theta, \;\; \omega_p^2 = \frac{N_e e^2}{m_e \varepsilon_0}, \;\; \omega_g = \frac{Be}{m_e}$$

n is the refractive index, N_e, e, m_e are the electron density, charge and mass respectively, ε_0 is the permittivity of free space, B is the flux density of the geomagnetic field. θ is the angle between the direction of propagation of the radio wave and the magnetic field (Rishbeth and Garriot, 1969). f

is frequency of the radio wave, f_p is the plasma frequency and f_g is the gyrofrequency. The + and - signs describe the propagation of the ordinary (O-) and extraordinary (X-) waves respectively. If the radio wave propagates in the same direction as the magnetic field, i.e. $\theta = 0$, it implies that $Y_L = Y$ and $Y_T = 0$ (Rishbeth and Garriot, 1969) and Equation 2.10 reduces to

$$n^2 = 1 - \frac{X}{(1 \pm Y)} \tag{2.11}$$

Neglecting the effect of the magnetic field on the propagation of radio waves (by setting $B = 0$) for the sake of simplicity implies that $\omega_g = 0$, $Y = 0$ and equation 2.11 becomes

$$n^2 = 1 - X = 1 - \frac{\omega_p^2}{\omega^2} \tag{2.12}$$

where the angular plasma frequency, ω_p is given by

$$\omega_p = 2\pi f_p \tag{2.13}$$

and $\omega = 2\pi f$ is the angular frequency of the radio wave.

Recall that

$$\omega_p^2 = \frac{N_e e^2}{m_e \varepsilon_0} = (2\pi f_p)^2 \tag{2.14}$$

Thus, the index of refraction, n, at frequency f is given by

$$n^2 = 1 - \frac{f_p^2}{f^2} = 1 - \frac{e^2 N_e}{4\pi^2 \epsilon_0 m_e f^2} \tag{2.15}$$

Substituting for $m_e = 9.11 \times 10^{-31}$ kg, $\varepsilon_0 = 8.854 \times 10^{-12}$ Fm^{-1} and $|e| = 1.602 \times 10^{-19}$ yields

$$n^2 = 1 - \frac{81N_e}{f^2} \tag{2.16}$$

which is a much more simplified form of the Appleton-Hartree equation.

The ionosphere is not a stable ionised medium, and its variations can strongly affect HF propagation. Sudden occurrence of strong disturbances (associated to solar activity) in the ionosphere may interrupt HF communication in a given band of frequency (McNamara, 1990; Sizun, 2005). The effect of the ionosphere to a radio wave can be described by assuming its propagation through layers with changing electron density, and refractive index.

Consider a ray incident on the ionosphere as shown in figure 2.3. The electron density increases from one layer to the next, reaches a maximum and then decreases again as illustrated in figure 2.2. Hence, as the radio signal penetrates the ionosphere it travels from a dense to a less dense medium (in refractive index terms), continuously bending away from its path until it suffers total internal reflection back to the Earth. Using Snell's law in figure 2.3,

$$\frac{sin(i)}{sin(r_1)} = \frac{n_1}{1}, \frac{sin(r_1)}{sin(r_2)} = \frac{n_2}{n_1}, ... \frac{sin(r_{k-1})}{sin(90)} = \frac{n_k}{n_{k-1}} \tag{2.17}$$

such that

$$\frac{sin(i)}{sin(r_1)} \times \frac{sin(r_1)}{sin(r_2)} \times ... \times \frac{sin(r_{k-1})}{sin(90)} = \frac{n_k}{1} \tag{2.18}$$

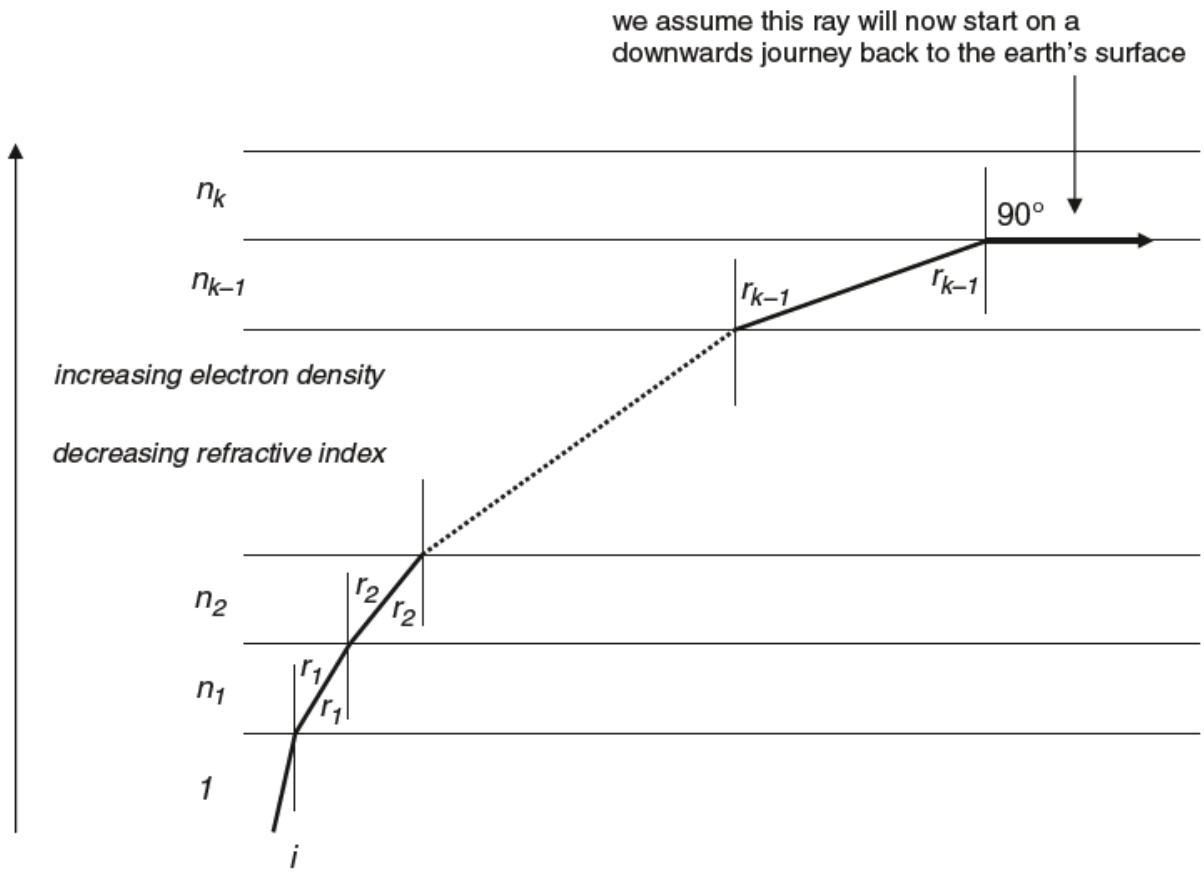

Figure 2.3: Schematic illustration of the propagation of an electromagnetic wave in the ionosphere. Adopted from Sizun (2005).

$$sin(i) = n_k \tag{2.19}$$

Equation 2.19 is the necessary condition for a ray to be reflected by the ionosphere back to Earth. In other words, for a given ray to be returned, there must be a region in the layer with an electron density that results in a refractive index that is equal to the sine of the incidence angle with which

the ray enters the ionosphere, otherwise the ray will penetrate further in the layer to encounter a refractive index that satisfies the condition. Using the expression for n obtained from equation 2.16, the condition for reflection to occur at vertical incidence, i.e. for $i = 0$ is

$$sin(i) = n = \sqrt{1 - \frac{81N_e}{f^2}} = 0 \tag{2.20}$$

$$f = 9\sqrt{N_e} \tag{2.21}$$

As long as Equation 2.21 is satisfied, at vertical incidence, the transmission frequency f will be reflected by the ionosphere from a region with electron density, N_e. As f is increased, the signal will come from higher up in the layer until a region of maximum electron density in a layer, N_{max}, which will reflect the highest frequency also known as the critical frequency, fo;

$$fo = 9\sqrt{N_{max}} \tag{2.22}$$

For oblique incidence,

$$sin(i) = n = \sqrt{1 - \frac{81N_{max}}{f^2}} = \sqrt{1 - \frac{f_v^2}{f^2}} \tag{2.23}$$

$$f = f_v sec(i) \tag{2.24}$$

Equation 2.24, otherwise known as the secant law gives the relationship between the frequency, f of a wave reflected obliquely (following path TBR

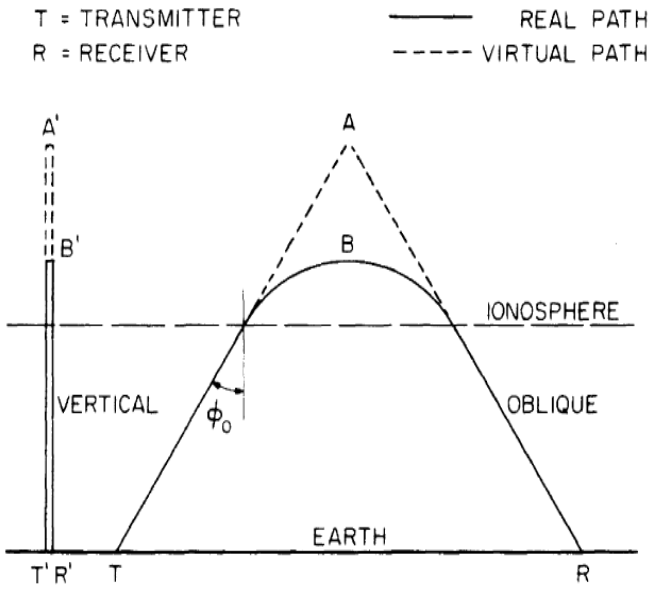

Figure 2.4: Schematic illustration of vertical and oblique HF propagation of a radio signal in the ionosphere. Adopted from Smith (1939).

in figure 2.4) at a certain real height, B and the frequency, f_v of a wave incident vertically ($T'B'R'$) and reflected at the same real height, B'. *seci* is called the propagation factor, also known as MUF- or M-factor. However, in practice, equation 2.24 is modified by introducing a constant k, which lies between 1.0 and 1.2 to account for the curvature of the ionosphere.

$$f = f_v k sec(i) \tag{2.25}$$

Equation 2.25 then becomes the 'corrected secant law'. Correction factors for different transmission distances were derived and graphically presented by

Smith (1939). A value of $k = 1.115$ is recommended by URSI for transmission distances greater than 500 km (Appleton and Beynon, 1940; Lockwood, 1983; Davies, 1989). The secant law shows that the ionosphere can reflect much higher frequencies with oblique propagation than with vertical propagation. The propagation factor is a useful factor in determining the MUF for the different layers of the ionosphere at given propagation distances. MUF can be computed by assuming a thin ionospheric layer and a curved Earth, with the geometry shown in figure 2.5.

$$AC = AB + BC, \quad AB = h_0, \quad BC = a(1 - cos(\theta)) \tag{2.26}$$

$$TC = asin(\theta) \quad AC = h_0 + a(1 - cos(\theta)) \tag{2.27}$$

From triangle TAC,

$$TA^2 = TC^2 + AC^2 = (asin(\theta))^2 + (h_0 + a(1 - cos(\theta)))^2 \tag{2.28}$$

$$TA = \left((asin(\theta))^2 + (h_0 + a(1 - cos(\theta)))^2\right)^{\frac{1}{2}} \tag{2.29}$$

$$cos^2(I_0) = \frac{(h_0 + a(1 - cos(\theta)))^2}{(asin(\theta))^2 + (h_0 + a(1 - cos(\theta)))^2} \tag{2.30}$$

For θ small,

$$cos(\theta) \sim 1, \quad sin(\theta) \sim \theta, \quad 1 - cos(\theta) \sim \frac{\theta^2}{2} \tag{2.31}$$

$$cos^2(I_0) = \frac{(h_0 + a\frac{\theta^2}{2})^2}{(a\theta)^2 + (h_0 + a\frac{\theta^2}{2})^2} \tag{2.32}$$

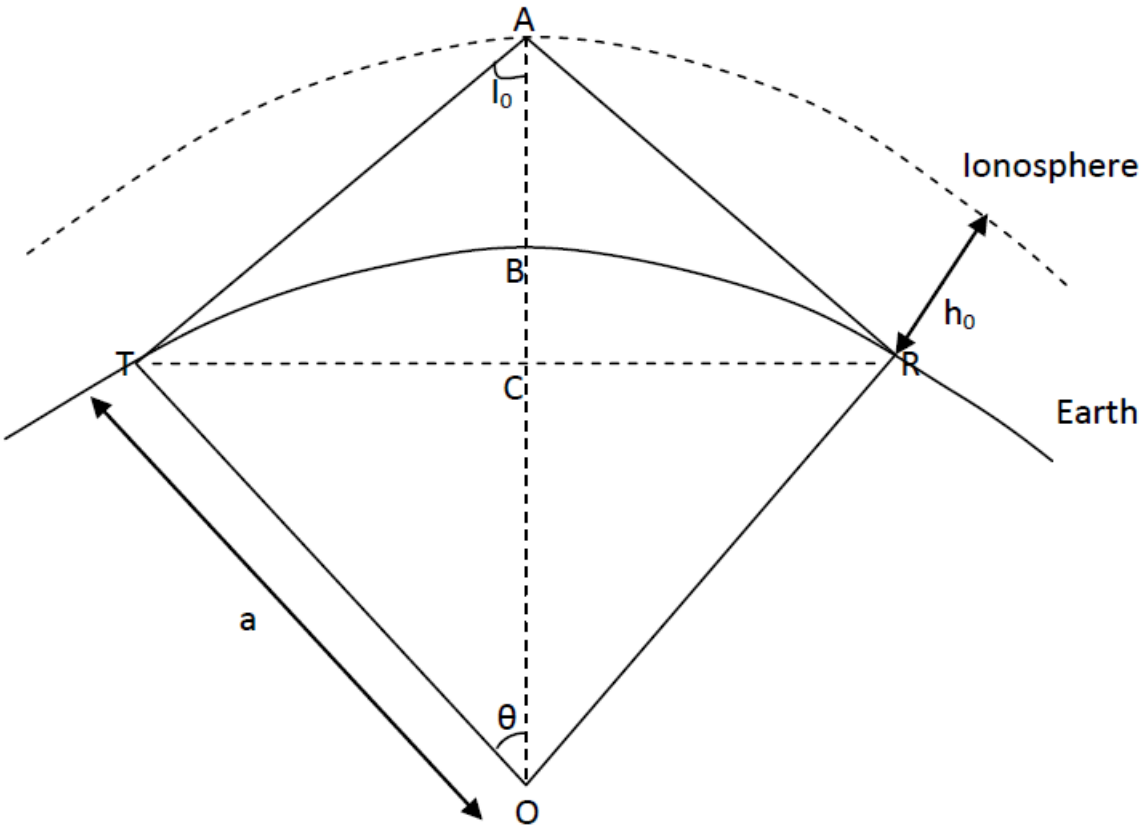

Figure 2.5: Geometry for a thin ionospheric layer and curved Earth (Appleton and Beynon, 1940; Davies, 1989).

$$cos^2(I_0) = \frac{(h_0 + a\frac{\theta^2}{2})^2}{(a\theta)^2 + (h_0 + a\frac{\theta^2}{2})^2} \tag{2.33}$$

The length of the chord TBR,

$$D = 2a\theta, \quad \theta = \frac{D}{2a} \tag{2.34}$$

Substituting for θ into Equation 2.33

$$cos^2(I_0) = \frac{(h_0 + \frac{D^2}{8a})^2}{\frac{D^2}{4} + (h_0 + \frac{D^2}{8a})^2} \tag{2.35}$$

In comparison with Equation 2.24, if f refers to the MUF for distance, D, then (Appleton and Beynon, 1940),

$$MUF = \frac{foF2}{cos(I_0)} \tag{2.36}$$

$$MUF(D) = foF2 \left(\frac{\frac{D^2}{4} + (h_0 + \frac{D^2}{8a})^2}{(h_0 + \frac{D^2}{8a})^2} \right)^{\frac{1}{2}} \tag{2.37}$$

where a is the Earth radius, D is the propagation distance and h_0 is the reflection height. For an obliquely transmitted radio signal reflected by the F2 layer, at a propagation distance of 3000 km,

$$MUF(3000)F2 = foF2 \times M(3000)F2 \tag{2.38}$$

3000 km is a useful practical limit for one hop propagation for the F2 layer for a lower elevation limit of 3°. MUF is the highest frequency for ionospheric transmission over an oblique path. M(3000)F2 is the propagation factor for the 3000 km propagation distance or range and MUF(3000)F2 is the corresponding maximum.

2.4 Ionospheric modeling

Ionospheric models have, for a long time, been used as a tool to predict the effect(s) of the ionosphere on radio propagation. Ionospheric predictions, alongside models, formulae and equations are known to aid the prediction of ionospheric and HF propagation characteristics. Ionospheric models are divided into three types, namely; theoretical, parametric and empirical. Theoretical models involve solving equations for ionospheric plasma and require significant time for computer algorithms and selecting suitable inputs in order to obtain meaningful results. Examples of theoretical models include the Time Dependent Ionospheric Model (TDIM), Coupled Thermosphere-Ionosphere Model (CTIM), Thermosphere-Ionosphere Global Circulation Model (TIGCM), Field Line Interhemispheric Plasma Model (FLIP) and Global Theoretical Ionospheric Model (GTIM). Parametric models are a simplified form of theoretical models, expressed in terms of solar-terrestrial parameters and geographical locations, representing the temporal and spatial structure of the ionosphere but they are limited to well-specified geophysical problems. Examples of parametric models include the Ionospheric Conductivity and Electron Density (ICED) model and Parameterised Ionospheric Model (PIM).

Empirical models are observation- or experiment-based models with ideas borrowed from theoretical and parametric models but with negligible depen-

dence on the progressing theories that describe the ionospheric plasma. They are very vital in the Sun-Earth environment because they provide the necessary reliable source-based empirical data for a parameter of interest. Some of the variations in the ionosphere, especially those that are geomagnetic-activity driven are complex and difficult or impossible to predict using theoretical models and therefore require data or observation-based models, which makes the use of empirical models a desirable approach. However, these models perform best in regions/ areas and time periods that have a sufficient database and reliable observations (Rush, 1986; Cander *et al.*, 1998; Ritchie and Honary, 2009). The Bent ionospheric model describes the electron density of the ionosphere as a function of longitude, latitude, season, time and solar radio flux. The model uses electron density values obtained from Alouette satellites, Ariel insitu measurements and bottomside ionograms. It finds its application in correcting ionospheric refraction in satellite tracking. However, it excludes the D, E and F1 regions. Using theoretical computations, Anderson *et al.* (1985) developed a semi-empirical model for the low-latitude region. The model uses electron density values (as a coefficient in the calculations) obtained from predicted vertical distribution and observed critical frequency (foF2) and the peak height of the F2 layer (hmF2). The other ionospheric electron density empirical models include the Penn state Mk III model, Chiu ionospheric model, Semi-Empirical Low-Latitude Ionospheric Model (SLIM), the Fully Analytical Ionospheric model (FAIM) and the International Reference Ionosphere (IRI). IRI, developed

and continuously improved by researchers from the Committee on Space Research (COSPAR) and the International Union of Radio Science (URSI), is an empirical model globally recognised for specifying ionospheric plasma parameters. These parameters include electron density and temperature, ion temperature and composition averaged over a month period at altitudes between 60 and 1500 km. The IRI model makes use of ionospheric plasma data obtained from a global network of ionosondes and incoherent scatter radars as well as satellites and rockets for topside and lower ionospheric measurements, respectively. This model can also generate TEC, predict the occurrence of spread F and the equatorial vertical ion drift. The IRI model is recommended for international use by COSPAR and URSI. (Bent *et al.*, 1975; Bilitza, 1990; Bilitza *et al.*, 2011).

2.5 HF propagation prediction models

2.5.1 Introduction

HF propagation prediction started in the early 1930s when the use of HF communication became apparent for long distance communication. Around this time, the knowledge of ionospheric conditions became significant and manual HF propagation models were developed. With the advancement in technology, computerised programs were developed. The first program to be developed was ITSA (Institute for Telecommunication Sciences and

Aeronomy)-1 which later evolved to the Ionospheric Communications Analysis and Prediction programme (IONCAP). IONCAP was later developed and improved to VOACAP in 1993 and the core model has not undergone any major changes since then. However, the VOACAP is limited to geomagnetically quiet conditions, and has poor performance in the polar regions. VOACAP was modified to the Ionospheric Communication Enhanced Profile Analysis and Circuit (ICEPAC) model to improve on high latitude HF predictions. ICEPAC was also developed from IONCAP by adding the Ionospheric Conductivity and Electron Density (ICED) profile model. The ICED profile model is a statistical model that takes into account the different physical processes of the large-scale features of the high latitude ionosphere. It includes distinct algorithms for the polar cap, subauroral trough, the equator-ward and pole-ward regions of the auroral zone. VOACAP and ICEPAC models are not good for hour-to-hour or day-to-day predictions because they work with median values. However, ICEPAC can be interpolated for short term predictions depending on the user's judgement (Tascione *et al.*, 1988; Stewart and Hand, 2008; Guest and Guest, 2013). The third common model is the Recommendation 533 (REC533) propagation model developed and updated by the International Telecommunication Union (ITU). The ICEPAC, VOACAP and REC533 models use monthly median values of foF2 and M(3000)F2 obtained from worldwide maps established using historical data at various ionosonde sites around the world. The commonly used world maps include the URSI and International Radio Consultative Committee (CCIR) maps

(Tanyer and Erol, 1998). The CCIR maps, used in VOACAP and ICEPAC, are based on monthly median values obtained by the worldwide network of ionosondes from about 150 stations during 1954 - 58. Long term models depend on the reliability and accuracy of ionospheric models: VOACAP uses an ionospheric model based on the parabolic layer theory, while ICEPAC uses Chapman layers for the E, F1 and F2 layers as well as coefficients approved by URSI (Bilitza, 1990). ICEPAC contains the Ionospheric Conductivity and Electron Density (ICED) profile model, a statistical model that takes into account the different physical processes of the large scale features of the high latitude ionosphere (Tascione *et al.*, 1988; Thrane *et al.*, 1994; Stewart and Hand, 2008). REC533 uses the NeQuick ionospheric model, referred to as version 1 or ITU-R, which was accepted by ITU-R sector in the early 2000s. NeQuick is a position- and time-dependent 3-D model that provides ionospheric electron density (Leitinger *et al.*, 2005; ITU-R, 2013).

2.5.2 ICEPAC

The ICEPAC prediction program is a simple FORTRAN code designed in such a way that it is not affected by replacement of any subsection. However, caution should be taken while joining the various sections and sub-models to mantain consistency and continuity of the program as a whole (Stewart and Hand, 2008). It is a combination of subroutines designed for the performance of HF sky wave systems and ionospheric-parameter analysis. The program is divided into seven independent sections (Stewart and Hand, 2008);

1. input subroutines,
2. path geometry subroutines,
3. antenna subroutines,
4. ionospheric parameter subroutines,
5. maximum usable frequency subroutines,
6. system performance subroutines, and
7. output subroutines.

Various input options such as the circuit parameters, numeric coefficients for ionospheric parameters, geomagnetic latitude and longitude for the polar model are handled by the input subroutines. The path geometry subroutines handle the selection of sample areas of the ionosphere and evaluation of the magnetic field at these areas. The path geometry subroutines also determine the geometry of the circuit. The antenna subroutines compute antenna parameters. The ionospheric parameter subroutines evaluate the ionospheric parameters required in the program. The MUF subroutine processes the E, F1, F2 and Es layer MUFs. The output subroutines produce the program output.

The ICEPAC prediction program can be implemented in diferent ways (Stewart and Hand, 2008) e.g.

- ICEPAC which is a point-to-point mode where calculations are made for a transmitter-reciever propagation.

- ICEAREA which produces area coverage predictions.
- S/I ICEPAC which calculates signal-to-interference in point-to-point mode.

It has a number of command lines, each having a name identifier to specify the associated input data (see table 2.1). When the user provides a valid name identifier, the program performs the analysis. However, at this stage, mistakes in the data may go unnoticed, thus the user should examine the output image. A detailed description of these command lines can be found in Stewart and Hand (2008). The method, Execution and Quit command lines are briefly discussed here.

- METHOD command line

  This command defines and controls the program analysis and prediction tasks to be performed. There are 30 tasks or methods or output options to choose from when predicting HF propagation conditions. A brief description of the available methods is given in table 2.2. Most of these tasks vary only in the way the output is presented but have more or less the same computations. The output options are divided into four basic analysis tasks performed by the ICEPAC program, namely;

  1. Ionospheric Parameters (METHOD 1 or 2):

     This task provides two outputs; a list of ionospheric parameters including the height of maximum ionization, the critical frequency, the reflection height of the Es layer, the location, time of the day

Identifier	Description of input parameters
METHOD	Program run option and beginning page number
MONTH	Year and month
SUNSPOT	12 month smoothed mean sunspot number and effective Q index
CIRCUIT	Transmitter-receiver locations
SYSTEM	Power, noise, min. angle, SNR, time delay, e.t.c
TIME	Time of day loop (and indicator for LMT or UT)
ANTENNA	Transmitter or receiver, antenna type and parameters
FREQUENCY	Operating frequencies
LABEL	Alphanumeric label for identification
INTEGRATE	.GE. 0 will do a fast integration when no F1 is present
EXECUTE	Execute program with parameters currently set
SAMPLE	Optional geophysical samples (for a specified area)
EFVAR	Optional E, F1 and F2 parameters (for a specified area)
EDP	True heights and electron density (for a specified area)
ANTOUT	Write antenna patterns on a file
OUTGRAPH	Request output of several methods
COMMENT	Comment line in user defined input
QUIT	Termination of program execution
FPROB	Critical frequency multipliers
TOPLINES	User specified heading lines (for method 23)
BOTLINES	User specified output lines (for method 23)

Table 2.1: Input parameters. Adopted from Stewart and Hand (2008)

for a given sample area of the ionosphere and an ionogram. The ionospheric parameters describe the E, F1, F2 and Es layers and are used to predict the ionosphere. The result is used to find an electron density profile which may be used to construct a predicted ionogram.

2. Antenna Patterns (METHOD 13, 14 OR 15):

   This task performs a precalculation of the antenna gain pattern

required for the system performance predictions.

3. Maximum usable frequency (METHOD 3 to 12):

   This task provides the MUF prediction. It also provides information about the MUF distributions of each ionospheric layer.

4. Systems Performance (METHOD 16 to 29):

   This task provides a comprehensive prediction of radio system performance parameters of a communication system operating between two points on the Earth's surface. This task is considered to be the main output of the ICEPAC program. The main outputs in this task include a table of up to 22 performance variables and a table or graph of the LUF. Examples of performance variables include number of hops for MUF, mode type, time delay and virtual height for the most reliable mode (MRM).

- EXECUTE command line

  When a system configuration is defined, this command executes the defined analysis task.

- QUIT control command

  This command terminates the ICEPAC program.

Method	Description
1	Ionospheric parameters
2	Ionograms
3	MUF - FOT lines (nomogram)
4	MUF - FOT graph
5	HPF - MUF - FOT graph
6	MUF - FOT - Es graph
7	FOT - MUF table (full ionosphere)
8	MUF - FOT graph
9	HPF - MUF - FOT graph
10	MUF - FOT - ANG graph
11	MUF - FOT - Es graph
12	MUF by magnetic indices, K (not implemented)
13	Transmitter antenna pattern
14	Receiver antenna pattern
15	Both transmitter and receiver antenna patterns
16	System performance (S.P.)
17	Condensed system performance, reliability
18	Condensed system performance, service probability
19	Propagation path geometry
20	Complete system performance (C.S.P.)
21	Forced long path model (C.S.P.)
22	Forced short path model (C.S.P.)
23	User selected output lines (set by TOPLINES and BOTLINES)
24	MUF-REL table
25	All modes table
26	MUF - LUF - FOT table (nomogram)
27	FOT - LUF graph
28	MUF - FOT - LUF graph
29	MUF - LUF graph

Table 2.2: Output methods. Adopted from Stewart and Hand (2008)

2.5.3 VOACAP

Like ICEPAC, VOACAP predicts the propagation of a radio signal from a transmitter to receiver at any location on Earth. It is also designed to

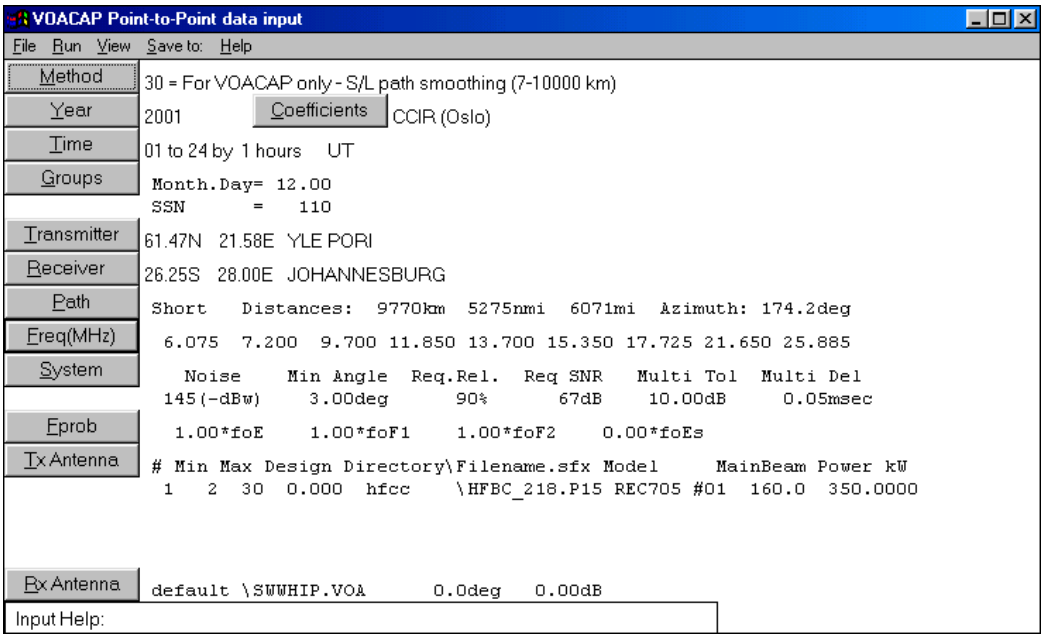

Figure 2.6: Input screen for the VOACAP point-to-point propagation prediction (http://www.voacap.com).

predict worldwide area coverage for a single transmitter at any time and point on Earth. VOACAP is able to predict 22 parameters including MUF, LUF, signal to noise ratio, signal power, reliability, propagation angle, field strength at receiver and required power gain. The model outputs monthly median ionospheric and HF propagation parameters based on a large number of observations provided by CCIR, URSI among other sources, and inputs such as the SSN, F10.7 and the planetary magnetic index. VOACAP is not suitable for predicting disturbed events such as geomagnetic storms and solar flares but it takes the diurnal and solar cycle variations into account. The model, however, allows knowledgeable users to input an electron density

multiplier in the ionospheric layers to represent the effects related to space weather. The Graphical User Interface (GUI) for the VOACAP prediction

Parameter	Recommendation
Method	Select Method Number 20 (Complete System Performance). If you are running circuits over 7000 km, use Method 30 (Short/Long Path Smoothing).
Year	This is a user-specified value. It has no effect on calculations.
Coefficients	Select CCIR (Oslo). This is the default for using VOACAP in long-term predictions. **Do not use URSI88 (Australian)**.
Time	Select UT (Universal Coordinated Time). Local Mean Time does not mean your local time but the local sun time at the receiver.
Transmitter	Select the transmitter location from the pre-defined lists, sorted by city (worldwide), by nation (worldwide) and by state (USA). You can also enter the coordinates manually.
Receiver	Select the receive location from the pre-defined lists, sorted by city (worldwide), by nation (worldwide) and by state (USA). You can also enter the coordinates manually.
Path	Select Short or Long Path. The default is Short Path.
Freq(MHz)	Enter the frequencies to be used for calculation. Use the zero (0) value to remove a frequency from the set. A set of 11 user-specified frequencies can be defined. Also three pre-defined frequency sets are available which can be modified if needed.
Fprob	Do not use all default values. Set foE to 1, foF1 to 1, foF2 to 1 and foEs to 0 (zero, instead of 0.7).

Figure 2.7: Basic input settings VOACAP point-to-point propagation prediction (http://www.voacap.com).

model is shown in figure 2.6 and a brief description of the input settings is given in figure 2.7. The user can specify up to 10 months of predictions at a time using the mm (month).dd (day) format. The monthly sunspot number for the specified month is also required. A list of system parameters: man-made noise level (140.4 - industrial area, 144.7 - residential, 150.0 - rural and 163.6 - remote), minimum take off angle (3° is recommended for a radio amateur user), the default required circuit reliability and maximum tolerable

time delay is 90 percent and 0.10 milliseconds, respectively, and so on.

2.5.4 REC533

Figure 2.8: Basic input settings REC533 point-to-point propagation prediction (http://www.voacap.com).

The REC533 prediction method is an implementation of the ITU's propagation model Recommendation ITU-R PI.533. The model development and maintainance was and is, respectively, done by the United States Department of Commerce, National Telecommunications and Information Administration, Institute for Telecommunication Sciences (NTIA/ITS) found in Boulder, Colorado. The user-friendly GUI for the input parameter modification is shown in figure 2.8. REC533 is also capable of producing point-to-point and area coverage predictions. The basic input settings are similar to ICEPAC and VOACAP shown in figure 2.7. The model aims at predicting HF communication performance for the different solar cycles, seasons, days and hours for any given geographic location, for purposes of circuit planning and frequency management. REC533 propagation from a transmitter to a receiver is assumed to follow the great circle path, and is used in estimating compatibility and reliability between frequencies in the HF range.

Chapter 3

Instrumentation and Data analysis techniques

3.1 Instrumentation

3.1.1 Ionosonde

As stated in Chapter 1, an ionosonde is one of the instruments used in studying the effects of the ionosphere on HF propagation. It is an HF radar which transmits and receives radio wave signals in a frequency range of 3 to 30 MHz. The ionosonde transmits signals of radio energy and records the time delay of the reflection of the echo by the ionosphere. The virtual height of reflection (h') is the apparent height of an ionized layer had the wave continued to travel (paths TAR and $T'A'R'$ as opposed to TBR and $T'B'R'$ in

figure 2.4) at the speed of light, as determined from the time interval between the transmitted signal and the ionospheric echo at vertical incidence. It is given by

$$h' = \frac{c\tau}{2} = c\int_0^{h_r} \frac{dh}{u} = \int_0^{h_r} \mu' dh \tag{3.1}$$

where c is the speed of light, τ is the echo delay and the factor 2 accounts for the fact that the pulse has to traverse the distance h' twice. u is the group speed and h_r is the real height of reflection (Davies, 1989).

Records of the variation of the virtual reflection height with frequency are known as ionograms. Examples are shown in figure 3.1. The ionogram shown in figure 3.1(top) is atypical of observations seen in the polar cap. While figure 3.1(bottom) gives a typical example, characterised by spread F and sporadic E as a result of reflections of the radio signal on irregularities in the ionosphere. The two traces with the black and red dashed fitted curves in figure 3.1(top) are the Ordinary (O-) and Extraordinary (X-) modes of reflection, respectively. To convert these traces to real height, the profiles are inverted using the Polynomial Analysis (POLAN) program (Titheridge, 1985, 1988). The black and red curves under the traces are the POLAN-inverted real height profiles corresponding to the X- and O-mode reflections, respectively. It should be pointed out that the electron density profile is independent of the the modes of reflection, and thus the black curve represents the real height profile for this example. The real height profiles corresponding to the X- and O-mode reflections are due to the fact that the POLAN soft-

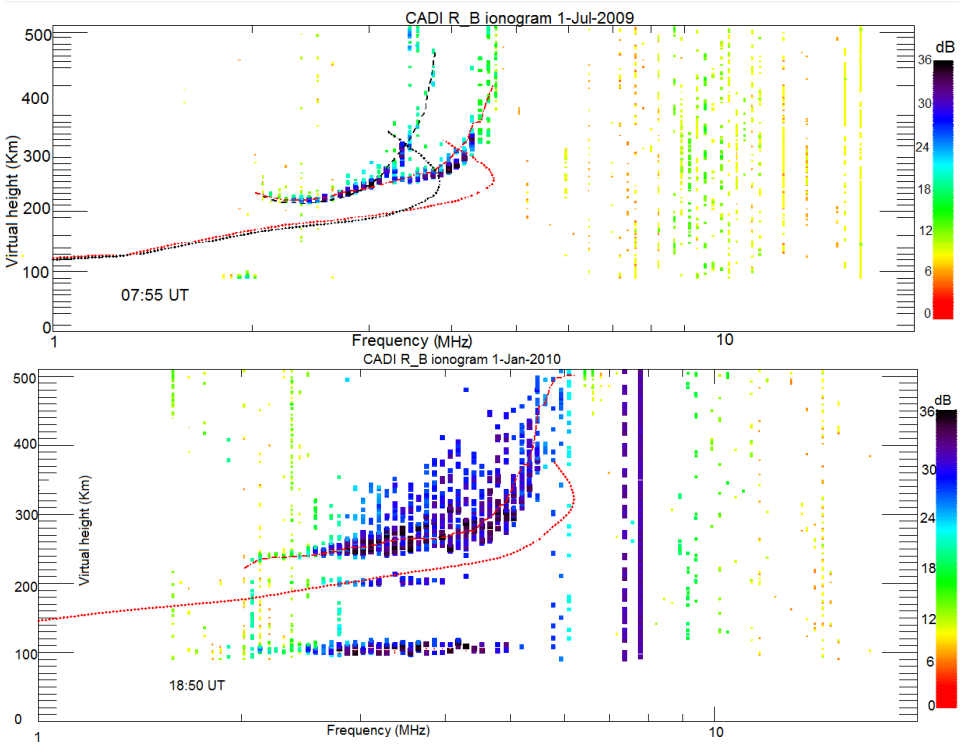

Figure 3.1: Examples of CADI generated ionograms for an undisturbed period (top) and a disturbed period (bottom).

ware automatically produces two different profiles for the different modes. Figure 3.2 shows the transmitter and receiver antennas for CADI at Hall Beach, NU (68.77° N, 278.74° E), one of the CHAIN stations. CADI consists of a transmitter with a delta antenna, and the receiver antenna array comprised of four dipoles arranged as a square. CADI ionograms are available in either 1 or 5 minute temporal and 6 km altitude resolutions from CHAIN. The CADI ionograms are manually scaled at 10 minute intervals to obtain the relevant ionospheric characteristics such as critical frequencies, the heights and the MUF.

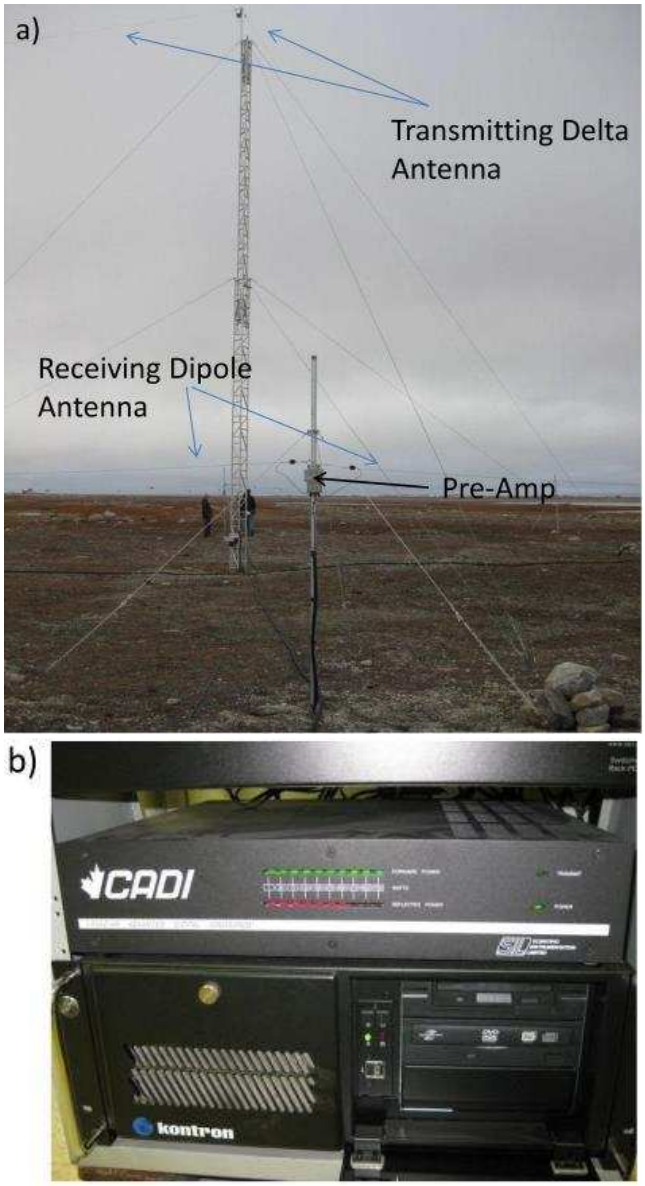

Figure 3.2: Transmitting and receiving antennas (a) and box containing receivers (b) of CHAIN CADI located in Hall Beach, NU. Adopted from Watson (2015).

3.2 Data analysis techniques

As mentioned in Chapter 1, the neural network (NN) has been used as a data analysis technique in this study. This section gives a brief introduction about the technique, and detailed information can be found in Haykin (1994); Hagan *et al.* (1996).

3.2.1 Neural Networks

A neural network is a vast, nonlinear, parallel distributed processor with a natural ability to learn and generalise tasks or data presented by the user (Haykin, 1994; Oyeyemi and McKinnell, 2008). The learning process involves adjusting the network free parameters through the environment-stimulation process, while generalisation is the ability to apply the learned knowledge during the training process to a completely new set of data. The NN is similar to the human brain in that knowledge acquisition is through a learning process, and the knowledge is stored in the neuron-neuron links otherwise known as synaptic weights. The learning process is effected following a procedure known as a learning algorithm, whose role is to adjust the synaptic weights of the NN to obtain a desired response. As the name suggests, a neural network is made up of neurons. A neuron is a fundamental unit of a neural network, made up of three basic elements, namely; synapses, an adder and an activation function. Figure 3.3 shows an illustration of a neuron model with input signals $x_1, x_2, ...x_m$, multiplied by synaptic weights, ω_{ki}

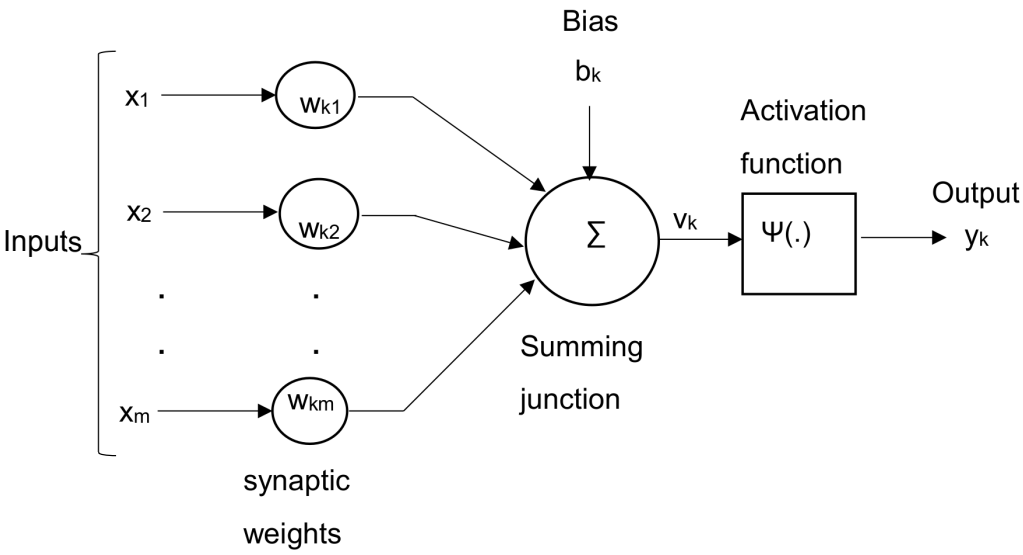

Figure 3.3: Neuron model. Adopted from Haykin (1994)

connected to neuron k. Each input x_i at synapse i is multiplied by a synaptic weight ω_{ki}. The weighted input signals are added at the summing junction and an activation function is applied to limit the neuron output amplitude. The bias b_k or threshold θ_k may be applied externally to lower or increase the net input to the activation function, respectively.

3.2.1.1 Activation functions

Basic types of activation functions include the threshold, piecewise linear, and sigmoid functions. The graphical representation of each of these functions is shown in figure 3.4.

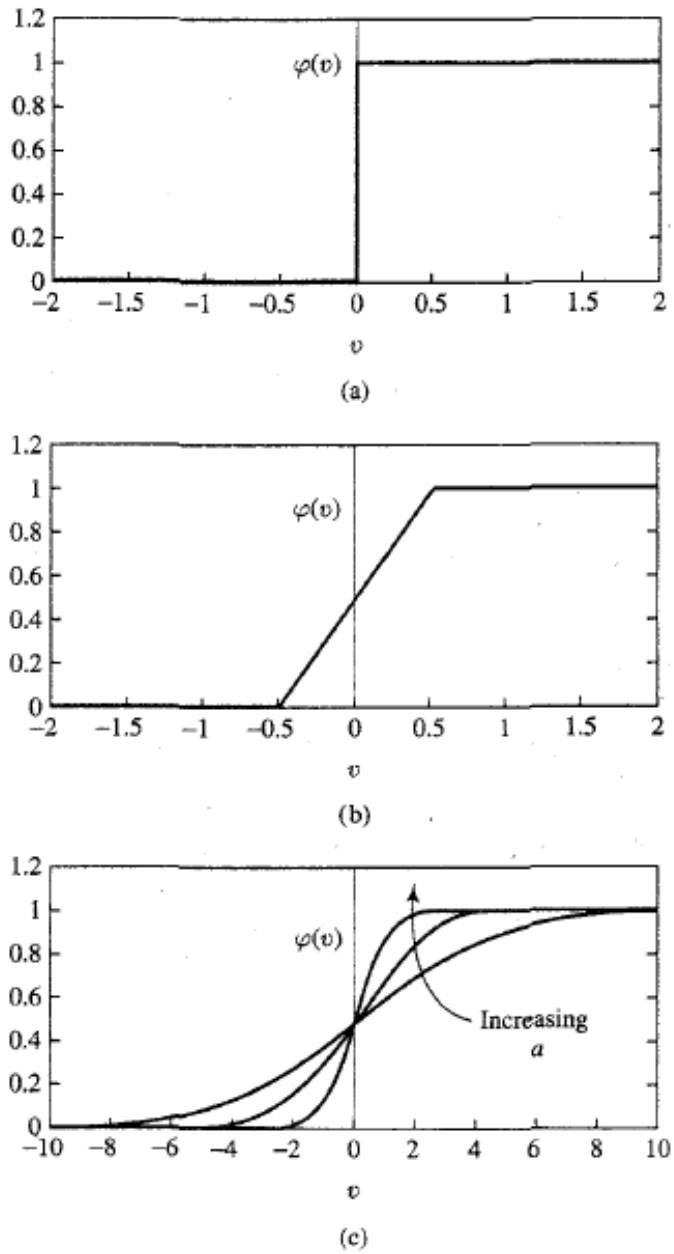

Figure 3.4: Basic types of activation functions: (a) Threshold, (b) Piecewise linear and (c) Sigmoid functions. Adopted from Haykin (1994)

- **Threshold function**: A neuron model with the threshold function, also known as the McCulloch-Pitts model generates an output of one if V_k is nonnegative or zero otherwise.

$$\phi(V_k) = \begin{cases} 1 & V_k \geq 0 \\ 0 & V_k < 0 \end{cases} \tag{3.2}$$

where

$$V_k = \sum_{i=0}^{m} \omega_{ki} x_i + b_k \tag{3.3}$$

- **Piecewise linear function**: The piecewise linear function is defined in the following limits,

$$\phi(V_k) = \begin{cases} 1 & V_k \geq \frac{1}{2} \\ V_k & \frac{1}{2} > V_k > -\frac{1}{2} \\ 0 & V_k \leq -\frac{1}{2} \end{cases} \tag{3.4}$$

- **Sigmoid function**: This is the preferred activation function in neural network applications because it is continuous in the range of 0 to 1 and differentiable. It demonstrates both linear and nonlinear characteristics and is a strictly increasing function. A common example of the sigmoid function is the logistic function given as

$$\phi(V_k) = \frac{1}{1 + exp(-aV_k)} \tag{3.5}$$

a is the slope parameter and the effect of varying a in the logistic function is shown in figure 3.4. The sigmoid function becomes a threshold function as the slope parameter tends to infinity except that the latter only takes up values of 0 and 1 and is not differentiable.

$$\lim_{a \to \infty} f(a)_{sigmoid} = f_{threshold} \tag{3.6}$$

3.2.1.2 Network architectures

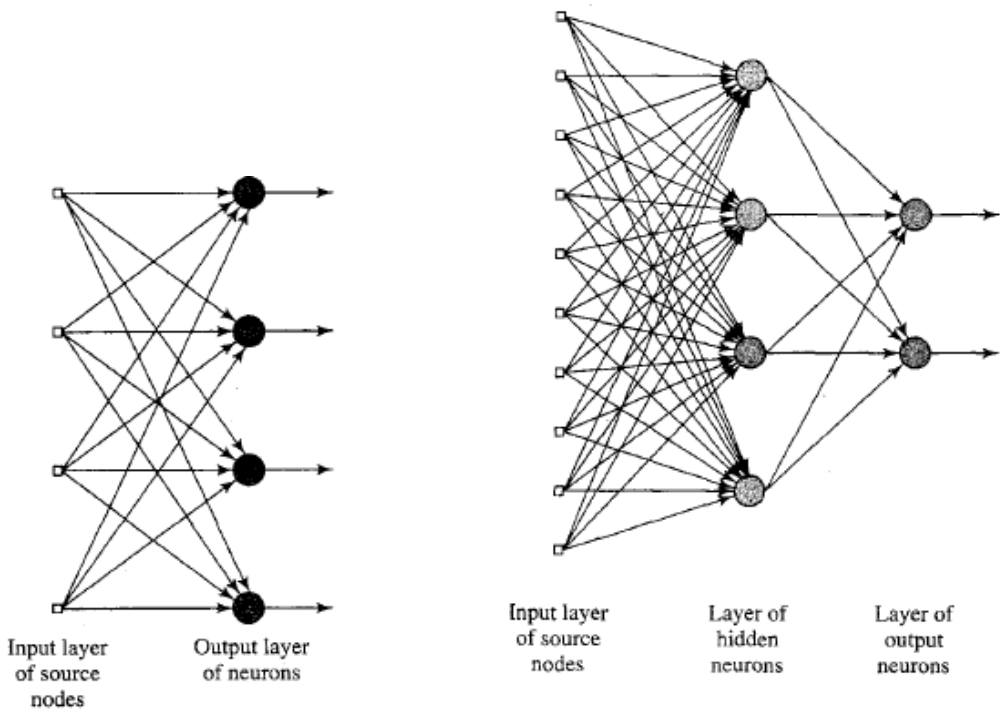

Figure 3.5: Examples of layered networks: single layered (left) and multiple layered (right) feedforward network. Adopted from Haykin (1994).

The manner in which the neurons are structured in a particular network is

known as a NN architecture, examples of which include the single layer and multilayer feedforward networks. The single layer network is the simplest type of a layered network, and it is made up of strictly the input and output layers. It is single layered because computations only occur in the neurons that make up the output layer. The multilayer feedforward network differs from a single layered one by having one or more hidden layers whose corresponding computation nodes are known as hidden neurons or units. The role of the hidden neurons is to establish a useful link between the network inputs and output(s), as well as enabling the network to extract high order statistics from available information. The choice of the number of hidden layers is specifically relevant to a network with a large input layer. The inputs of one hidden layer of a multilayer feedforward network are the outputs of the preceeding one, and the output signals at the final layer are simply the total network response to the stimulation at the input. An example of a single and multi layer feedforward network is shown in figure 3.5 (Haykin, 1994). The input vectors are presented to the network and they propagate forward to produce an output. The network output is subtracted from a desired output, usually called the target, to obtain an error, also known as a performance index. This is a step-by-step process that aims at obtaining the smallest possible error by adjusting the network parameters (weights and biases) after each iteration, a process also known as learning (Haykin, 1994).

3.2.1.3 Learning

The learning process involves a stimulation of the NN by the environment which results in changes in the network free parameters. The network is consequently induced to respond accordingly. The learning algorithm describes a set of rules that govern a particular learning process. The difference between algorithms are steps followed in adjusting the network parameters. The basic learning algorithms include the error-correction, memory-based, Hebbian, competitive and Boltzman learning. Below is a description the error-correction algorithm which has been used in this work.

- **Error-correction learning algorithm**

  The error-correction rule is illustrated in figure 3.6, the input vector

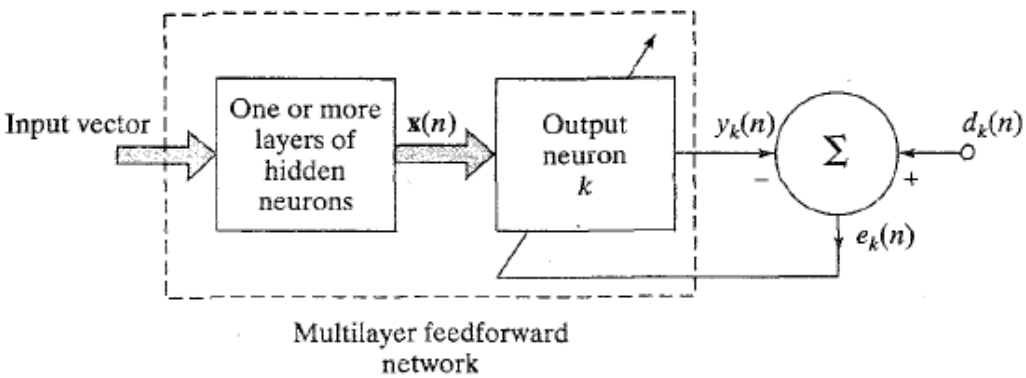

Figure 3.6: An illustration of the error-correction rule. Adopted from Haykin (1994).

presented to the network by the user acts as stimulus to the computational node(s), otherwise known as hidden node(s), which in turn

generate a response $x(n)$. $x(n)$ becomes a stimulus to the output neuron. n symbolises a time step in the iteration process of adjusting the synaptic weights that correspond to a neuron k. The output signal correponding to neuron k, $y_k(n)$, which is the network output in this case, is subtracted from the target, $d_k(n)$ to obtain an error signal, $e_k(n)$, denoted as

$$e_k(n) = d_k(n) - y_k(n) \tag{3.7}$$

The error signal activates a mechanism that applies a series of corrective adjustments to the respective synaptic weights in such a way as to obtain a $y_k(n)$ that is as close to $d_k(n)$ as possible in an iterative manner. The iteration continues until the synaptic weights are stabilised, i.e., a steady state is reached, at which point the learning process is terminated. The error-correction algorithm employs the Delta or Windrow-Hoff learning rule in the process of minimising $e_k(n)$. According to the Delta rule, the correction adjustment, $\triangle\omega_{ki}(n)$, to the synaptic weight, ω_{ki}, at the nth iteration is denoted as

$$\triangle\omega_{ki}(n) = \eta e_k(n) x_i(n) \tag{3.8}$$

The learning rate in the iterative process is determined by η, which is a positive constant. The adjusted synaptic weight is then denoted as

$$\omega_{ki}(n+1) = \omega_{ki}(n) + \triangle\omega_{ki}(n) \tag{3.9}$$

3.2.1.4 Generalisation

The complexity of a given neural network is dependent on the number of free parameters, which are determined by the amount of neurons in that particular network. Determining the suitable number of neurons in a network, otherwise known as regularisation, is a key feature in designing multilayer networks. The more complex the network is, i.e., the more free parameters the network has, the more likely it is to have poor generalisation of a given dataset, while a well-trained network is able to perform well on new data as it does on the training set. One of the goals of a neural network user is to design a suitable network with the least number of free weights and biases. Figure 3.7 shows examples of poor and good generalisation, both figures are outputs of the same network trained at two different times. The blue curve represents the underlying function. The noisy target plotted data is represented by open circles, the trained network output is represented by the black curve, and the network output at the training data points is represented by circles with crosses. figure 3.7 (top) represents an output of an overtrained network. There is an exact match between the network output and the training data points, and a poor match of the function. Such a network is said to overfit, and thus has poor generalisation because of its failure to interpolate points in the neighborhood of the training data. However, the overfitting occurs for input values that correspond to the training dataset (between -3 and 0). For input values outside the range corresponding to the training dataset (between 0 and 3), the network fails to extrapolate points

in this region. While using neural networks, it is thus important that the user makes an effort to obtain training data that covers all regions of input space that the network is to be applied. Figure 3.7 (bottom) illustrates an example of good generalisation. The network was trained such that only the necessary number of weights were used (not all the available weights). The network output does not perfectly fit the function but it performs much better than the previous case. However, even in the good generalisation case, the network fails to accurately extrapolate for reasons mentioned earlier.

Generalisation can be improved by two common methods: early stopping and regularisation. In the early stopping method, the available data is divided into the training (used for training the network) and validation set (used for testing the ability of the network to approximate the underlying function). The user monitors the error obtained from the validation set and stops the training once the minimum error is obtained. However, the validation dataset as well as the training set should have a good representation of all regions of input space that the network is going to be used. While the regularisation method modifies the sum squared error performance index by adding a term that aims at penalising the complexity of the network. One of the effective regularisation approaches is the Bayesian regularisation that uses an algorithm outlined in Foresee and Hagan (1997) and detailed in Hagan *et al.* (1996). The goal is to adjust the network parameters so as to minimise the difference between the network output and the target or to develop an algorithm that minimises the performance index.

The performance function used in the Bayesian regularisation algorithm is given by (Hagan *et al.*, 1996),

$$F(w) = \beta \sum_{k} (d_k - y_k)(d_k - y_k) + \alpha \sum_{i=1}^{n} w_i^2 \tag{3.10}$$

where d is the target, y is the network output, α and β are regularization parameters, the first summation term on the right is the sum squared error computed from the training dataset and the second summation term is the sum squared weight. The performance function, $F(w)$ is minimised by adjusting the weights as

$$w_{k+1} = w_k - \frac{1}{2\mu_k} \bigtriangledown F(w) \tag{3.11}$$

μ_k is the Marquardt adjustment parameter. μ_k is initially set to a small arbitrary value e.g. 0.01, if $F(w+1)$ is not smaller than $F(w)$, then μ_k is multiplied by some factor $\phi > 1$ at the next iteration, otherwise it is divided by the same factor. The effective number of network parameters, γ is obtained at each iteration using the equation

$$\gamma = n - 2\alpha t(H)^{-1} \tag{3.12}$$

where n is the total number of network parameters and the Hessian, H, is given by

$$H = \bigtriangledown^2 F(w) \sim 2\beta J^T J + 2\alpha I_n \tag{3.13}$$

J is the Jacobian matrix of the errors obtained from the training dataset. The Bayesian algorithm computes and adjusts α and β using the effective number of parameters, the sum squared errors and weights, iteratively until convergence is reached, that is, there is no significant change in $F(w)$ over consecutive loops. The Bayesian regularisation has an advantage that as long as the network has the effective number of parameters, and convergence has been reached, there is no need to use trial and error to determine the suitable size of the network .

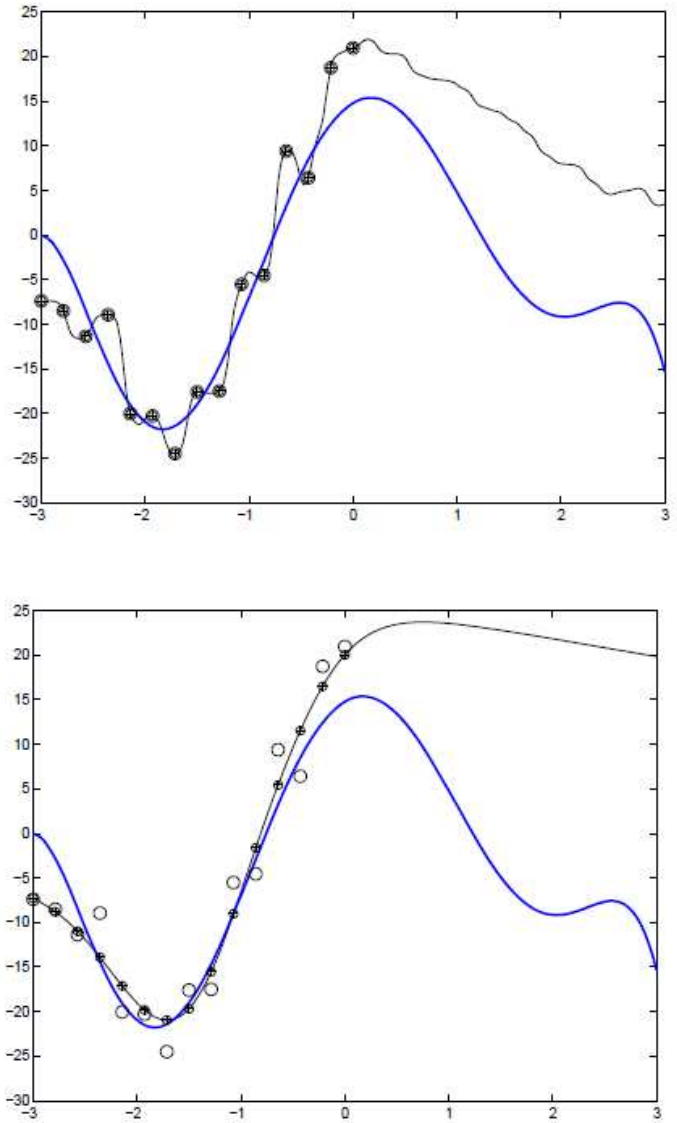

Figure 3.7: Examples of poor (top) and good (bottom) generalisation. The blue curve represents the underlying function. The noisy target plotted data is represented by open circles, the trained network output is represented by the black curve, and the network output at the training data points is represented by circles with crosses. Adopted from Hagan *et al.* (1996).

Chapter 4

Comparison of observed and predicted MUF(3000)F2 in the polar cap region

4.1 Introduction

Ionospheric communication in the HF band is known for its ability to provide world-wide coverage, using relatively little power and low-cost equipment. Studies have shown that HF communication at high latitudes is more vulnerable to the dramatic changes of the high latitude ionosphere, mainly driven by the nature of its geophysical environment, briefly descussed in section 2.2, and solar activity (Cannon, 1989; Hunsucker and Hargreaves, 2003). This is especially true with polar HF radio communication, which is

strongly affected by the presence of features such as patches and sun-aligned arcs, briefly described in section 2.2 (Tobiska *et al.*, 2002; Goodman and Ballard, 2004; MacDougall and Jayachandran, 2007; Warrington *et al.*, 2009, 2012). Known effects of these features on HF communication include delay spread, Doppler shift and spread and displacement of radio signals from the great circle path (Warrington *et al.*, 1997; Stocker *et al.*, 2003; Hunsucker and Hargreaves, 2003). Various studies have been undertaken to account for off-great circle propagation over northerly regions (Zaalov *et al.*, 2003, 2005; Stocker *et al.*, 2007; Warrington *et al.*, 2012). Recently, there has been renewed interest in comparing long term model predictions and observations over different paths at high latitudes (Thrane *et al.*, 1994; Jodalen *et al.*, 2001; Goodman and Ballard, 2004; Stocker *et al.*, 2007). Thrane *et al.* (1994) presented preliminary comparisons of measured and predicted reliability of the HF communication channel at high latitudes and found an overestimation of the reliabilities and MUFs by VOACAP and ICEPAC prediction programs. Goodman and Ballard (2004) compared observations and VOACAP predictions of the Maximum Observable Frequency (MOF) in the polar cap and found the upper decile predicted by VOACAP was lower than the observations, which was attributed to polar patches. Stocker *et al.* (2007) compared measurements and VOACAP predictions of HF propagation parameters for paths along the midlatitude trough and within the polar cap and found that signal strength was underestimated by VOACAP in the presence of off-great circle propagation. Similar studies have been done in the mid lat-

itudes (Zolesi *et al.*, 2008; Pietrella *et al.*, 2009; Tshisaphungo *et al.*, 2011). Efforts to explore the polar region have been limited by inadequate data, where most of the available ionospheric communication studies in the polar region have used limited data, mostly acquired in the 1960s - 70s. Adequate data is an essential requirement for validation and development of empirical models, as already mentioned in Chapter 1. In this study, the performance of three long term HF propagation prediction models over two paths within the polar cap region have been examined. This work takes advantage of new data obtained from CHAIN. CHAIN has been briefly described in Chapter 1, and details can be found in Jayachandran *et al.* (2009). Observations of ionosonde-derived MUF(3000)F2 at the stations shown in figure 4.1 and model predictions have been compared.

4.2 Data and analysis

The instantaneous MUF(3000)F2 was obtained, as described in sections 2.3 and 3.1, from two CHAIN ionosondes at Resolute (74.75° N, 265.00° E) and Pond Inlet (72.69° N, 282.04° E) stations shown in figure 4.1. The monthly median MUF(3000)F2 was then computed from the instantaneous values for the different hours within a month. For instance, the MUF(3000)F2 values for a particular month are sorted according to hours, and a median is obtained for each hour, generating 24 values in a given month. The monthly median values were compared with predictions obtained from ICEPAC, VOACAP

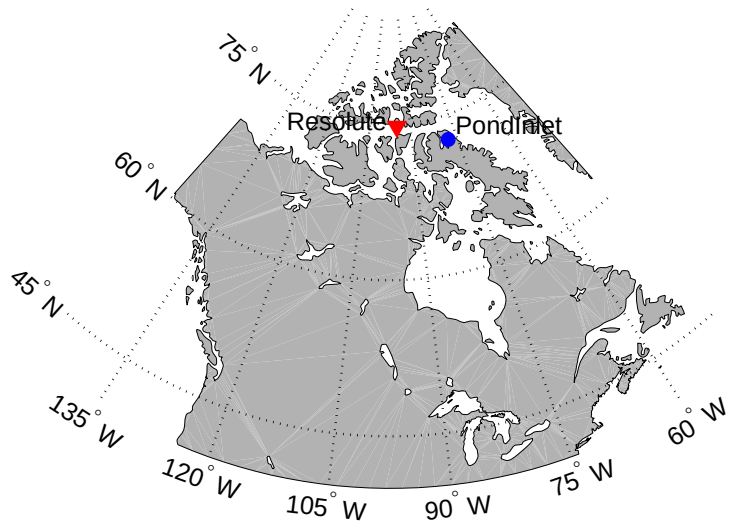

Figure 4.1: A map showing the locations of Resolute (74.75° N, 265.00° E) and Pond Inlet (72.69° N, 282.04° E).

and REC533 models over a four year period. Data analysis at Resolute covers 2009, 2011, 2012 and 2013 while that at Pond Inlet covers the same period except that 2011 is replaced by 2010. The reason for the replacement was because there was more scaled Resolute data for 2011 compared to 2010. The performance of the long term models was characterised using the root mean square error (RMSE) defined as

$$RMSE = \sqrt{\frac{1}{N}\sum_{i=1}^{N}(MUF^e - MUF^p)^2} \tag{4.1}$$

Where N is the number of data points, MUF^e and MUF^p are the experimental and predicted MUF respectively.

.

4.3 Comparison of observations with model predictions

MUF is an essential parameter to radio users, because of its key role in circuit planning and radio frequency management. The HF radio community mostly relies on long term model predictions. It is important to examine the model predictions using ionospheric measurements. The monthly median MUF(3000)F2 and values predicted by the models for the analysed period are displayed in figures 4.2 to 4.7. The error bars on the measurements represent the standard deviations during each month, at a particular hour. Months have been classified into seasons as: November, December, January, February (winter), May, June, July, August (summer) and March, April, September, October (equinoxes). The time format of 01:00 - 24:00 UT, used in the three prediction models, as opposed to the traditional format, 00:00 - 23:00 UT, was adopted in this work for easy comparison. In figures 4.2, 4.3 and 4.4, results are presented for Resolute during the winter, summer and equinoxes, respectively. The left and right panels represent results for low and moderate solar activity, respectively. The observed values, VOACAP, REC533 and ICEPAC predictions are plotted in blue, black, red and green colours, respectively. The observed MUF(3000)F2 is noticeably affected by solar activity across all seasons with lower values during low solar activity.

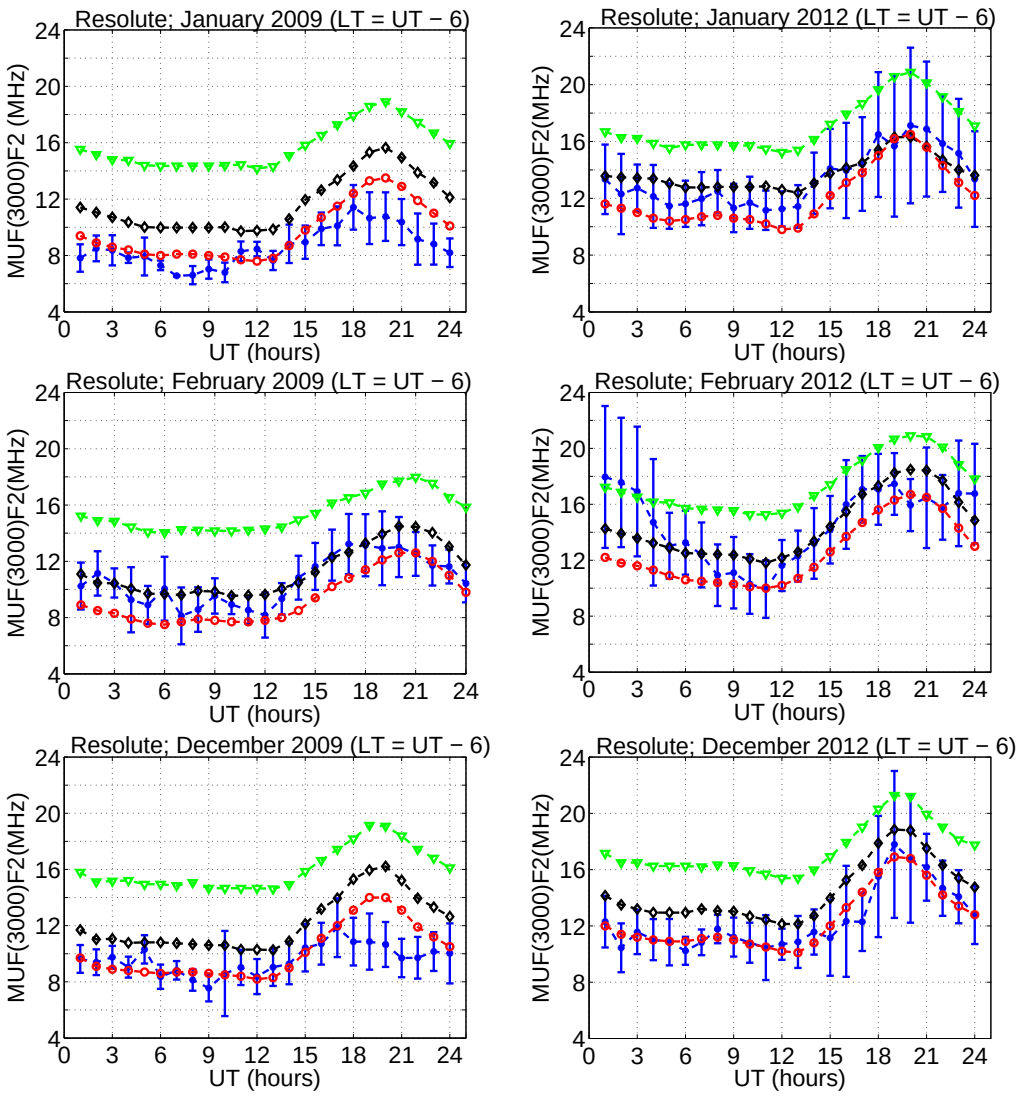

Figure 4.2: Monthly median values for the MUF(3000)F2 calculated from measurements at Resolute (blue) and predicted values: ICEPAC (green), VOACAP (black) and REC533 (Red) for winter 2009 and 2012. The error bars are standard deviations in the observed values.

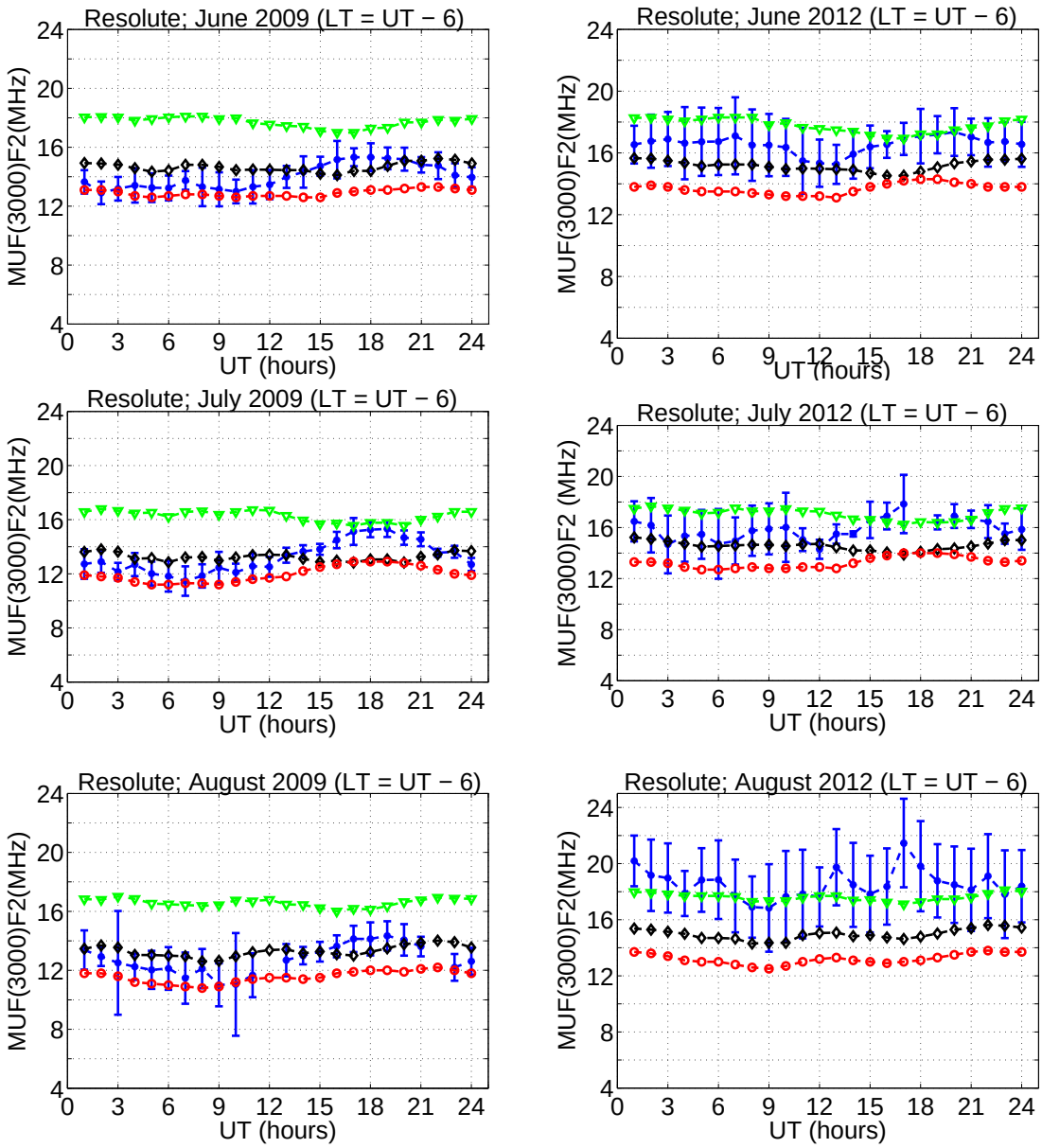

Figure 4.3: Monthly median values for the MUF(3000)F2 calculated from measurements at Resolute (blue) and predicted values: ICEPAC (green), VOACAP (black) and REC533 (Red) for summer 2009 and 2012. The error bars are standard deviations in the observed values.

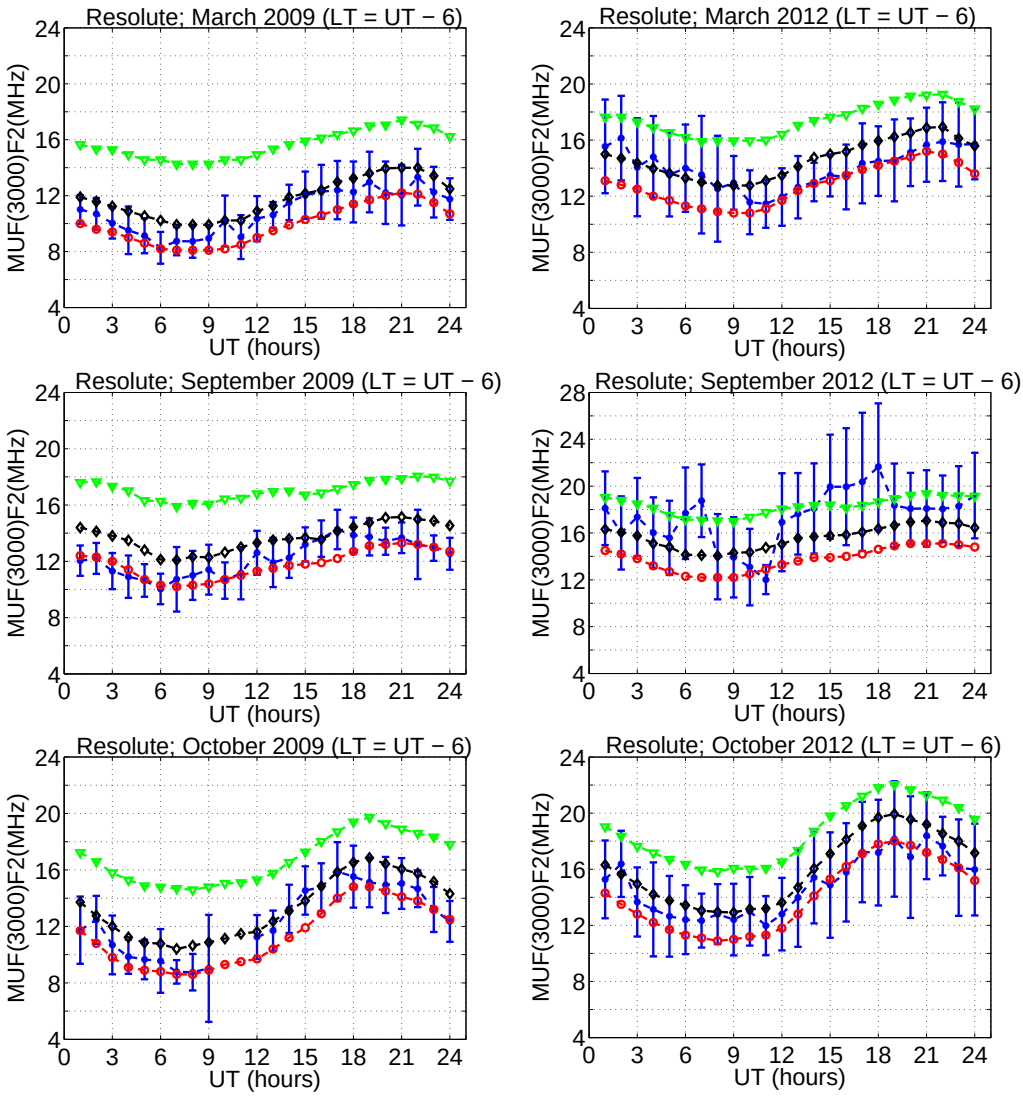

Figure 4.4: Monthly median values for the MUF(3000)F2 calculated from measurements at Resolute (blue) and predicted values: ICEPAC (green), VOACAP (black) and REC533 (Red) for equinoxes of 2009 and 2012. The error bars are standard deviations in the observed values.

This is associated with the effect of solar activity on the variation of the ionosphere, as pointed out in section 2.1.3. For instance, high solar activity increases photoionisation levels which in turn leads to an enhancement in the ionospheric electron density, which requires higher MUF(3000)F2 for meaningful communication as described in section 2.3.

During winter, the observed MUF(3000)F2 is relatively constant between 01:00 UT to ∼12:00 UT (local nighttime), gradually increasing to a maximum at ∼18:00 UT (local noon) followed by a reduction until 24:00 UT (local midnight). All models roughly reproduce this general diurnal trend except that the peak is at 20:00 UT. It is important to note that the polar winter ionosphere is exposed to extended periods of darkness, even though the electron density in the region is still high, and shows diurnal variation. The contribution to the F layer electron density in the polar winter is by particle precipitation and transport of plasma from the sunlit ionosphere (Whitteker *et al.*, 1978; Goodman and Ballard, 2004; MacDougall and Jayachandran, 2007; Hosokawa *et al.*, 2014). Research studies that demonstrate the uniqueness of the polar F region date back to the 1950s and 1960s. For example, Maehlum (1969) presented one of the significant differences between the mid latitude and polar F regions: the fact that the ionisation at the latter is Universal Time (UT) controlled, with the $foF2$ at the North pole having its peak around 20:00 UT, and the south pole peak at 06:00 UT. The diurnal peaks were reported to be more and less pronounced during the winter and summer, respectively. The UT variation is attributed to the separation of the

geographic and magnetic poles. The thermospheric neutral-air wind blows over the polar regions in an antisunward direction. At 06:00 UT and 18:00 UT, the South and North geographic poles, respectively, lie on the magnetic pole midnight side, and thus the ionosphere during those times is lifted by the drag of the neutral particles against the ions. At these times, transport of ionisation produced in the sunlit hemisphere is also effective (Hunsucker and Hargreaves, 2003). A combination of all these factors explains the HF radio ionospheric support achieved in the dark winter. In summer, the diurnal variation in MUF(3000)F2 is less pronounced than during other seasons but the values are higher. Goodman and Ballard (2004) also observed the variation of MUF to be least during summer and greatest in the equinox and winter periods. During the polar summer, solar radiation prevails the entire time with a slight variation in the intensity due to the changing solar elevation angles (Zheng *et al.*, 2014).

Looking at the results in figures 4.2, 4.3 and 4.4, ICEPAC systematically overestimates the MUF(3000)F2 throughout all the hours during low solar activity, while VOACAP and REC533 give values close to observations with a few exceptions where divergences occur. Overestimation in VOACAP and ICEPAC MUF predictions have been observed at high latitudes (Thrane *et al.*, 1994; Goodman and Ballard, 2004). Thrane *et al.* (1994) observed a tendency of VOACAP and ICEPAC predictions to overestimate MUF up to a factor of 2 at noon time. They noted that the overestimation is an indicator that the models overestimate the daytime F region electron density. During

moderate solar activity, ICEPAC overestimates the winter nighttime MUF but shows an improvement during the daytime winter and the equinoxes, while VOACAP underestimates the daytime summer MUF. During summer, VOACAP and ICEPAC modelled values demonstrate opposite diurnal variations from the CADI observations, with maxima occuring during local night time and minima during local daytime. These results are similar to the errors in the IRI-derived propagation factor observed in the polar cap region by Themens *et al.* (2014). Even though it underestimates the MUF(3000)F2, REC533 captures the same variability as the observations.

During the equinoxes (figure 4.4), the diurnal variation is more pronounced with a minimum and maximum around 09:00 UT and between 18:00 and 21:00 UT, respectively. VOACAP and REC533 fall within the error bars while ICEPAC overestimates the values with a slight improvement during high solar activity.

Similar diurnal and seasonal variations are observed at Pond Inlet in figures 4.5 to 4.7. Results for Pond Inlet are displayed in the same format as Resolute results. Pond Inlet has a 1 hour local time difference from Resolute. The CADI at Pond Inlet became operational in the summer of 2009, so the analysis for that particular year covers only 6 months.

ICEPAC is still seen to overestimate the MUF during low solar activity while VOACAP and REC533 generate values close to observations with some cases of deviations. During moderate solar activity, however, ICEPAC still overestimates the winter nighttime MUF, while REC533 underestimates values

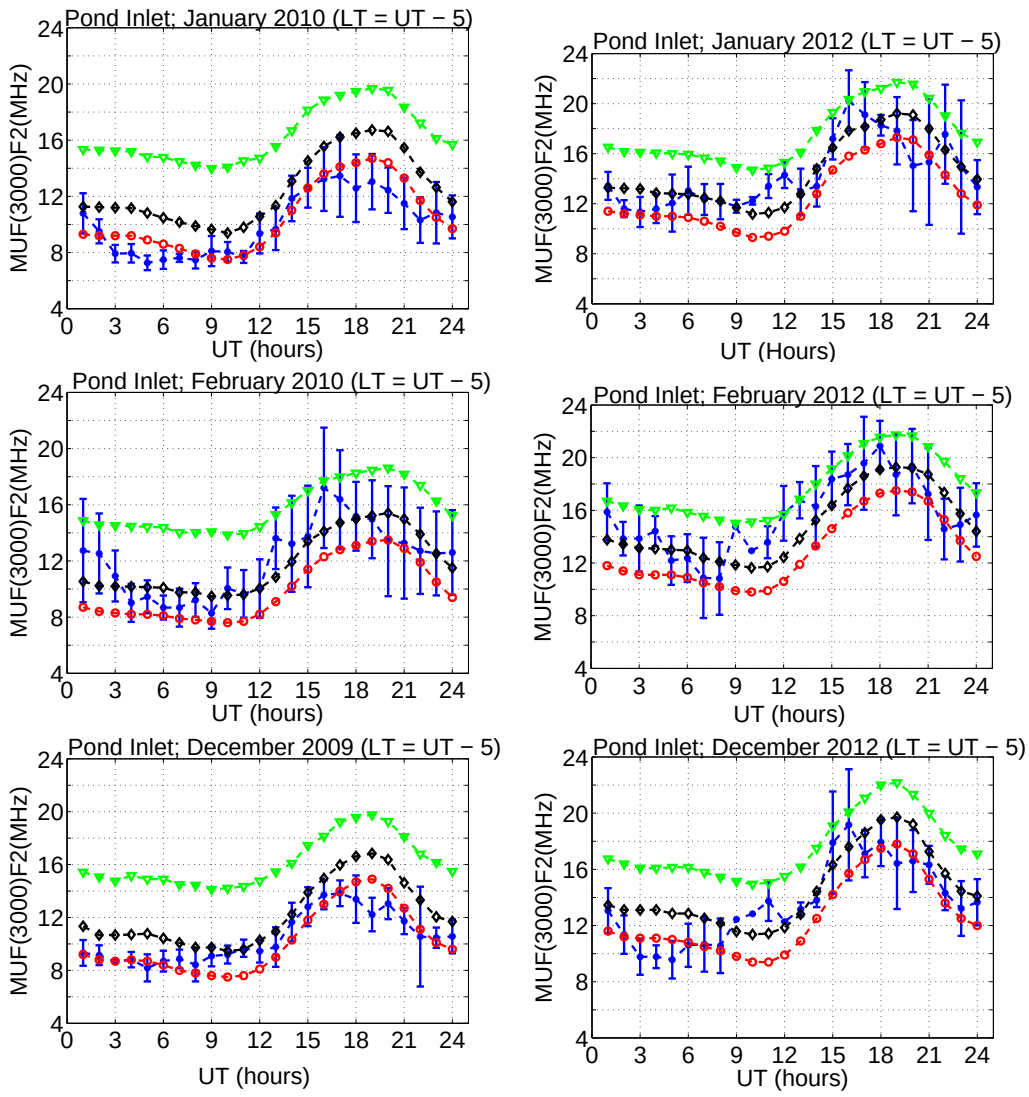

Figure 4.5: Monthly median values for the MUF(3000)F2 calculated from measurements at Pond Inlet (blue) and predicted values: ICEPAC (green), VOACAP (black) and REC533 (Red) for winter 2009, 2010 and 2012. The error bars are standard deviations in the observed values.

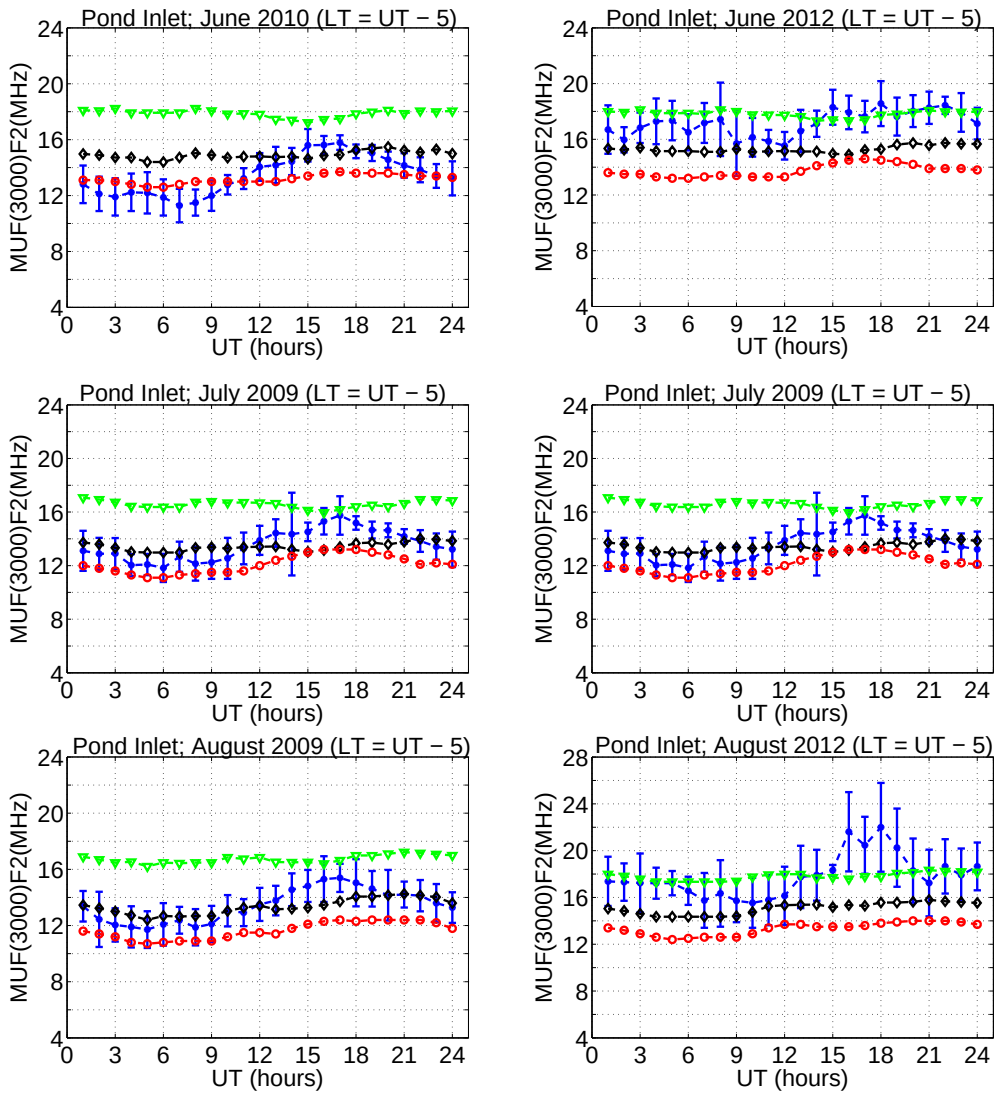

Figure 4.6: Monthly median values for the MUF(3000)F2 calculated from measurements at Pond Inlet (blue) and predicted values: ICEPAC (green), VOACAP (black) and REC533 (Red) for summer 2009, 2010 and 2012. The error bars are standard deviations in the observed values.

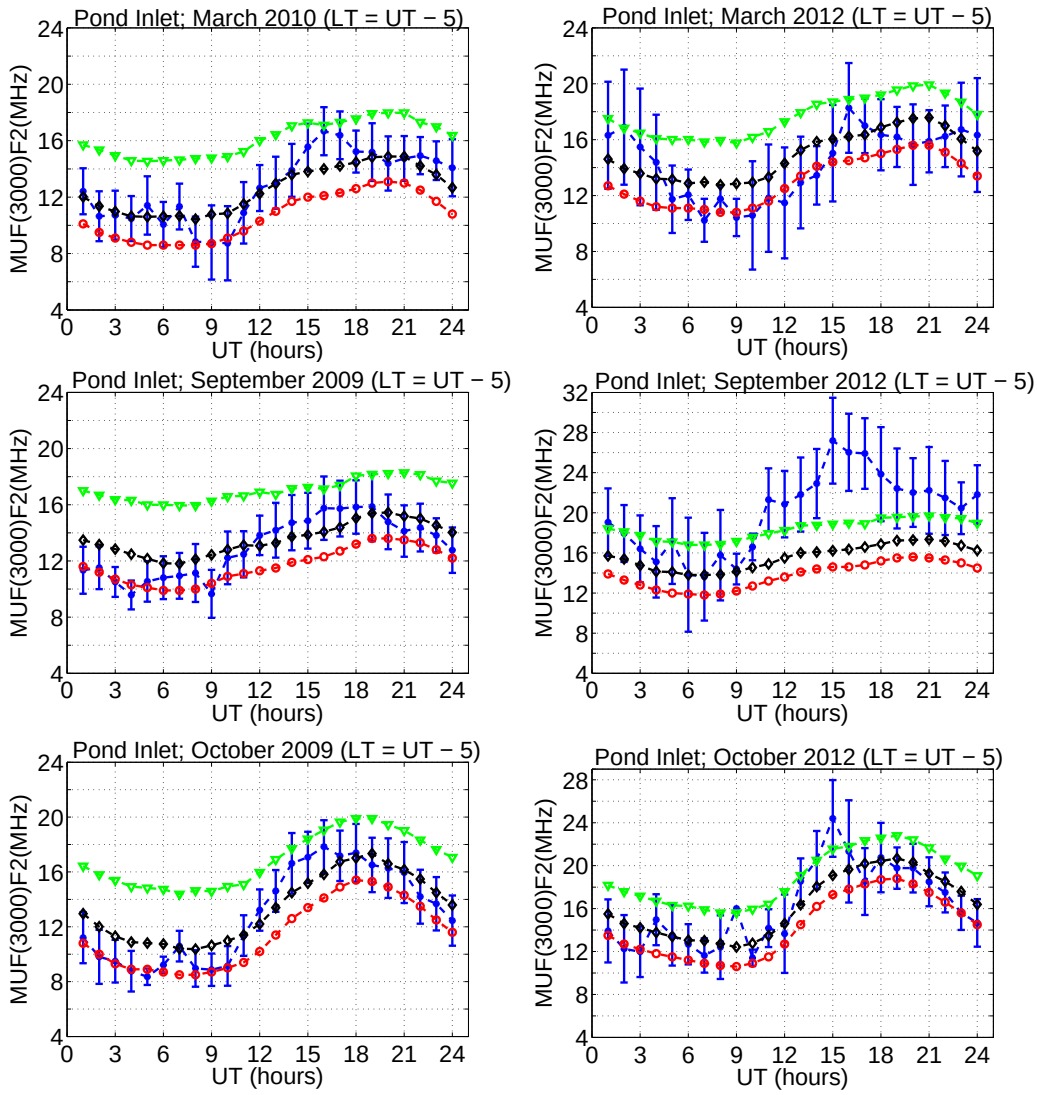

Figure 4.7: Monthly median values for the MUF(3000)F2 calculated from measurements at Pond Inlet (blue) and predicted values: ICEPAC (green), VOACAP (black) and REC533 (Red) for the equinoxes of 2009, 2010 and 2012. The error bars are standard deviations in the observed values.

between the post-midnight - noon period. VOACAP generally shows a better performance compared to other models. During summer, VOACAP and ICEPAC predict MUF values close to observations, except the observed opposite diurnal variation mentioned earlier. REC533 still underestimates MUF during this season but reproduces the diurnal variation seen in observations. Notice also that all three models are unable to reproduce the daytime enhancement in MUF observed in measurements during September 2012.

The ICEPAC and VOACAP prediction models are sister models developed from IONCAP. The difference between the two models is that VOACAP mantains the original ionospheric structure based on parabolic layer theory while ICEPAC ionospheric structure is based on the Chapman layer theory. As stated in section 2.5, ICEPAC was mainly developed to improve predictions at the high latitudes and polar regions by the inclusion of the ICED model (Tascione *et al.*, 1988; Thrane *et al.*, 1994; Stewart and Hand, 2008). Thrane *et al.* (1994) point out that the replacement of the parabolic layer with the Chapman layer causes a slight increase of the predicted MUFs as a result of enhanced electron densities below the maximum of the layer. This could explain the overestimation of the MUF(3000)F2 by ICEPAC.

The RMSE between observed and modelled values, and the standard deviation in the measurements for Resolute and Pond Inlet are presented in figures 4.8(a) and (b). In these figures, the case of RMSE values being greater than the standard deviations in the observed data is considered poor perfor-

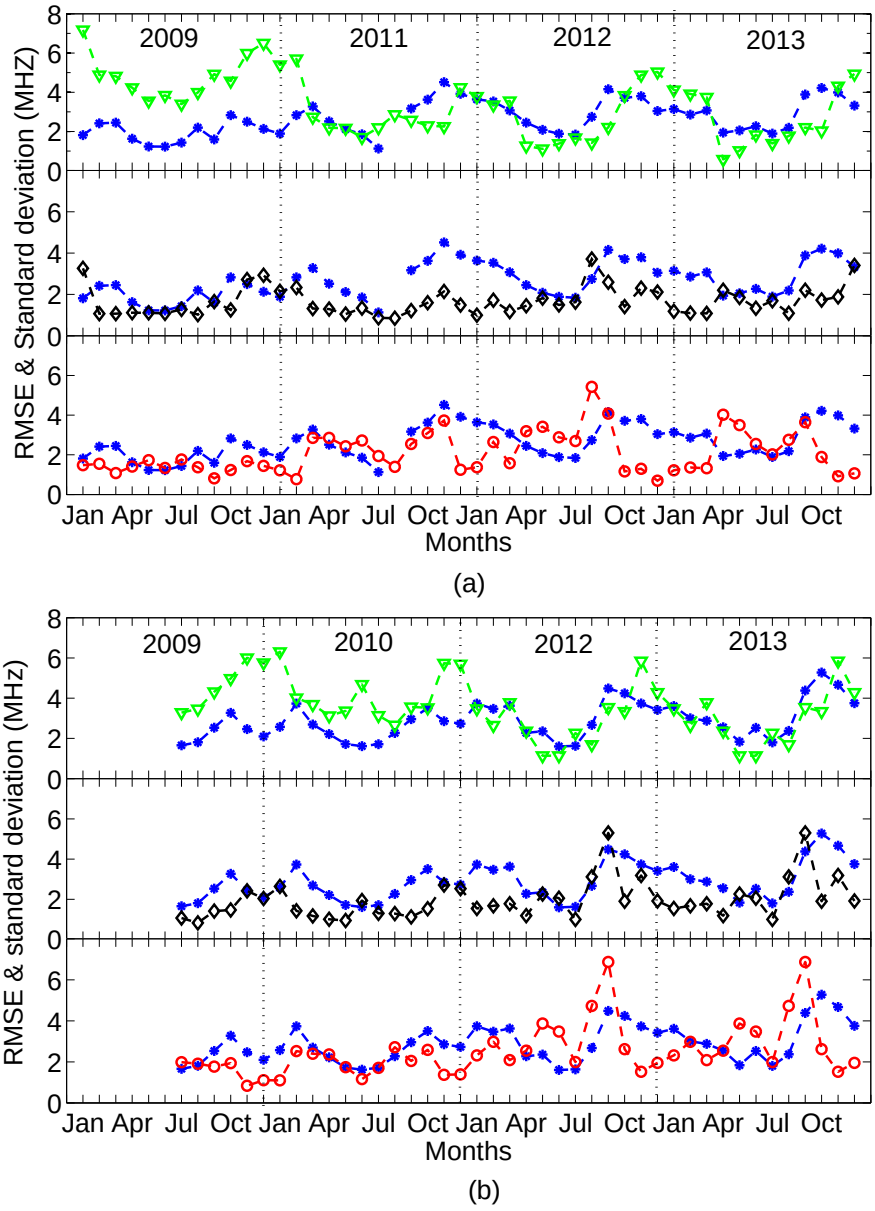

Figure 4.8: RMSE between observed MUF(3000)F2 values and ICEPAC (green), VOACAP (black), REC533 (red) modelled values and standard deviation (blue) in the measured data at (a) Resolute and (b) Pond Inlet.

mance. The standard deviations, as well as RMSE values seem to increase with solar activity. A seasonal variation in the standard deviation is evident in the results. The variation is clearly depicted by the ICEPAC RMSE and fairly well by the VOACAP RMSE but not so evident in the REC533, especially during high solar activity.

In the upper panel of figures 4.8(a), the ICEPAC model performs poorly during low solar activity, particularly, during the entire year of 2009. This may be a result of solar activity being well below expected or previously observed levels during the extended solar minimum of cycle 23/24. ICEPAC improves in performance as solar activity increases, especially during summer; however, the poor performance during the months of January, February, December 2011, January, November, December 2012, March 2012, March 2013 and the winter of 2013 is still noticeable. In the next panel, VOACAP performs well except during winter in 2009 and August 2012.

While in the third panel, REC533 performs well during winter and equinox months except during the summers of 2011, 2012 and 2013. REC533 shows poor performance in May, July 2009 and April 2009, 2011, 2012, 2013.

At Pond Inlet (figures 4.8(b)), ICEPAC still performs poorly during low solar activity except in March and September 2010. ICEPAC performance gets better as solar activity increases with exceptions of January, November, December 2012 and April, August, November 2013. In the second panel, VOACAP RMSE values fall within the standard deviation except in July 2010, July, September, October 2012 and April, August, November 2013.

In the last panel, REC533 RMSE values fall within the standard deviation except during the summers of 2012 and 2013. REC533 also shows poor performance in July 2009, August 2010, September 2012 and 2013.

4.4 Discussion and Conclusion

Measurements and modelled values of MUF(3000)F2 have been compared for two paths in the polar cap region. The diurnal variation in equinox months is characterised by a pronounced minimum and maximum around local midnight and noon, respectively. The diurnal variation in summer is less pronounced but the MUF(3000)F2 values are higher compared to the other seasons. The winter variation of MUF(3000)F2 has a maximum around local noon. All models roughly reproduce the general diurnal trend observed in the measurements during the winter and equinox periods. This observation is consistent with the results of Thrane *et al.* (1994) in their comparison of measured and modelled reliability and MUF at high latitudes. Both predictions and observations show diurnal and seasonal variations, however, the models do not reproduce the actual hourly variability observed in the measurements. VOACAP and ICEPAC modelled values do not reproduce the daytime variations observed in the CADI measurements. One of the most discussed features in the polar ionosphere are the polar patches: Enhancements of electron density caused by different mechanisms (Smith *et al.*, 2000; Carlson *et al.*, 2004; Lockwood *et al.*, 2005; Oksavik *et al.*, 2006). MacDougall

and Jayachandran (2007) observed a higher patch activity in winter than in summer but also noted that the seasonal variation depends on the patch definition used. In general terms, it is background electron density versus the enhancements associated with patches. The models used in this study are empirical, not physics-based, and do not account specifically for features such as patches.

A statistical analysis of the performance of the three models was also examined using the RMSE approach. The standard deviations, as well as RMSE values, seem to increase with solar activity, indicative of greater inter-month variability. The ICEPAC model performs poorly during low solar activity. Some general differences across seasons for the studied period were noticed. REC533 gives a better performance in winter and some equinox months while VOACAP has a better performance for both equinox and summer months and ICEPAC shows poor performance during low solar activity. Even though ICEPAC performance improves with solar activity, poor performance during winter and some equinoctal months is still noticeable.

The long term models considered in this study are empirical, implying that data collection has to be sufficiently large to provide good results. However, the models were developed at a time when exploration of the high latitudes, especially the polar ionosphere was almost impossible due to insufficient data. Deductions at the high latitudes were mostly based on extrapolation using data at low and mid latitudes. The models also assume propagation along the great circle contrary to studies that have suggested off-great circle prop-

agation in the polar cap, a result that has been attributed to the presence of patches. Warrington *et al.* (2012) developed a ray tracing model for the polar ionosphere to account for the HF radio propagation that results from the off-great circle mechanism. They compared their results with model predictions and suggested an improvement of the current prediction models by the inclusion of additional measured parameters such as patch intensity. They pointed out a plan for extensive observations to obtain data at high latitudes to validate and improve the current models. This work lays a foundation for the validation and improvement of the current HF propagation models in the polar cap region using data from CHAIN.

Chapter 5

MUF variability in the Arctic region

5.1 Introduction

As described in section 2.3, the ionosphere plays a significant role as a medium of HF radio propagation. However, from section 2.1.3, it is also true that it is highly variable, which can be a limitation to ionospheric-dependent communication. Ionospheric variability ranges from within the hour to solar cycle timescales. It is necessary to establish ranges and limits for ionospheric variability for different seasons, regions and solar cycles for the smooth operation of radio communication systems (Davies, 1989; McNamara, 1990; Kouris *et al.*, 2000a). Reliable and precise estimates of MUF variability are particularly important to radio users for purposes of circuit

planning and radio frequency management (Fotiadis *et al.*, 2004). A significant effort has been made in studying ionospheric variability using different indices and ionospheric parameters by various researchers (Bradley *et al.*, 1999; Forbes *et al.*, 2000; Kouris *et al.*, 2000a,b; Ezquer *et al.*, 2002, 2004; Bradley *et al.*, 2004; Wilkinson, 2004). For instance, studies of the foF2 and peak electron density (NmF2) variability have been undertaken by various groups (Rishbeth and Mendillo, 2001; Mendillo *et al.*, 2002; Altadill, 2007; Deminov *et al.*, 2013). In their investigations of the day-to-day variation of foF2 and M(3000)F2 in the European sector, Kouris *et al.* (1998) found the relative deviations (relative daily deviations normalised to the corresponding monthly median values) of hourly daily M(3000)F2 from corresponding monthly medians to be below ± 0.10 while the F2 layer critical frequency (foF2) deviations ranged from ± 0.2 to ± 0.3. MUF and foF2 variabilities are of the same order with a slight difference during high solar activity (Kouris *et al.*, 1994; Bradley *et al.*, 1999; Kouris *et al.*, 1999, 2000a).

Using results of foF2 observations obtained by Davis and Groome (1964) in the American longitudinal sector, Recommendation P.533 of the International Telecommunication Union (ITU-R) gives tabulated estimates of the diurnal variability of the MUF as a function of solar activity, seasons, local time and geographical latitude (ITU-R, 1997; Kouris *et al.*, 2000a; Fotiadis *et al.*, 2004; Wilkinson, 2004; Bradley *et al.*, 2004). The results provided by Davis and Groome (1964) were values of the foF2 fractional decile deviations from the monthly median, obtained from 13 stations mostly covering one

solar cycle of measurements. The stations used in the Davis and Groome (1964) MUF distribution analysis include: Thule (77.00° N, 69.00° W) for the polar cap, Barrow (71.30° N, 156.80° W), Byrd (80.00° S, 120.00° W), Fairbanks (64.90° N, 147.80° W), and Reykjavik (64.10° N, 21.80° W) for the auroral oval, Adak (51.90° N, 8176.60° W), Washington (38.70° N, 77.10° W) and White Sands (32.30° N, 106.50° W) for the high temperate regions, Concepcion (36.50° S, 73.00° W), Maui (20.80° N, 156.50° W), Okinawa (26.30° N, 127.80° E) and Puerto Rico (18.50° N, 67.20° W) for the lower temperate regions. The equatorial latitudes were represented by Huancayo (12.00° S, 75.30° W). These results were adopted and applied to MUFs by the ITU-R to assess radio system performance and operations (Wilkinson, 2004; Bradley *et al.*, 2004). The direct application of foF2 results to MUFs is based on the assumption that the variability of M(3000)F2 is negligibly smaller compared to that of foF2 and to a first order, MUF variability is not a function of path length (Bradley *et al.*, 1999; Kouris and Fotiadis, 2002; Bradley *et al.*, 2004; Fotiadis *et al.*, 2004). Kouris *et al.* (2000a) found that the ITU-R reference values over estimate MUF variability compared to observations made in the European area. Fotiadis *et al.* (2004) investigated the day-to-day ionospheric variations using data obtained from a worldwide network ionospheric stations, with an aim to establish a new set of bounds and concluded that their model was not a viable replacement of the ITU-R reference figures. There have been suggestions of adopting the ITU-R estimated values in the IRI to provide an estimate of ionospheric variability (Wilkinson, 2004).

The ITU-R reference values are considered by the global HF radio community as acceptable and are adopted by radio system operators and users. As stated in section 4.1, data scarcity in the high latitude region was a major drawback to the exploration of the ionosphere in the early 1960s, when the reference values were established. It is thus important to ensure the validity of the estimates using ionospheric observations as a first step towards establishing global and regional ionospheric variability bounds, a vital but lacking specification in ionospheric and HF prediction models.

5.2 Data and analysis

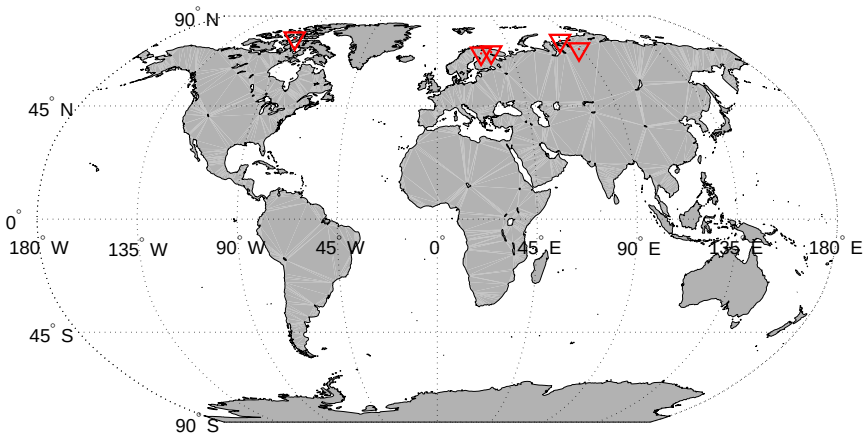

Figure 5.1: A map showing the geographic locations of the stations listed in Table 1.

The MUF(3000)F2 data used in the analysis was obtained from five stations located in the northern arctic region: Resolute (74.75° N, 265.10° E), Dikson (73.50° N, 80.40° E), Norilsk (69.40° N, 88.10° E), Loparskaya (68.00° N, 33.00° E), and Sodankyla (67.40° N, 26.60° E). The geographical locations of the stations considered in the study are shown in figure 5.1. The periods of

Table 5.1: Stations used in the data analysis.

Station	Latitude (°) (Geographic)	Longitude (°)	Period of data
Resolute	74.70	265.10	1961, 1966 - 1967, 1971 - 1973, 1977 - 1978, 1983 - 1984, 1987 - 1988, 1992 - 1993
Sodankyla	67.40	26.60	1961 - 1989
Loparskaya	68.00	33.00	1961 - 1962, 1964 - 1977, 1981 - 1984, 1986 - 1994, 2000-2002
Norilsk	69.40	88.10	1968 - 1988,2010 - 2013
Dikson	73.50	80.40	1982 - 2001

data used for each station are shown in table 5.1. The foF2 and M(3000)F2 data was obtained from the SPIDR for a period ranging from 1961 to 2013, spanning over three solar cycles. SPIDR has been briefly described in Chapter 1. foF2, the maximum frequency beyond which radio waves transmitted at vertical incidence become escape rays, is related to the F2 peak density (NmF2) by equation 2.5. The hourly daily MUF(3000)F2 are computed from the corresponding hourly daily foF2 and M(3000)F2 values using equation 2.38, The ratio of hourly MUF(3000)F2 to the corresponding monthly median value, R, computed as

$$R = \frac{MUF_{hourly}}{MUF_{monthlymedian}} \tag{5.1}$$

was obtained for a particular station, and classified according to solar activity (low, moderate, high), season (winter, equinoxes, summer), local time 4-hour interval of the day (22h00 - 02h00, 02h00 - 06h00, 06h00 - 10h00, 10h00 - 14h00, 14h00 - 18h00, 18h00 - 22h00). The seasons have been classified according to the ITU-R standard, as already stated in section 4.3. The three levels of solar activity are determined using the 12-month running mean of the sunspot number (R12): $R12 < 50$, $50 < R12 < 100$ and $R12 > 100$ for low, moderate and high solar activity, respectively. The upper and lower deciles were determined for each 4-hour local time interval grouping. The ITU-R MUF variability method of analysis was adopted for the measurements for easy comparison. The ratio, R, was obtained for a particular station, using equation 5.1, and classified according to solar activity, season, local time 4-hour interval of the day, and the upper and lower deciles were determined for each 4-hour local time interval grouping for each of the stations shown in table 1 and compared with the ITU-R reference values.

5.3 Results

First, the observed and ITU-R lower and upper deciles were plotted against the local time grouping for the different seasons, as shown in figures 5.2, 5.3 and 5.4 for low, moderate and high solar activity, respectively. The summer MUF diurnal variability, represented by lower and upper decile values, obtained in a manner described in section 5.2, is mostly within ± 0.2 while the

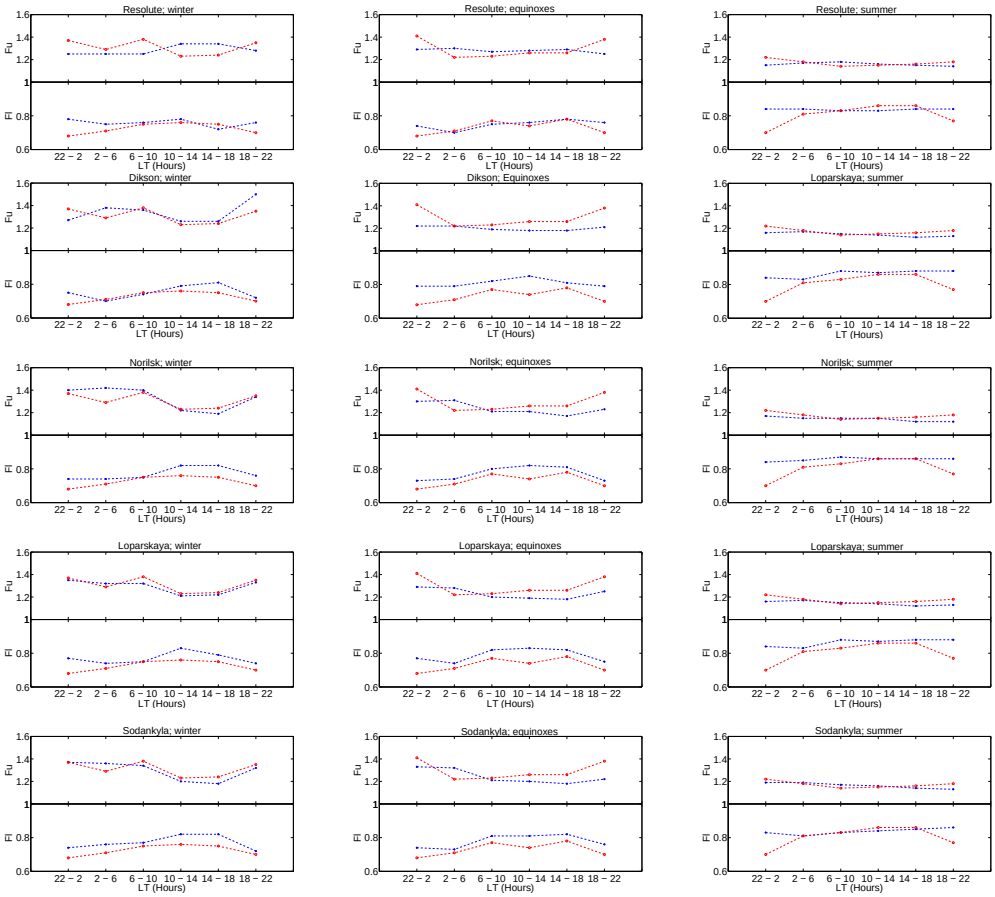

Figure 5.2: Upper (Fu) and Lower (Fl) decile factors for observations at the respective stations (blue) and ITU-R estimates (red) for the R12 $<$ 50 solar activity grouping.

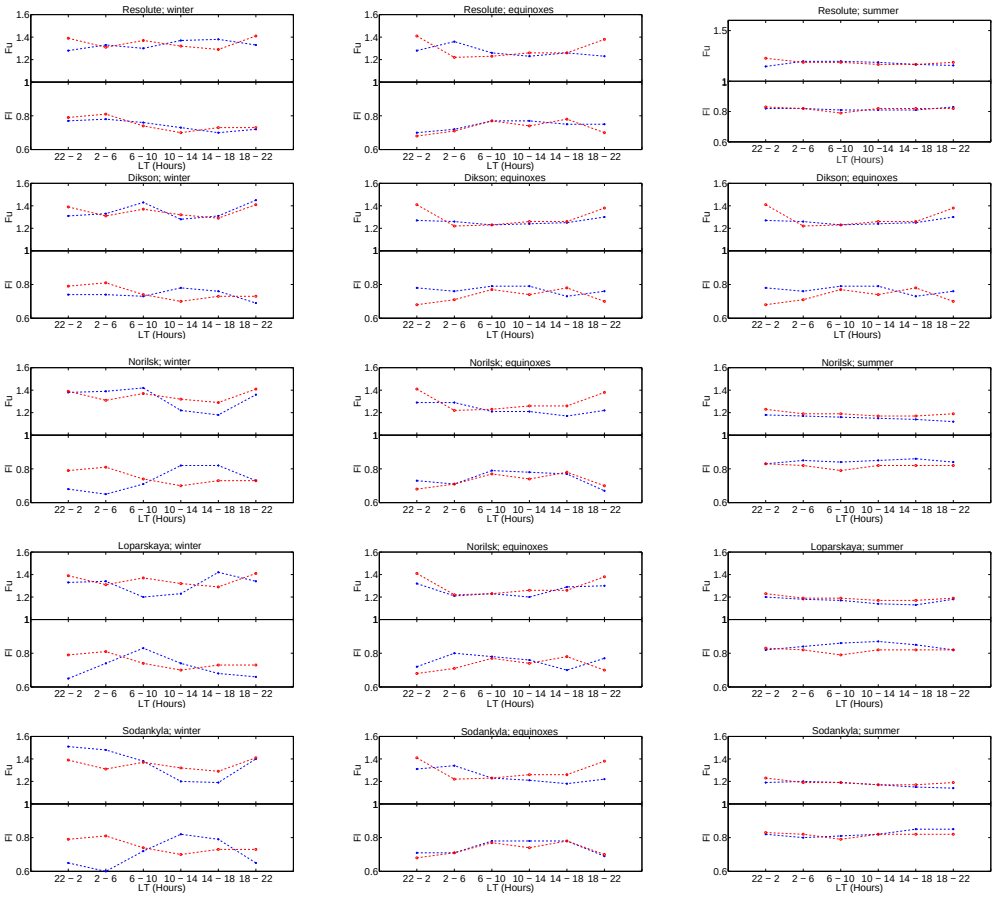

Figure 5.3: Upper (Fu) and Lower (Fl) decile factors for observations at the respective stations (blue) and ITU-R estimates (red) for the $50 < R12 < 100$ solar activity grouping.

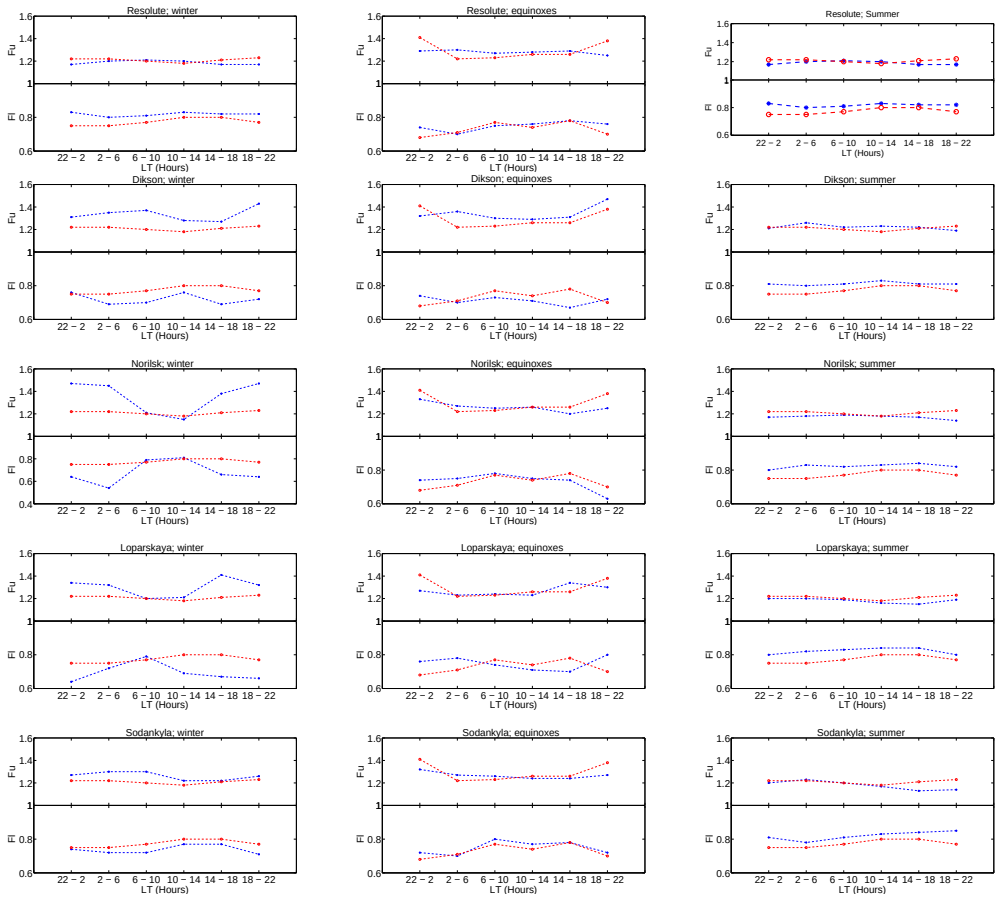

Figure 5.4: Upper (Fu) and Lower (Fl) decile factors for observations at the respective stations (blue) and ITU-R estimates (red) for the R12 > 100 solar activity grouping.

equinox variability lies in the range ±0.3 and in winter it is seen to be up to ±0.5, which indicates that the high latitude ionosphere, and thus the MUF is highly variable in winter, followed by the equinox and experiences a low variability in summer. This observation seems to directly translate into high differences between the observed and ITU-R decile factors in winter and the smaller values for summer, as shown in figures 5.5 to 5.7. The variability of MUF has been reported elsewhere to be between ±0.2 and ±0.3 or higher during high solar activity (Kouris *et al.*, 2000a). The decile factors obtained from measurements have been found to exhibit a diurnal trend that is not always reproduced by the ITU-R reference values. For example, the upper deciles are seen to be lower during the day and higher at night with a minimum around local noon, especially in winter. This observation is not always clear in the summer and equinoxes. A similar observation of the diurnal variation of the MUF variability factors was reported by Kouris *et al.* (2000a). Rishbeth and Mendillo (2001) suggested that the greater night time variability, particularly in winter, is partly associated with the lower electron density: (i) mainly due to magnetic activity of auroral origin which gets stronger and moves to lower latitudes at night, and (ii) partly due to the absense of strong photochemical control that is present in the daytime F2 layer.

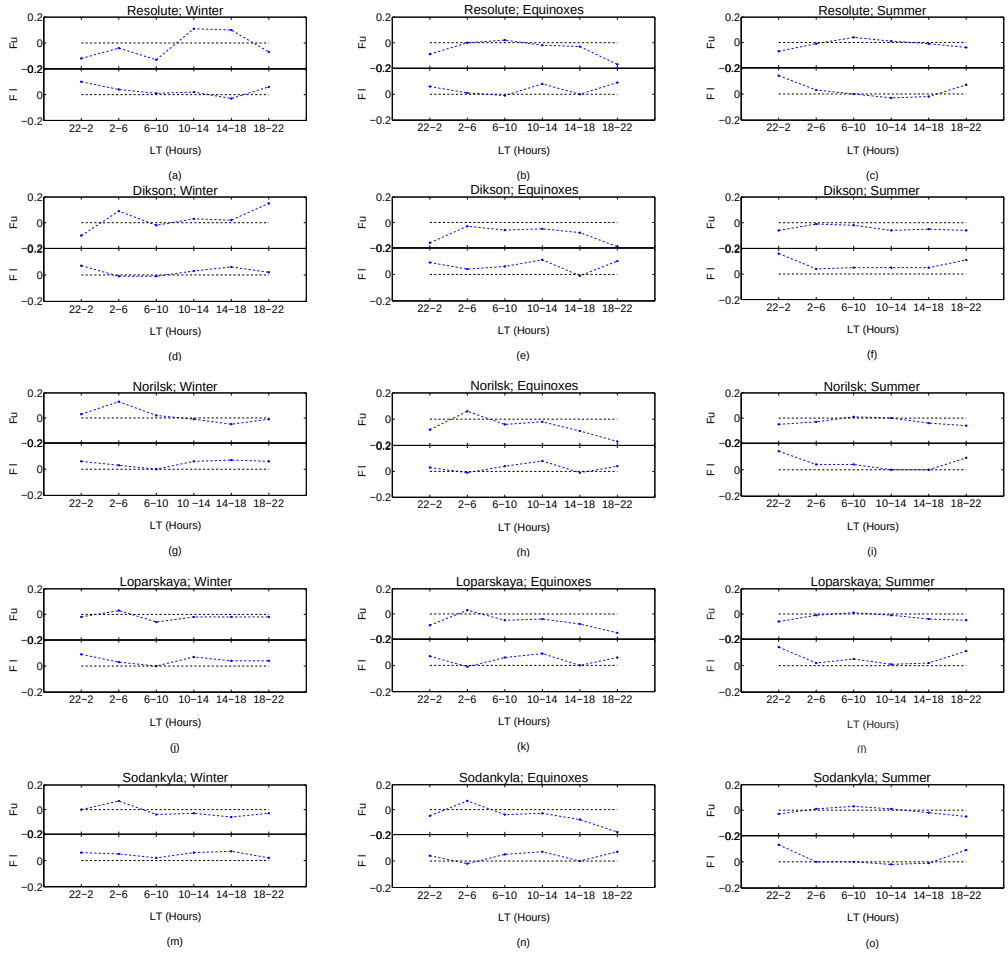

Figure 5.5: Differences between the observed and ITU-R decile factors, Fu (for upper deciles) and Fl (for lower deciles) for the R12 < 50 solar activity grouping. The black (at zero) line indicates Fu and Fl if the measured and ITU-R values were the same.

Secondly, for better comparisons, the factors Fu and Fl were modified as,

$$F = F_{observed} - F_{ITU-R} \tag{5.2}$$

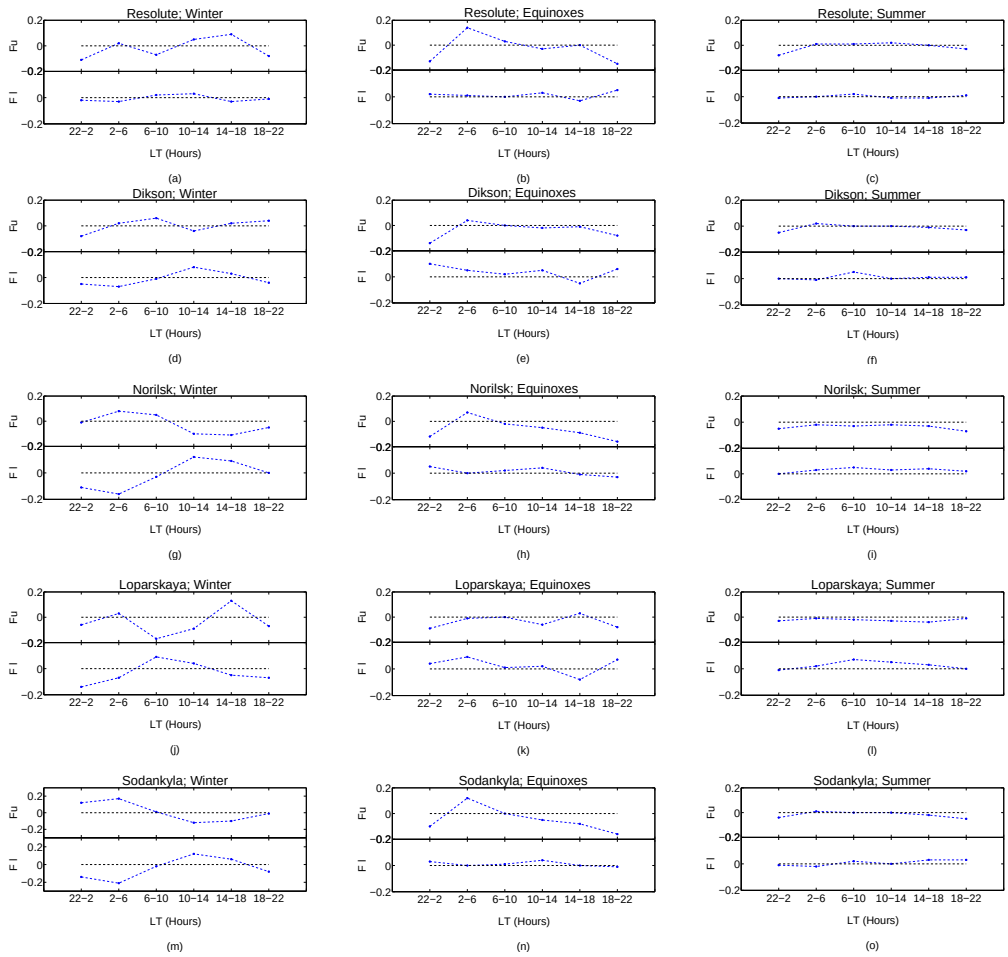

Figure 5.6: Differences between the observed and ITU-R decile factors, Fu (for upper deciles) and Fl (for lower deciles) for the $50 < R12 < 100$ solar activity grouping. The black (at zero) line indicates Fu and Fl if the measured and ITU-R values were the same.

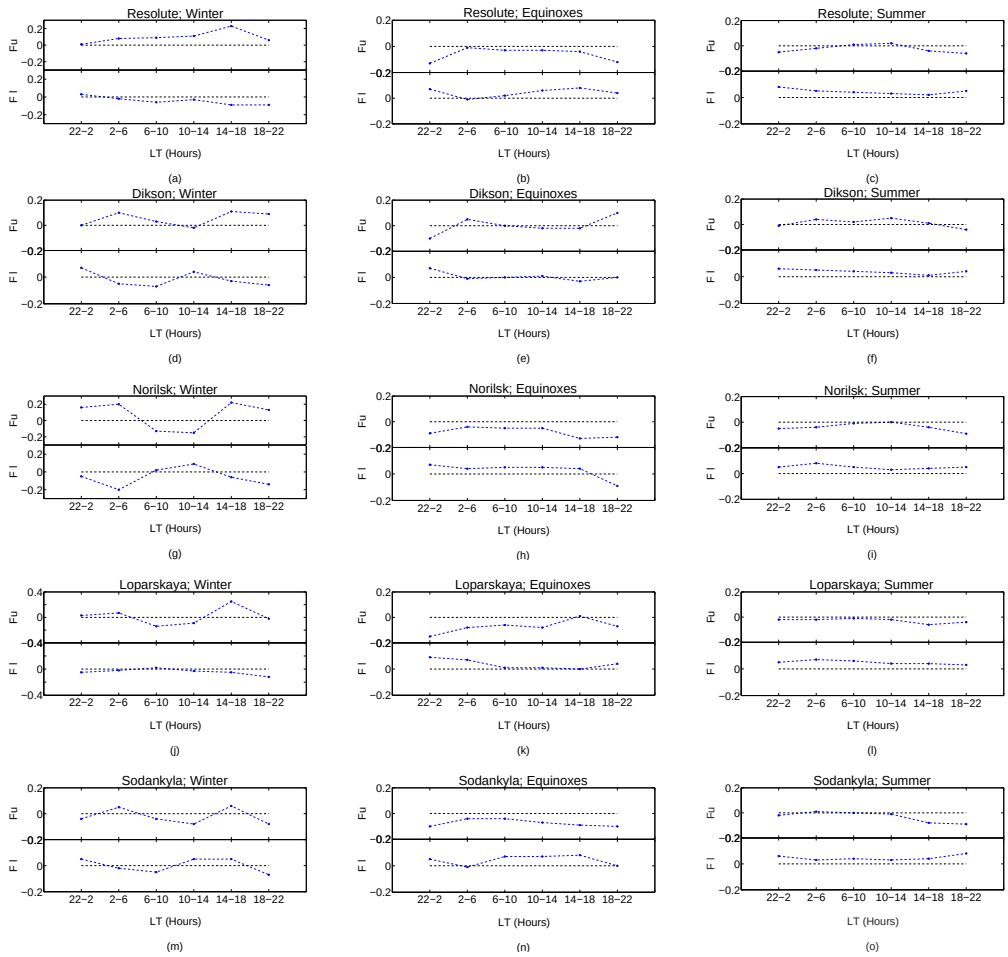

Figure 5.7: Differences between the observed and ITU-R decile factors, Fu (for upper deciles) and Fl (for lower deciles) for the R12 > 50 solar activity grouping. The black (at zero) line indicates Fu and Fl if the measured and ITU-R values were the same.

where F represents Fu and Fl, $F_{observed}$ corresponds to decile factors computed from measurements while F_{ITU-R} are ITU-R reference values. The modified Fu and Fl values calculated using equation 5.2 are presented in figures 5.5, 5.6 and 5.7 for low, moderate and high solar activity, respectively. The left (figures (a), (d), (g), (j) and (m)), middle (figures (b), (e), (h), (k) and (n)) and right (figures (c), (f), (i), (l) and (o)) panels illustrate results for winter, equinoxes and summer, respectively. The black line indicates the expected F (see equation 5.2) if the observed and ITU-R values were the same, below and above this line indicates an over- and under-estimation of the variability factors by the ITU-R reference values, respectively. A close look at figures 5.5(c), (f), (i), (l), (o), figures 5.6(c), (f), (i), (l), (o), and figures 5.7(c), (f), (i), (l), (o) shows that the summer Fu and Fl values are smaller compared to the other seasons, implying that the ITU-R reference factors do not significantly deviate from the measurement-derived deciles during this season. However, the ITU-R underestimation of the summer lower decile factors during high solar activity is noticeable in figures 5.7(c), (f), (i), (l), (o). Figures 5.5(a), (d), (g), (j), (m), figures 5.6(a), (d), (g), (j), (m), and figures 5.7(a), (d), (g), (j), (m) illustrate notable differences between the measurement-derived and ITU-R deciles, demonstrated by higher Fu and Fl values observed during the winter. The differences between observations and ITU-R decile factors during the equinoxes, shown figures 5.5(b), (e), (h), (k), (n), figures 5.6(b), (e), (h), (k), (n), and figures 5.7(b), (e), (h), (k), (n) are also noticeable. The high winter differences during moderate and high solar

activity are even more evident for stations outside the American longitudinal sector.

5.4 Discussion and Conclusion

Results for the comparison of the ITU-R MUF variability estimates with values computed from measurements have been reported. The analysis has been performed for several years (in the period of 1961 - 2013) of data covering three solar cycles at five stations in the arctic region. The summer MUF variability has been found to lie in the range of ± 0.2 while the limits for winter and equinox seasons are ± 0.5 and ± 0.3, respectively. The differences between measurement-derived and ITU-R factors (Fu and Fl) have been found to be smaller in summer compared to other seasons. This could partly be due to the low summer MUF variability at the high latitudes that has been reported by researchers (Araujo-Pradere *et al.*, 2005; Athieno *et al.*, 2015). The lower summer variability has been attributed to the exposure of the ionosphere to longer periods of solar radiation with slight changes in the intensity associated with varying solar elevation angles. Araujo-Pradere *et al.* (2005) attributed the lower summer variability to the greater chemical control and the longer daylight hours. The ITU-R underestimation of the summer lower decile factors during high solar activity is probably because the increased combined effect of solar and magnetic activity, the two key drivers of ionospheric variability, is underrepresented by the ITU-R reference figures. Significant over- and under-estimations have been observed in the winter, followed by the equinoxes. This could be linked to the vulnerability of the high latitude ionosphere to the dynamics of the magnetosphere and the

changes in the solar wind flow (Cannon, 1989; Hunsucker and Hargreaves, 2003; MacDougall and Jayachandran, 2007). Known effects of such dynamics include electron density enhancements described in section 2.2 as patches and blobs, known to occur any time of the year, with a higher and lower frequency in the winter and summer respectively. Their occurrence in summer is suppressed by the large electron densities produced by photoionisation in the sunlit ionosphere (Rodger and Graham, 1996; Hunsucker and Hargreaves, 2003; Carlson, 2012). The intensity of the enhancements, despite the fact that they are mostly observed during the winter night, can be compared to a daylit ionosphere at the mid-latitudes (Rodger and Graham, 1996; Coley and Heelis, 1998; Cannon, 1989; Hunsucker and Hargreaves, 2003; Carlson, 2012; Burston *et al.*, 2014). Precipitation of low energy electrons is an additional source of electron density enhancements in the auroral oval, towards the pole reaching the polar cap. The higher, high, and low variability and differences (Fu and Fl) observed during the winter, equinox and summer, respectively agree with the seasonal occurrence of these enhancements, which could suggest that the electron density enhancements have a significant impact on the variability of the high latitude ionosphere. All these factors collectively affect the high latitude MUF variability in a way that cannot easily be reproduced by statistical models in addition to the fact that they were developed with less data from the high latitudes. The high winter differences during moderate and high solar activity for stations outside the American longitudinal sector is expected given that the ITU-R decile factors were processed from

data obtained from stations in the American sector.

The ITU-R variability factors were established to mitigate the problems encountered in scheduling and managing radio frequencies on High frequency circuits (Wilkinson, 2004). Previous studies have noted some shortcomings of the ITU-R factors, for instance, the ITU-R reference values were derived basing on latitude dependence, and longitude effects found by Fotiadis *et al.* (2004) were ignored. It has also been noted that the ITU-R latitude groupings could be big enough to miss some effects of latitudinal dependence of the diurnal variabilities (Bradley *et al.*, 2004). In spite of the limitations mentioned above, the absence of an alternative global day-to-day variability statistical model qualifies the ITU-R model as a baseline model describing ionospheric variability. The aim of this work is to investigate the accurancy of the ITU-R MUF variability factors in the arctic region, as a starting point towards the establishment of a regional ionospheric variability statistical model using all available data sources including new data provided by CHAIN.

Chapter 6

A Neural Network based foF2 model for a single station in the polar cap

6.1 Introduction

The importance of foF2 in HF communication studies and applications has been a driving force in the development of various ionospheric and HF propagation models, examples of which have been mentioned in sections 2.4 and 2.5. The development and improvement of these models has recently recieved more attention due to the advancement in data acquisition and analysis techniques, as well as the installation of more ground- and space-based instruments for carrying out ionospheric research. For instance, empirical models

have been developed to predict the behaviour of foF2 over different timescales using various approaches including the nonlinear least square, Neural Network and AdaBoost techniques (Kumluca *et al.*, 1999; Yue *et al.*, 2006; Liu *et al.*, 2008; Zhang *et al.*, 2010; Hoque and Jakowski, 2012; Zhao *et al.*, 2014). Particularly, the NN approach, described in section 3.2, has proven to be a promising tool in modeling of ionospheric characteristics and solar wind effects on the magnetosphere as well as solving forecast problems in different geophysical applications, such as long term forecast of solar and geomagnetic indices and geomagnetic storm predictions (Williscroft and Poole, 1996; Lamming and Cander, 1999; Barkhatov *et al.*, 2000, 2001; Oyeyemi *et al.*, 2006). The NN technique has also been used in other applications such as image processing and recognition, system identification, financial forecasting, and adaptive filtering (Lundstedt and Wintoft, 1994; Gleisner *et al.*, 1996). Numerous global, regional and single station NN-based foF2 models have been developed with remarkable success except for the polar cap region, which has had an "almost inherent" challenge of data paucity in addition to the already well-documented dynamic nature of its ionosphere (Xenos, 2002; Mckinnell and Poole, 2004; Barkhatov *et al.*, 2005; Oyeyemi *et al.*, 2006; Yue *et al.*, 2006; Oyeyemi *et al.*, 2007; McKinnell and Friedrich, 2007; McKinnell and Oyeyemi, 2010; Oronsaye *et al.*, 2014). For example, a near-real time global NN foF2 model was developed by Oyeyemi *et al.* (2006), using hourly daily values of foF2 obtained from 26 worldwide ionosonde stations. McKinnell and Oyeyemi (2010) also developed a NN foF2 model for the equatorial re-

gion as a suitable replacement for the URSI and CCIR model options, used in the IRI model for NmF2. McKinnell and Friedrich (2007) applied the NN to model the lower ionosphere in the auroral zone. NNs have also been applied to improve model predictions at single stations (Williscroft and Poole, 1996; Xenos, 2002; Mckinnell and Poole, 2004). All the models developed are compared with the IRI as the baseline empirical ionospheric model. In fact, most of the available empirical models have been developed with an aim to improve on the IRI model predictions of the various ionospheric parameters. Inspite of such tireless efforts, recent studies by Themens *et al.* (2014); Themens and Jayachandran (2016) still show persistent limitations of the IRI at high latitudes especially in the polar cap. Previous research has also emphasized the disadvantage of data scarcity to the exploration of the polar ionosphere especially in the empirical modelling and prediction of important HF and ionospheric parameters (Oyeyemi and McKinnell, 2008; Themens *et al.*, 2014; Athieno *et al.*, 2015). CHAIN has made a tremendous improvement in data availability especially in the high arctic which includes the polar cap region. With the persistent limitations of the IRI at high latitudes and an improvement in data availability, it is necessary to develop alternatives to the IRI for the polar regions. This study attempts to empirically model foF2 at a single station located in the polar cap using both historical and new data obtained from SPIDR and CHAIN, respectively.

6.2 Data analysis

The foF2 data for Resolute (see figure 4.1), was used in this study, and was obtained from SPIDR (SPIDR-foF2) for the period between 1975 and 1995, the earliest date was dictated by the availability of the polar cap index data, while the CADI data (CADI-foF2) ranged between 2009 and 2013. SPIDR and CADI have been briefly described in Chapter 1 and Section 3.1. A Neural Network based foF2 model for the Resolute station was developed using this data. SPIDR-foF2 and CADI-foF2 values were used to train and evaluate the ability of the NN to predict foF2, respectively. The NN prediction results (NN-foF2) were compared with foF2 values obtained from the IRI model (IRI-foF2).

As pointed out in Section 3.2, the suitable choice of the network inputs also plays a vital role in the ability for the network to learn and generalise a given relationship between the inputs and the target. In this study, parameters with a known significant impact on foF2 were used as inputs. The diurnal, seasonal, solar and magnetic activity dependence of the ionosphere, specifically the F2 region, is well documented (e.g. Rishbeth and Garriot, 1969; Davies, 1989; McNamara, 1990; Baumjohann and Treumann, 1997; Hunsucker and Hargreaves, 2003; Saha, 2008). The existence of the F2 layer is directly influenced by the effect of solar extreme ultra violet (EUV) radiation and X-ray flux. The complex structure of the F2 layer is also influenced by the processes of photoionisation, recombination, and transport of plasma

from lower latitudes (Rishbeth and Garriot, 1969; McNamara, 1990; Forbes *et al.*, 2000; Hunsucker and Hargreaves, 2003; Carlson, 2012). The diurnal and seasonal dependence of foF2 is represented by the universal time (00h00 - 23h00) and day of the year (1 - 365), respectively. To ensure continuity from day 1 to 365 and 00h00 to 23h00, the two inputs are split into their cyclic components (Williscroft and Poole, 1996):

$$HOD1 = sin\left(\frac{2\pi \times HOD}{24}\right) \qquad HOD2 = cos\left(\frac{2\pi \times HOD}{24}\right) \tag{6.1}$$

$$DOY1 = sin\left(\frac{2\pi \times DOY}{365.25}\right) \qquad DOY2 = cos\left(\frac{2\pi \times DOY}{365.25}\right) \tag{6.2}$$

The acronyms DOY and HOD represent day of year and hour of day, respectively. The significant dependence of foF2 on solar, magnetic, and seasonal variations has been well established in previous studies (e.g. Williscroft and Poole, 1996; Bilitza, 2000; Richards, 2001; Sethi *et al.*, 2002; Mendillo *et al.*, 2002). The solar dependence has been represented by the F10.7 cm solar flux. The solar flux data was obtained from SPIDR but it is originally obtained from observations made at the Dominion Radio Astrophysical Observatory near Pentictin, British Columbia, Canada. Details of how the F10.7 cm solar radio flux is processed can be found in Tapping (2013). Previous work on NN based ionospheric studies used the 1-day (A1) and 2-day (A2) running means of the 3-hour planetary magnetic index (A_p) in modeling Total Electron Content (TEC) and foF2, respectively (e.g. Williscroft and Poole, 1996; Habarulema *et al.*, 2007). The NN in this work was trained using

each of the two indices, in addition to the inputs shown in figure 6.1(top), and A1 was found to be optimum with a mean square error, MSE (the performance index given by equation 3.10) of 0.0103 MHz compared to 0.0108 MHz obtained by using A2. A1 was then replaced by the Dst index, and retraining the network yielded a MSE of 0.0114 MHz compared to 0.0103 MHz obtained with A1. Hence, the 1-day running mean of the 3-hour planetary magnetic index and the polar cap index have been used to represent the geomagnetic activity dependence of foF2. The Ap indices were obtained from http://wdc.kugi.kyoto-u.ac.jp/. The polar cap index data is processed and provided by the Danish Space Research Institute (Stauning, 2013). It was found that adding more inputs to the network, shown in figure 6.1(top), yielded very slight decrements in the MSE but did not necessarily make a significant change to the performance of the model. For instance, adding the solar zenith angle yielded a MSE of 0.0102 MHz. The other inputs that were used in the process of finding the optimum inputs include the Auroral Electrojet (AE) index and the 28-day running mean of sunspot number (R28). It should be noted that a suitable NN is one that can approximate an underlying problem with the least number of network parameters.

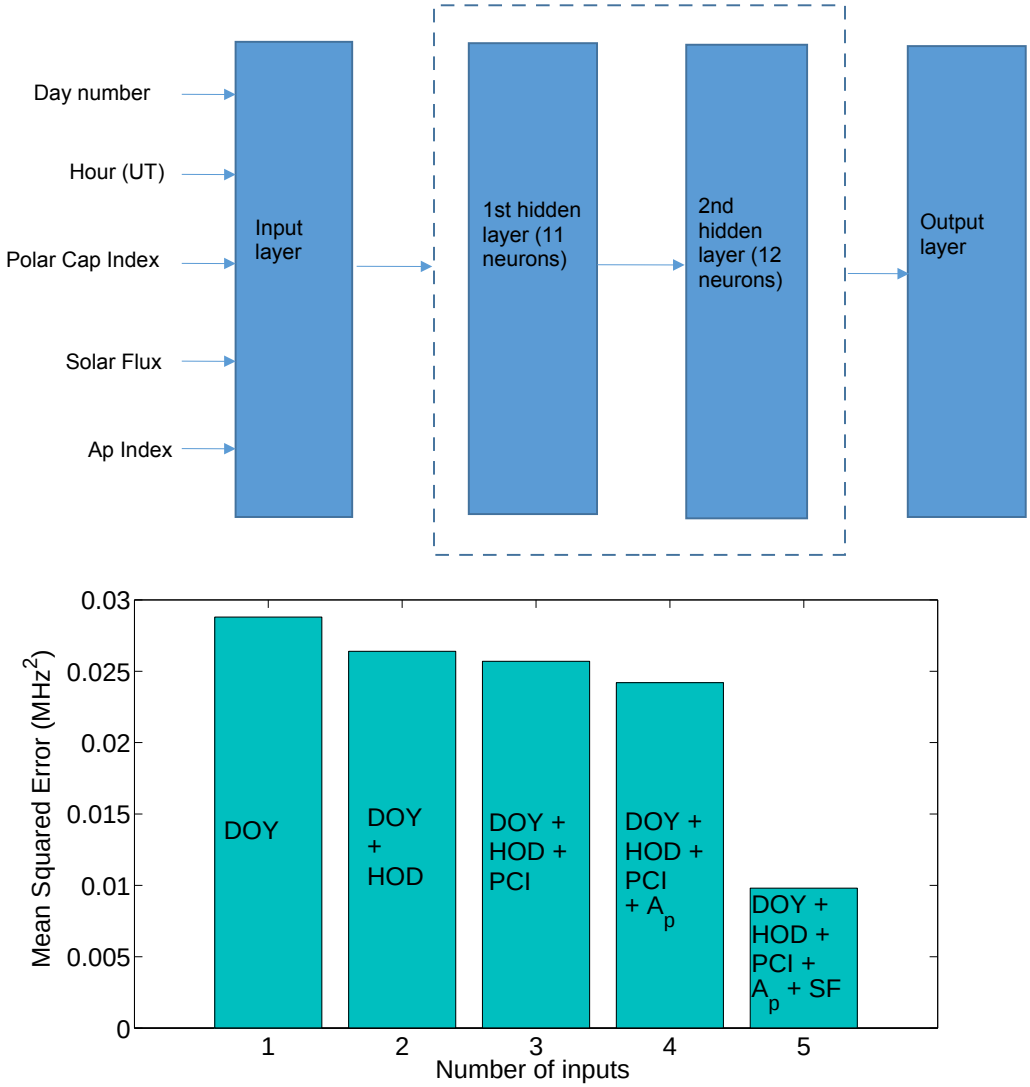

Figure 6.1: Neural Network architecture used in this study (top) and a bar graph showing the contribution of the input parameters to the NN-foF2 model (bottom).

The architecture used in the NN is shown in figure 6.1(top). The NN consists of one input, two hidden, and one output layer(s). The input layer consists of the input parameters: Day number, Universal Time, Polar cap index, Ap

index and the F10.7 cm solar flux, the two hidden layers consist of 11 and 12 neurons, respectively, while the network output is NN-foF2. The contribution of each of the inputs to the NN model is given in figure 6.1(bottom). The acronyms PCI, A_p, and SF represent polar cap index, A_p magnetic index and F10.7 cm solar flux, respectively. The MSE is plotted for the respective combination of inputs. This figure illustrates that each addition of an input parameter reduces the MSE, by some value which implies that each of the inputs has an effect on the foF2 prediction. Note that different combinations of inputs were used during the training and only the optimum input parameters have been listed.

6.3 Results and Discussion

6.3.1 Day-to-day variations

The day-to-day variations of the observed foF2 and model predictions are shown in this section. NN-foF2 and IRI-foF2 have been compared with CADI-foF2 values for a period ranging from 2009 to 2013. The comparison of the NN daily predictions with the IRI monthly median model is justified by the fact that the output of the former is an average that can be obtained by a set of input vectors (Oyeyemi and McKinnell, 2008). The NN-foF2 (red), IRI-foF2 (black) and CADI-foF2 (blue) hourly values for randomly selected days are plotted in figure 6.2 for low (2009 and 2010) and moderate (2012

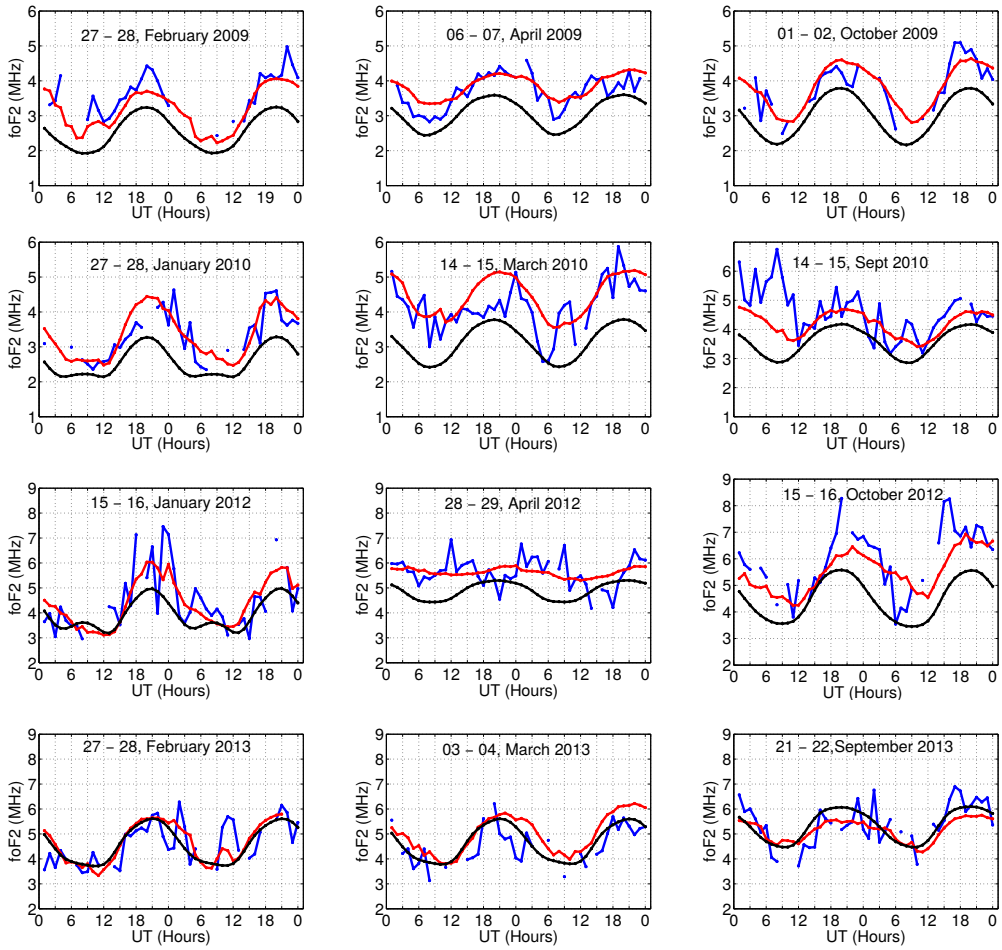

Figure 6.2: Hourly foF2 values for CADI observations at Resolute (blue) and predicted values: NN (red) and IRI (black) for selected days in the period of 2009 - 2013.

and 2013) solar activity. The NN and IRI models are able to reproduce the expected diurnal variation of foF2: a gradual increment from morning up to a maximum around local noon and a decrement towards midnight (local time at Resolute is UT - 6). During low solar activity (2009 - 2010), the IRI tends to underestimate foF2, while the NN seems to show a good agreement with the observations.

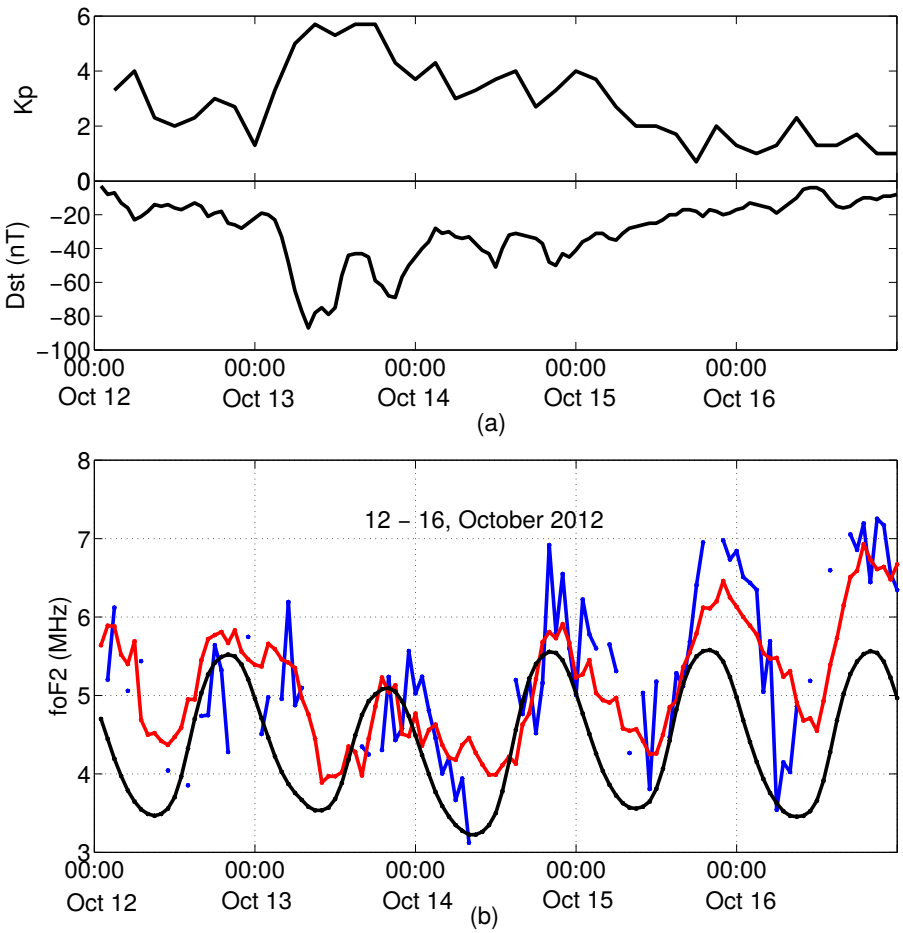

Figure 6.3: K_p and D_{st} values for the period of 12 - 16 October 2012 (a). Hourly foF2 from CADI at Resolute (blue) and predicted values: NN (red) and IRI (black) for the same period (b).

A comparison of CADI-foF2, NN-foF2 and IRI-foF2 from 12-16 October 2012, one of the storm periods with available CADI data, is shown in figure 6.3. It includes both quiet and disturbed days with minor storms that occurred between 13 - 14 October 2012 with a maximum K_p and D_{st} of 5.7 and -90 nT, respectively, as seen in figure 6.3(a). It is important to note

that the ionograms in the polar cap on disturbed days are hard to hand-scale due to strong absorption and enhancement of the E-layer. It is clear from figure 6.3(b) that the NN-foF2 values have a good agreement with the CADI-foF2 during this period compared to IRI-foF2. The missing CADI-foF2 data on 13 October does not permit the model performance analysis during the onset of the first storm but the NN model seems to represent the observations in the CADI-foF2 during the recovery phase of the first 13 October storm and also during both phases of the proceeding storms that occured 13 - 14 October 2012.

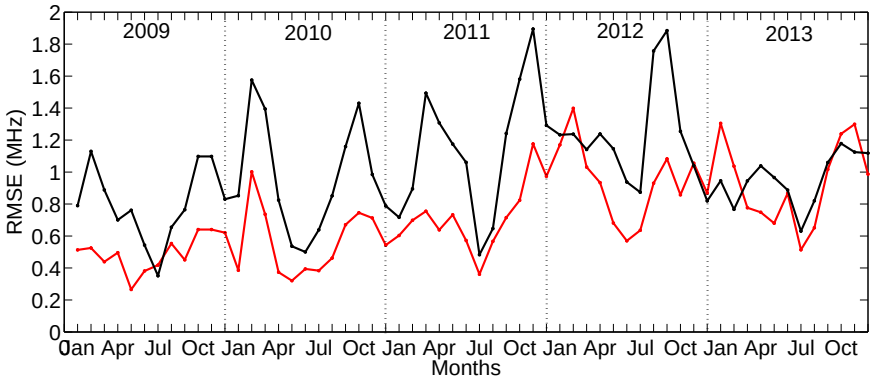

Figure 6.4: RMSE between CADI-foF2 and NN-foF2 (red), and IRI-foF2 (black) for each month in the period 2009 - 2013.

Evaluation of the model performance has been done using the RMSE approach, using equation 4.1, RMSE were computed between the CADI-foF2 and model predictions for 2009 - 2013. The results are shown in figure 6.4. RMSE values are seen to increase with solar activity with lowest values observed in summer, possibly due to the low summer variability of the ionosphere manifested in the ionospheric parameters such as foF2 and MUF(3000)F2 seen in sections 4.3 and 5.3. Based on the RMSE values, the performance of the NN model seems to be better than that for the IRI from 2009 to 2011 and the summers of 2012 and 2013. The IRI model shows an improvement in its predictions as solar activity increases especially during the winter. The high RMSE values generated by the IRI model comparison with the CADI-foF2 is also noticeable during the equinoxes of 2009 - 2012, indicative of its failure to reproduce the equinox enhancements in foF2 observed in CADI-foF2.

A comparison of the seasonal variation of NN-foF2 and IRI-foF2 with CADI-

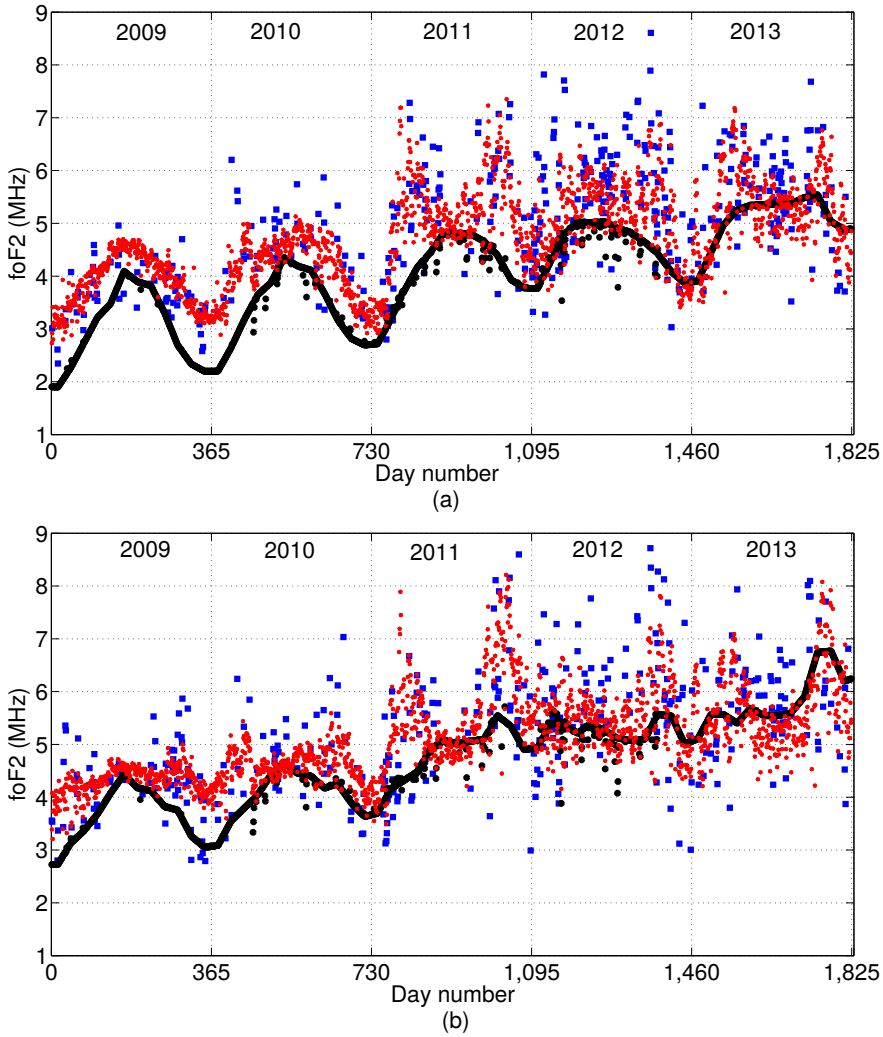

Figure 6.5: Seasonal variations of CADI-foF2 (blue), NN-foF2 (red) and IRI-foF2 (black): at 01h00 (a) and 19h00 (b) UT.

foF2 at 01h00 UT (19h00 LT) and 19h00 UT (13h00 LT) for analysed period (2009 - 2013) is illustrated in figure 6.5. These two hours were chosen because they have more CADI-foF2 data to fairly represent the seasonal variation in foF2. Looking at figure 6.5(a): The models are able to successfully predict the seasonal variation of foF2 at 01h00 UT. There is also a noticeable underestimation of the foF2 values by the IRI model during low solar activity (2009 - 2010) and the equinoxes during moderate solar activity (2011 - 2013). While the NN model seems to fit the CADI-foF2 across the entire analysed period and interestingly reproduces the foF2 enhancements observed in the CADI-foF2. From figure 6.5(b): The IRI shows an improvement in the estimation of foF2 during low solar activity but still fails to reproduce the equinox enhancements in foF2 during moderate solar activity. This could be an explanation for the high IRI RMSE during the equinoxes shown in figure 6.4. The NN model attempts to reproduce the scatter in the observed foF2 compared to IRI, which could be an indication of the ability of the NN model to predict the foF2 seasonal variability observed in CADI-foF2.

6.3.2 Monthly median foF2

The monthly median foF2 variations were also analysed using the model predictions and CADI-foF2 values. The CADI-foF2 (blue), NN-foF2 (red) and IRI-foF2 (black) monthly median values have been plotted from 2009 - 2013 (figure 6.6(a)). The general trend of foF2 increasing and decreasing towards the summer and winter, respectively is demonstrated by both observed and

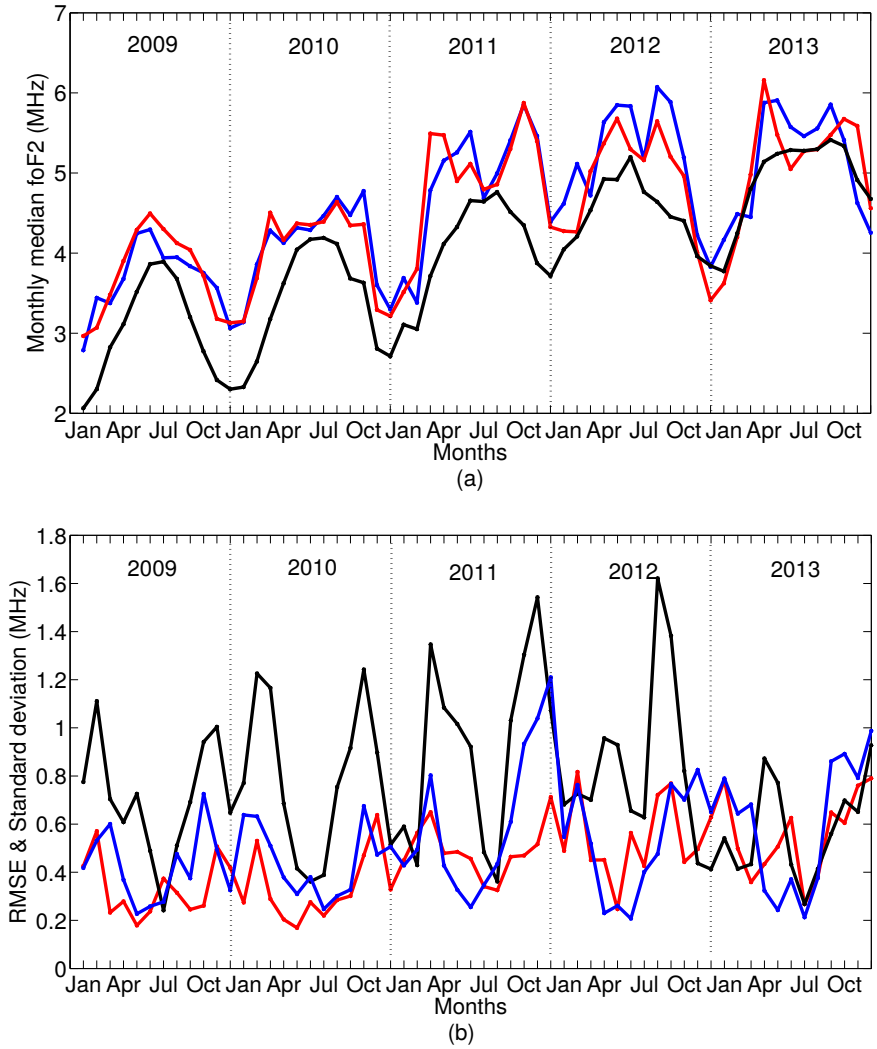

Figure 6.6: Monthly median CADI-foF2 (blue), NN-foF2 (red) and IRI-foF2 (black) values for each month in 2009 - 2013 (a). RMSE between CADI-foF2 and NN-foF2 (red), CADI-foF2 and IRI-foF2 (black) and the standard deviation in CADI-foF2 (blue dashed) (b).

modeled foF2. The increment in foF2 with solar activity is also noticeable in this figure. However, the IRI-foF2 is seen to underestimate the monthly median foF2 during low solar activity, especially during winter and equinoxes. The NN-foF2 shows an improvement in the monthly median predictions especially during low solar activity. Figure 6.6(b) illustrates RMSE computed between NN-foF2 (red), IRI-foF2 (black) and CADI-foF2, and plotted with the standard deviations in the CADI-foF2 (blue). While there are cases of NN-RMSE being higher than the standard deviation, its performance is still seen to be better than that of IRI especially during low solar activity and the summers of 2012 and 2013. Figure 6.7 demonstrates a comparison between diurnal variability of the monthly median CADI-foF2, NN-foF2 and IRI-foF2. The IRI tends to underestimate the nighttime monthly median foF2 observed in CADI-foF2 during low solar activity compared to the NN model. The NN model seems to reproduce the foF2 daytime enhancements seen in CADI-foF2 in the equinoxes of 2011 and 2012, while the IRI shows an underestimation. In 2013, both models seem to reproduce the foF2 daytime enhancements during the equinoxes except that they demonstrate a seasonal phase shift in which the enhancements seem to appear about a month later (also see figure 6.6(a)). Similar observations in the CADI and IRI monthly median F2 layer peak electron density (NmF2) enhancements were reported by Themens *et al.* (2014), a result they attributed to the significant role of transport processes in the high latitude F region dynamics. On the whole, the NN model seems to show an improvement in modeling the monthly median

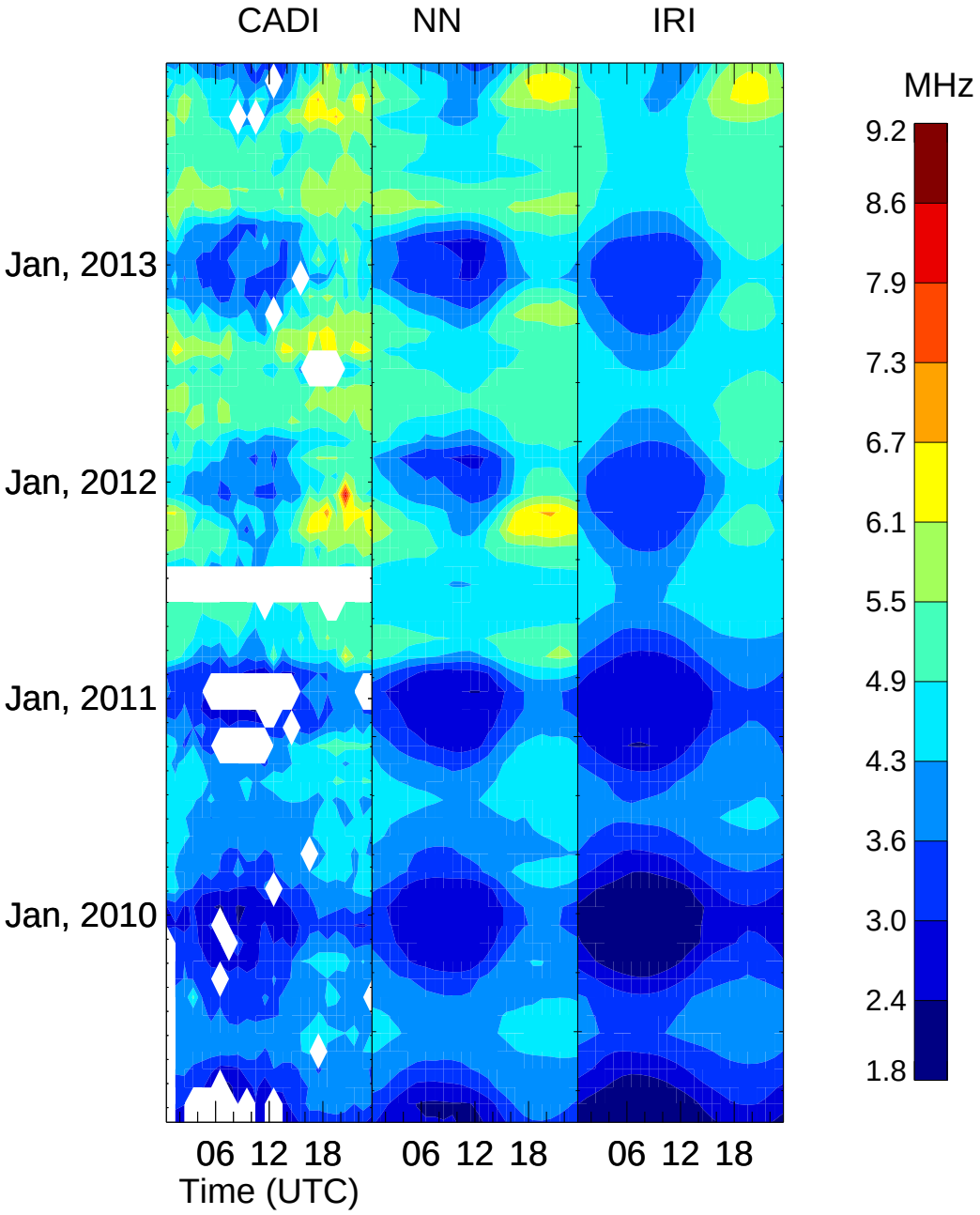

Figure 6.7: A contour plot of monthly median diurnal variation for CADI-foF2 (left), NNN-foF2 (middle) and IRI-foF2 (right) between 2009 and 2013.

foF2 compared to the IRI. The correlations, slopes and y-intercepts of the fit

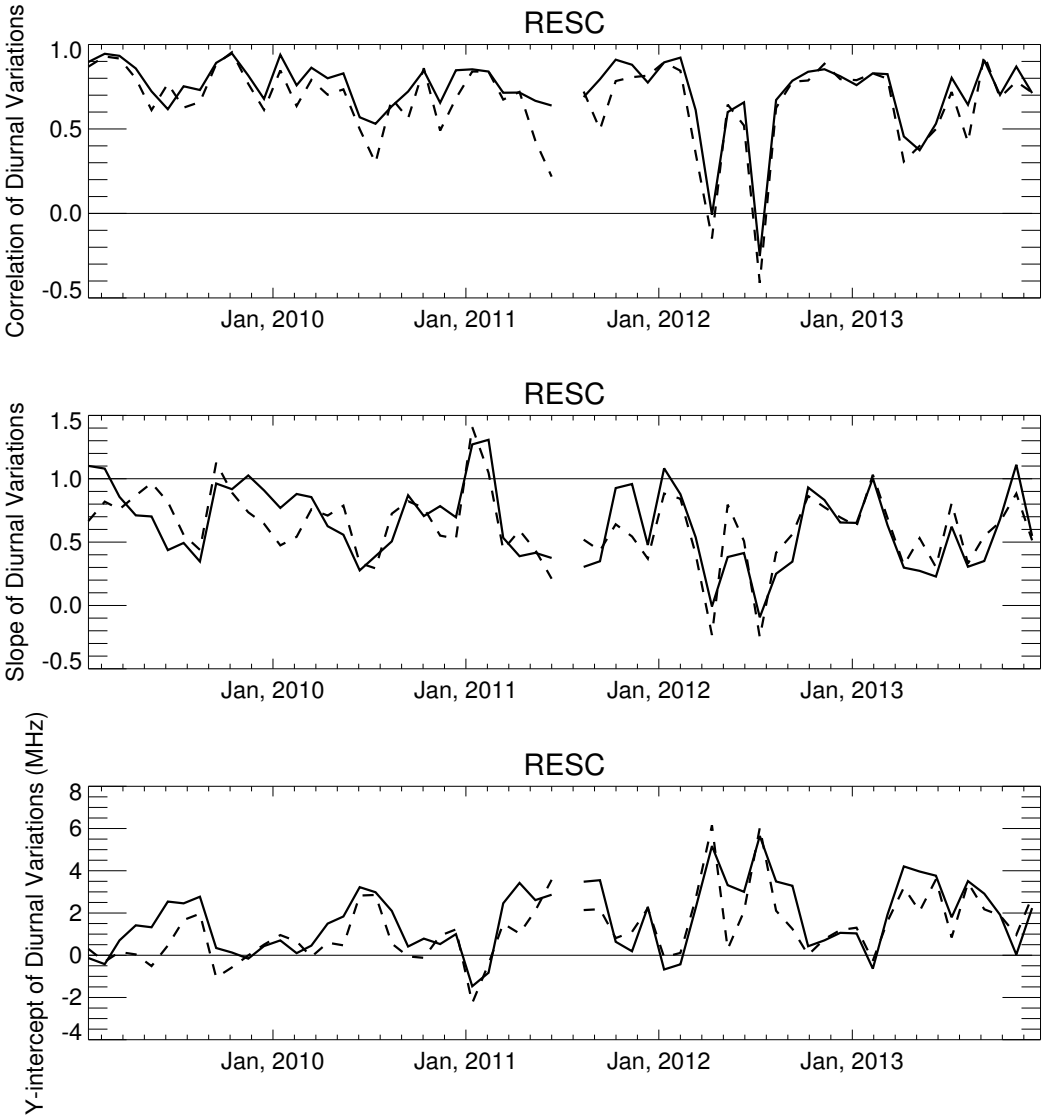

Figure 6.8: Correlations (top panel), slopes (middle panel) and y-intercept (bottom panel) between the NN (solid line) and IRI (dashed line) model monthly medians with observations.

between modeled and observed monthly median foF2 diurnal variability are

shown in Figure 6.8. A close look at figure 6.8(top) shows that the NN model seems to outperform the IRI in terms of correlation to the observations especially during low solar activity. Both models show poor correlation in May 2012 and July 2012. There was limited hourly CADI-foF2 data during this period, in most cases the monthly median was computed using two or three data points, which to a greater extent, could have contributed to the very poor correlation seen in the models. However, Themens and Jayachandran (2016) also reported the sharp decrease (with latitude and solar activity) in the Pearson correlation coefficients for the monthly diurnal variation fits between GPS (Global Positioning System) and IRI vTEC (vertical Total Electron Content) in the polar cap during summer periods, a result they attribute to the small magnitude of the summer diurnal variation, implying that even a small error can translate into significant differences. The slopes of diurnal variation are shown in figure 6.8(middle) where better performance is measured by the closeness of the values to unity. Below and above the reference line at unity is an indication of under- and over-estimation of diurnal variability, respectively. Themens and Jayachandran (2016) observed a progressively worse performance in the IRI TEC diurnal variability in winter and equinox periods in the polar cap. Similar results have been observed with the foF2 diurnal variability. The NN model shows an improvement over the IRI in the representation of the magnitude of diurnal variations during the winter months but seems to perform poorly during the summer. Both models seem to only underestimate the diurnal variability especially as solar

activity increases. The similarity could be due to the fact that the foF2 data used to train the NN model is a subset of that used in the IRI model. The y-intercept of the fit, an indication of the potential bias in the modeled data, is shown in figure 6.8(bottom). The NN model seems to perform better than the IRI model during the winter while the IRI shows a better performance during the summer.

6.4 Conclusion

A NN model has been developed for foF2 using data from SPIDR and CADI at Resolute (74.75° N, 265.00° E). The data obtained from SPIDR was used to train the network, and that from CADI was used to evaluate the ability of the NN model to predict foF2. The network was trained using the day of year, hour of day, polar cap index, A_p index, the F10.7 cm solar flux inputs and historical values of hourly foF2 for the period of 1975 - 1995. The NN model predictions (NN-foF2) were compared with foF2 values obtained from the IRI model (IRI-foF2) and CADI (CADI-foF2) for the period of 2009 - 2013.

NN-foF2 and IRI-foF2 demonstrate the expected diurnal and seasonal patterns, except the underestimation made by IRI during low solar activity, and its failure to represent foF2 daytime equinox enhancements observed in CADI-foF2. The NN model has been found to perform better than the IRI at representing the equinox enhancements seen in both the hourly and monthly median CADI-foF2. The enhancements in foF2 during the equinoxes could be as a result of the balance between transport and photoionisation effects as compared to the winter and summer that are almost entirely dependent on transport and photoionisation, respectively, for electron production. The NN also shows an improvement in the predictions of foF2 during disturbed periods compared to the IRI, demonstrated by a minor storm shown in the results. Based on the RMSE analysis, the NN model gives improved predictions

compared to the IRI model especially during low solar activity and the summers during high solar activity. The RMSE values are also seen to increase with solar activity with lowest values observed in summer. The increment of the errors with solar activity is probably due to an increase in solar and geomagnetic activity which translate into increased ionospheric variability, to a level that can not easily be matched by the model predictions, while low values in summer could just be due to the low foF2 variability owing to the exposure of the ionosphere to extensive periods of solar radiation. Analysis of the diurnal variation in the monthly median foF2 reveals an improvement in nighttime foF2 predictions by the NN compared to the IRI.

The results of the NN model presented in this paper are impressive, and could even get better if more data from Resolute and other stations is ingested into the model. The data from CHAIN is available but requires more time to manually scale especially for other CHAIN polar cap stations such as Eureka (79.99° N, 274.10° E) and Pond Inlet (72.69° N, 282.04° E) that do not have archived processed data on other data sites. Empirical modeling may not be the ultimate solution to all prediction and forecasting problems, but it offers an alternative approach to solving such problems compared to using analytical approaches that get complicated, trying to account for the diverse ionospheric processes that depend on numerous factors and parameters. The model presented in this work, is an interesting starting point towards developing an foF2 empirical model for the polar region and the high latitude in

general, a project that has always been limited by data paucity, in addition to the unique impact of the solar wind-magnetosphere-ionosphere coupling.

Chapter 7

Conclusions and Future work

7.1 Conclusions

Ionospheric radio propagation is preferred for long distance communication because of its associated low equipment cost and low power, as well as its ability to provide a world-wide coverage. However, using the ionosphere as a medium of communication is a challenge due to the fact that it varies under several conditions as described in Chapter 2. It is always good to hope for the best but even much better to prepare for the 'worst', in which case, HF propagation and ionospheric models were and still are being developed for forecasting and prediction purposes. For instance, as stated in section 2.5, HF prediction model development dates back to the 1930s. The previous models went through a series of updates and improvements as more ionospheric data became available, but up until the 21st century, the high

latitudes have always been faced with the challenge of data scarcity. With the improvement in data acquisition and analysis techniques, coupled with the installation of suitable instruments at the high latitudes, it has become necessary to test the performance of the available 'traditional' HF propagation models at these latitudes.

The comparison of HF propagation prediction models; VOACAP, ICEPAC and REC533 with observations at two stations in the polar cap has been presented in Chapter 4. The comparison has been done using MUF(3000)F2, obtained from observations at the Resolute and Pond Inlet CADIs as discussed in Chapters 2 and 3. The choice of the MUF(3000)F2 parameter is based on its vital role in radio communication in terms of circuit planning and frequency management. Predictions and observations showed diurnal and seasonal variations, except for the failure of VOACAP and ICEPAC to reproduce the diurnal variation trend observed in CADI measurements during summer. The statistical analysis of the performance of the models revealed that REC533 performs better in equinox months, while VOACAP does better for both equinox and summer and ICEPAC shows poor performance during low solar activity. It was also found that the models do not reproduce the hour-to-hour variability that is seen in the observations. The available models do not have specifications and or indices for ionospheric variability, which is important especially for short-time variations. The only currently available global variability factors are given by the ITU-R.

In Chapter 5, the MUF variability at high latitude stations was studied by statistically comparing observations with ITU-R factors. The study was aimed at investigating the accuracy of the ITU-R diurnal variability estimates as a first step towards establishing accurate and reliable ionospheric variability bounds. The bounds could be included in the available ionospheric and HF prediction models to improve on the variability of the predicted HF propagation and ionospheric characteristics. Resolute (74.75° N, 265.10° E), Dikson (73.50° N, 80.40° E), Norilsk (69.40° N, 88.10° E), Loparskaya (68.00° N, 33.00° E), and Sodankyla (67.40° N, 26.60° E), were chosen because they were the high latitude stations with observations spanning over 3 solar cycles. The study was done using the ITU-R method of analysis for easy comparison. The summer MUF(3000)F2 variability was found to lie in the range of ±0.2 whereas limits for equinox and winter seasons were ±0.3 and ±0.5, respectively. This observation directly translated into high differences between the measurement-derived and ITU-R decile values in winter and the smaller values for summer. These results illustrate that the high latitude ionosphere, and thus the MUF is highly variable in winter, followed by the equinox and experiences a low variability in summer.

Besides the variability specification, the ionospheric models used in the HF propagation prediction models are very important. A suitable ionospheric model implies that the forecasts and or predictions will, to a greater extent,

be able to reproduce the observations. As mentioned earlier, the IRI model is the available baseline ionospheric model against which all new models are compared. It has been updated and improved over the years. However, as discussed in Chapter 6, it still shows limitations at high latitudes, particularly the polar cap regions. With these limitations and improvements in data availability, this study has also attempted to empirically model foF2 at Resolute, a polar cap station, using neural networks. The foF2 data used was obtained from SPIDR and CADI at Resolute. The NN model predictions (NN-foF2) were compared with foF2 values obtained from the IRI model (IRI-foF2) and CADI (CADI-foF2) for the period of 2009 - 2013. The NN and IRI models were able to reproduce the diurnal variations observed in hourly CADI measurements. While the IRI underestimates the nighttime monthly median foF2 variation observed in CADI-foF2. The models are also able to demonstrate the seasonal variation in foF2, specifically the NN is able to reproduce the enhancements in the foF2 observed in CADI measurements during the equinoxes. IRI underestimates foF2 values in winter and the equinoxes during low solar activity. The NN model also shows an improvement in foF2 predictions during disturbed days. Root Mean Square Errors (RMSE) were computed between hourly and monthly median model predictions and observations. RMSE values seem to increase with solar activity, and are lowest in summer. On the whole, the NN model seems to perform better during low solar activity and the equinoxes. The IRI shows an improvement in its predictions as solar activity increases especially in

winter.

7.2 Future work

The improvement in data availability cannot be questioned, for example, CHAIN is a promising data resource especially for the 'data-troubled' polar cap region. However, as stated in Chapter 3, processing this data to a usable format, specifically for statistical studies is a huge task, which when tackled head-on, can be an asset to empirical modeling in the polar cap, and the high latitudes as a whole. The NN-based foF2 model presented in this can be applied to M(3000)F2 modeling, with the same inputs and corresponding historical M(3000)F2 values. Obtaining foF2 and M(3000)F2 will then allow a comparison of the NN-modeled MUF(3000)F2 with VOACAP, ICEPAC and REC533 predictions. The single models would then be modified to regional ones, particularly by using data obtained from CHAIN polar cap stations: Eureka (79.99° N, 274.10° E), Resolute (74.75° N, 265.00° E), Pond Inlet (72.69° N, 282.04° E), in addition to the historical data for Alert (82.50° N, 297.70° E) and Qaanaaq/ Thule (77.50° N, 290.80° E). This would eventually be upgraded to an NN-foF2 model for the high latitudes by including the auroral stations such as Cambridge Bay (69.12° N, 254.97° E), Hall Beach (68.78° N, 278.74° E) and Iqaluit (63.73° N, 2291.46° E), all of which are

CHAIN stations. The same data can be used to establish variability bounds in form of an index. The overall aim is to modify or replace the IRI, and obtain a reliable ionospheric model with a variability specification, which can be used in HF propagation models to improve on the observation-model comparison results discussed in chapter 4.

Bibliography

Altadill D., "Time/altitude electron density variability above Ebro. Spain", *Advances in Space Research*, **39**, pp. 962–969, 2007.

Anderson D.N., Mendillo M. and Herniter B., "A semi-empirical low-latitude ionospheric model", *Air Force surveys in geophysics*, 1985.

Appleton E.V. and Beynon W.J.G., "The application of ionospheric data to radio-communication problems: part I", *Proceedings of the Physical Society*, volume 52, pp. 518–533, 1940.

Araujo-Pradere E.A., Fuller-Rowell T.J., Codrescu M.V. and Bilitza D., "Characteristics of the ionospheric variability as a function of season, latitude, local time, and geomagnetic activity", *Radio Science*, **40**(RS5009), doi:10.1029/2004RS003179, 2005.

Athieno R., Jayachandran P.T., Themens D.R. and Danskin D.W., "Comparison of observed and predicted MUF(3000)F2 in the polar cap region", *Radio Science*, **50**(6), pp. 509–517, doi:10.1002/2015RS005725, 2015.

Barkhatov N.A., Bellustin N.S., Levitin A.E. and Sakharov S.Y., "Comparison of efficiency of artificial Neural Networks for forecasting the geomagnetic activity index DST", *Radiophysics and Quantum Electronics*, **43**(5), 2000.

Barkhatov N.A., Korolev A.V., Ponomarev S.M. and Sakharov S.Y., "Long-term forecasting of solar activity indices using Neural Networks", *Radiophysics and Quantum Electronics*, **44**(9), 2001.

Barkhatov N.A., Revunov S.E. and Uryadov V.P., "Artificial Neural Network technique for predicting the critical frequency of the ionospheric F2 layer", *Radiophysics and Quantum Electronics*, **48**(1), 2005.

Baumjohann W. and Treumann R.A., *Basic Space Plasma Physics*, Imperial College Press, 1997.

Bent R.B., Llewellyn S.K., Nesterczuk G. and Schmid P.E., "The development of a highly-successful world-wide empirical ionospheric model and its use in certain aspects of space communications and world-wide total electron content investigations", *Effect of the Ionosphere on Space Systems and Communication*, pp. 23–28, Arlington, VA, 1975.

Bilitza D., "Solar-Terrestrial Models and Software Application", National Space Science Data Center/ World Data center A for Rockets and Satellites, 1990.

Bilitza D., "The importance of EUV indices for the International Reference Ionosphere", *Physics and Chemistry of the Earth*, **Part C**(25), pp. 515–521, 2000.

Bilitza D., McKinnell L.A., Reinisch B. and Fuller-Rowell T., "The International Reference Ionosphere (IRI) today and in the future", *Journal of Geodesy*, **85**, pp. 909–920, doi:10.1007/s00190-010-0427-x, 2011.

Bradley P.A., Kouris S.S., Stanislawska I., Fotiadis D. and Juchnikowski G., "Day-to-day variability of the IRI electron density height profile", *Advances in Space Research*, **34**, pp. 1869–1877, 2004.

Bradley P.A., Kutiev I. and Muhtarov P., "Day-to-day variability of the basic MUF", *COST251 Workshop on Procedures and Testing of the models for Ionospheric Telecommunications Application*, pp. 133–156, Universidad de Huelva, Trieste, 1999.

Burston R., Hodges K., Astin I. and Jayachandran P.T., "Automated identification and tracking of polar-cap plasma patches at solar minimum", *Annales Geophysicae*, **32**, pp. 197–206, 2014.

Cander L.R., Leitinger R. and Levy M.F., "Ionospheric models including the auroral environment", *the ESA Workshop on Space Weather, ESTEC*, Noordwijk, the Netherlands, 1998.

Cannon P.S., "Morphology of the high latitude ionosphere and its impli-

cations for HF communications systems", *Communications, Speech and Vision, IEE Proceedings I*, volume 136, pp. 1–10, 1989.

Carlson H.C., "Sharpening our thinking about polar cap ionospheric patch morphology, research, and mitigation techniques", *Radio Science*, **47**(RS0L21), doi:10.1029/2011RS004946, 2012.

Carlson H.C., Oksavik K., Moen J. and Petersen T., "Ionospheric patch formation: Direct measurements of the origin of a polar cap patch", *Geophysical Research Letters*, **31**(L08806), doi:10.1029/2003GL018166., 2004.

Chum J., Athieno R., Baše R., Burešová D., Hruška F., Mckinnell L.A. and Šindelářová T., "Statistical Investigation of Horizontal Propagation of Gravity Waves in the Ionosphere over Europe and South Africa", , 2011.

Coley W.R. and Heelis R.A., "Structure and occurrence of polar ionisation patches", *Journal of Geophysical Research*, **103**(A2), pp. 2201–2208, 1998.

Davies K., *Ionospheric Radio (Ionospheric Radio Wave Propagation)*, Boulder, Colorado, 1989.

Davis R.M. and Groome N.L., *Variations of the 3000 km MUF in time and space*, Technical Report 8496, National Bureau of Standards, US Government Printing Office, Washington, DC, 1964.

Deminov M.G., Deminova G.F., Zherebtsov G.A. and Polekh N., "Statistical properties of variability of the quiet ionosphere F2-layer maximum param-

eters over Irkutsk under low solar activity", *Advances in Space Research*, **51**, pp. 702–711, 2013.

Ezquer R.G., Mosert M. and Corbella R., "Day to day variability of ionospheric characteristics in the American sector", *Advances in Space Research*, **34**(9), pp. 1887–1893, 2004.

Ezquer R.G., Mosert M. and Radicella S.M., "The study of the electron density variability at fixed heights over San Juan and Tucuman", *Advances in Space Research*, **29**(6), pp. 993–997, 2002.

Forbes J.M., Palo S.E. and Zhang X., "Variability of the ionosphere", *Journal of Atmospheric and Solar-Terrestrial Physics*, **62**, pp. 685–693, 2000.

Foresee D. and Hagan M., "Gauss-Newtonian Approximation to Bayesian Learning", *Proceedings of the 1997 International Joint Conference on Neural Networks*, volume 3, pp. 1930–1935, 1997.

Fotiadis D.N., Baziakos G.M. and Kouris S.S., "On the global behaviour of the day-to-day MUF variation", *Advances in Space Research*, **33**, pp. 893–901, 2004.

Gleisner H., Lundstedt H. and Wintoft P., "Predicting geomagnetic storms from solar wind data using time-delay neural networks", *Annales Geophysicae*, **14**, pp. 679–686, 1996.

Goodman J.M. and Ballard J.W., "An examination of elevated fre-

quency propagation over a transpolar path", *Radio Science*, **39**, doi: 10.1029/2002RS002850, 2004.

Goodman M.J., *Space weather & Telecommunications*, Radio propagation service, inc, New York, 2005.

Guest P.S. and Guest A.A., *Validation of the Voice Of America Coverage Analysis Program (VOACAP)*, Technical report, Naval Postgraduate School, Monterey, California, 2013.

Habarulema J.B., Mckinnell L.A. and Cilliers P.J., "Prediction of global positioning system total electron content using Neural Networks over South Africa", *Journal of Atmospheric and Solar-Terrestrial Physics*, **69**, pp. 1842–1850, 2007.

Hagan M.T., Demuth H.B., Beale M.H. and Jesús O.D., *Neural Network Design*, Pws Pub. Boston, 1996.

Haykin S., *Neural Networks: A comprehensive Foundation*, Macmillan, New York, 1994.

Hoque M.M. and Jakowski N., "A new global model for the ionospheric F2 peak height for radio wave propagation", *Annales Geophysicae*, **30**, pp. 797–809, 2012.

Hosokawa K., Moen J.I., Jayachandran P.T., Shiokawa K. and Ostuka Y., "An unusual strolling motion of polar cap patches: an implication of the

influence of tail reconnection on the nightside polar cap convection", *Journal of Geophysical Research*, 2014.

Hunsucker R.D. and Hargreaves J.K., *The High-Latitude Ionosphere and its effects on Radio Propagation*, Cambridge University Press, 2003.

ITU-R, "HF propagation prediction method", Recomendation P.533, International Telecommunication Union, Geneva, 1997.

ITU-R, "Electron density models and data for transionospheric radio propagation", Report P.2297-0, Geneva, Switzerland, 2013.

Jayachandran P.T., Langley R.B., MacDougall J.W., Mushini S.C., Pokhotelov D., Hamza A.M., Mann I.R., Milling D.K., Kale Z.C., Chadwick R., Kelly T., Danskin D.W. and Carrano C.S., "Canadian High Arctic Ionospheric Network (CHAIN)", *Radio Science*, **44**(S0A03), doi: 1029/2008RS004046, 2009.

Jodalen V., Cannon T.B.P.S. and Arthur P.C., "Performance of HF modems on high-latitude paths using multiple frequencies", *Radio Science*, **36**(6), pp. 1687–1698, 2001.

Kelley M.C., *The Earth's Ionosphere: Plasma Physics & Electrodynamics*, Elsevier, London, 2009.

Kouris S.S. and Fotiadis D.N., "Ionospheric Variability: A Comparative Statistical Study", *Advances in Space Research*, **29**(6), pp. 977–985, 2002.

Kouris S.S., Fotiadis D.N. and Hanbaba R., "On the Day-to-Day Variation of the MUF over Europe", *Physics and Chemistry of the Earth*, **25**(4), pp. 319–325, 2000a.

Kouris S.S., Fotiadis D.N. and Xenos T.D., "On The Day-To-Day Variation of foF2 and M(3000)F2", *Advances in Space Research*, **22**(6), pp. 873–876, 1998.

Kouris S.S., Fotiadis D.N. and Zolesi B., "Specifications of the F-Region Variations for Quiet and Disturbed Conditions", *Physics and Chemistry of the Earth*, **24**(4), pp. 321–327, 1999.

Kouris S.S., Xenos T.D., Zolesi B., Barbatsi K. and Nissopoulos Y., "Preliminary results on correlation in daily foF2 and M(3000)F2 variations", *Annali di Geofisica*, **XXXVII**(2), 1994.

Kouris S.S., Zolesi B., Fotiadis D.N. and Bianchi C., "On the Variability Within-the-Hour Characteristics Above Rome and from Hour-to-Hour of the F-Region Characteristis Above Rome", *Physics and Chemistry of the Earth*, **25**(4), pp. 347–351, 2000b.

Kumluca A., Tulunay E., Topalli I. and Tulunay Y., "Temporal and spatial forecasting of ionospheric critical frequency using neural networks", *Radio Science*, **34**(6), pp. 1497–1506, 1999.

Lamming X. and Cander L.R., "Monthly median foF2 modelling COST 251

area by neural networks", *Physics and Chemistry of the Earth (c)*, **24**, pp. 349–354, 1999.

Laštovička J., "Forcing the ionosphere by waves from below", *Atmospheric and Solar- Terrestrial Physics*, **68**, pp. 479–497, doi: 10.1016/j.jastp.2005.01.018, 2006.

Leitinger R., Zhang M. and Radicella S.M., "An improved bottomside for the ionospheric electron density model NeQuick", *Annals of Geophysics*, **48**(3), 2005.

Liu C., Zhang M., Wan W., Liu L. and Ning B., "Modeling M(3000)F2 based on empirical orthogonal function analysis method", *Radio Science*, **43**(RS1003), doi:10.1029/2007RS003694, 2008.

Lockwood M., "Simple M-factor algorithm for improved estimation of the basic maximum usable frequency of radio waves reflected from the ionospheric F-region", *Communications, Radar and Signal Processing, IEE proceedings*, volume 130, pp. 296–302, 1983.

Lockwood M., Davies J.A., Moen J., Eyken A.P.V., Oksavik K., W.McCrea I. and Lester M., "Motion of the dayside polar cap boundary during substorm cycles: II Generation of poleward-moving events and polar patches by pulses in the magnetopause reconnection rate", *Annales Geophysicae*, **23**, pp. 3513–3532, 2005.

Lundstedt H. and Wintoft P., "Prediction of geomagnetic storms from solar wind data with the use of a neural network", *Annales Geophysicae*, **12**(19), 1994.

MacDougall J. and Jayachandran P.T., "Polar patches: Auroral zone precipitation effects", *Journal of Geophysical Research*, **112**, doi: 10.1029/2006JA011930, 2007.

Maehlum B.N., "On the high latitude, Universal Time controlled F-layer", *Journal of Atmospheric and Terrestrial Physics*, **31**, pp. 531–538, 1969.

McKinnell L.A. and Friedrich M., "A neural network-based ionospheric model for the auroral zone", *Journal of Atmospheric and Solar-Terrestrial Physics*, **69**, pp. 1459–1470, 2007.

McKinnell L.A. and Oyeyemi E.O., "Equatorial predictions from a new neural network based global foF2 model", *Advances in Space Research*, **46**, pp. 1016–1023, 2010.

Mckinnell L.A. and Poole A.W.V., "Neural network-based ionospheric modelling over the South African region", *South African Journal of Science*, **100**, pp. 519–523, 2004.

McNamara L.F., *The Ionosphere: Communications, Surveillance, and Direction Finding*, Krieger publishing company, Malabar, Florida, 1990.

Mendillo M., Rishbeth H., Roble R.G. and Wroten J., "Modelling F2-layer seasonal trends and day-to-day variability driven by coupling with the

lower atmosphere", *Journal of Atmospheric Solar Terrestrial Physics*, **64**, pp. 1911–1931, 2002.

Millward G.H., Rishbeth H., Fuller-Rowell T.J., Aylward A.D. and Quegan S., "Ionospheric F2 layer seasonal and semiannual variations", *Geophysical Research*, **101**(A3), pp. 5149–5156, 1996.

Oksavik K., Ruohoniemi J.M., Greenwald R.A., Baker J.B.H., Moen J., Carlson H.C., Yoeman T.K. and Lester M., "Observations of isolated polar cap patches by the European Incoherent Scatter (EISCAT) Svalbard and Super Dual Auroral Radar Network (SuperDARN) Finland radar", *Journal of Geophysical Research*, **111**(A05310), 2006.

Oronsaye S.I., MCkinnell L.A. and Habarulema J.B., "A new global version of M(3000)F2 prediction model based on artificial neural networks", *Advance in Space Research*, **53**, pp. 371–386, 2014.

Oyeyemi E.O. and McKinnell L.A., "A new global F2 peak electron density model for the International Reference Ionosphere (IRI)", *Advances in Space Research*, **42**, pp. 645–658, 2008.

Oyeyemi E.O., McKinnell L.A. and Poole A.W.V., "Near-real time foF2 predictions using neural networks", *Journal of Atmospheric and Solar-Terrestrial Physics*, **68**, pp. 1807–1818, 2006.

Oyeyemi E.O., MCkinnell L.A. and Poole A.W.V., "Neural network based

prediction techniques for global modelling of M(3000)F2 ionospheric parameter", *Advances in Space Research*, **39**, pp. 643–650, 2007.

Pietrella M., Perrone L., Fontana G., Romano V., Malagnini A., Tutone G., Zolesi B., Cander L.R., Belehaki A., I.Tsagouri, Kouris S., F.Vallianatos, Makris J. and Angling M., "Further oblique-incidence ionospheric soundings over Central Europe to test nowcasting and long term prediction models", *Advances in Space Research*, **43**, pp. 1611–1620, 2009.

Richards P.G., "Seasonal and solar cycle variations of the ionospheric peak electron density: comparison of measurement and models", *Journal of Geophysical Research*, **106**(A12), pp. 12803–12819, 2001.

Rishbeth H. and Garriot O.K., *Introduction to Ionospheric Physics*, volume 14 of *International Geophysics*, Academic Press, 1969.

Rishbeth H. and Mendillo M., "Patterns of F2 layer variability", *Journal of Atmospheric Solar Terrestrial Physics*, **63**(15), pp. 1661–1680, 2001.

Ritchie S.E. and Honary F., "Advances in ionospheric propagation modelling at high-latitudes", *Proceedings of IET 11th International Conference on Ionospheric Radio Systems and Techniques (IRST 2009)*, 2009.

Rodger A.S. and Graham A.C., "Diurnal and seasonal occurrence of polar patches", *Annales Geophysicae*, **14**(5), pp. 533–537, 1996.

Rodger A.S., Moffet R.J. and Quegan S., "The role of ion drfit in the formation of ionization troughs in the mid- and high-latitude ionsophere - a

review", *Journal of Atmospheric and Terrestrial Physics*, **54**(1), pp. 1–30, 1992.

Ruohoniemi J.M. and Greenwald R.A., "Dependencies of high-latitude plasma convection: Consideration of interplanetary magnetic field, seasonal, and universal time factors in statistical patterns", *Journal of Geophysical Research*, **110**(A09204), doi:10.1029/2004JA010815, 2005.

Rush C., "Ionospheric radio propagation models and predictions - A mini-review", *IEEE Transactions on Antennas and Propagation*, **34**(9), pp. 1163–1170, ISSN 0018-926X, 1986.

Saha K., *The Earth's Atmosphere (Its Physics and Dynamics)*, Springer-Verlag Berlin Heidelberg, USA, 2008.

Sethi N.K., Goel M.K. and Mahajan K.K., "Solar cycle variations of foF2 from IGY to 1990", *Annales Geophysicae*, **20**, pp. 1677–1685, 2002.

Seybold J.S., *Introduction to RF propagation*, John Wiley & Sons, inc, Hoboken, New Jersey, 2005.

Sindelarova T., Mosna Z., Buresova D., Chum J., McKinnell L.A. and Athieno R., "Observations of wave activity in the ionosphere over South Africa in geomagnetically quiet and disturbed periods", *Advances in Space Research*, **50**(2), pp. 182–195, 2012.

Sizun H., *Radio Wave Propagation for telecommunication Applications*, Springer-Verlag Berlin Heidelberg, New York, 2005.

Smith A.M., Pryse S.E. and Kersley L., "Polar patches observed by ESR and their possible origin in the cusp region", *Annales Geophysicae*, **18**, pp. 1043–1053, 2000.

Smith N., "The Relation of Radio Sky-Wave Transmission to Ionosphere Measurements", *Proceedings of the IRE*, volume 27, pp. 332–347, 1939.

Stauning P., "The Polar Cap index: A critical review of methods and a new approach", *Journal of Geophysical Research*, **118**, pp. 5021–5038, doi: doi:10.1002/jgra.50462, 2013.

Stewart F.G. and Hand G., *Ionospheric Communications Enhanced Profile Analysis & Circuit (ICEPAC) Prediction Program Technical Manual*, 2008.

Stocker A.J., Warrington E.M. and Jones T.B., "A comparison of observed and modeled deviations from the great circle direction for a 4490 km HF propagation path along the midlatitude ionospheric trough", *Radio Science*, **38**(3), p. 1054, doi:10.1029/2002RS002781, 2003.

Stocker A.J., Warrington E.M. and Siddle D.R., "Comparison between the measured and predicted parameters of HF radio signals propagating along the midlatitude trough and within the polar cap", *Radio science*, **42**(RS3019), doi:10.1029/2006RS003557, 2007.

Stocker A.J., Warrington E.M. and Siddle D.R., "Observations of Doppler and delay spreads on HF signals received over polar cap and trough paths

at various stages of the solar cycle", *Radio Science*, **48**(638), pp. 638–645, doi:10.1002/2013RS005264, 2013.

Tanyer S.G. and Erol C.B., "Broadcast analysis and prediction in the HF band", *Broadcasting, IEEE Transactions on*, **44**, doi:10.1109/11.713075, 1998.

Tapping K.F., "The 10.7 cm solar radio flux (F10.7)", *Space Weather*, **11**, pp. 394–406, doi:doi:10.1002/swe.20064, 2013.

Tascione T.F., Kroehl H.W., Creiger R., Jr J.W.F., Wolf R.A., Spiro R.W., Hilmer R.V., Shade J.W. and Hausman B.A., "New Ionospheric and Magnetospheric Specification Models", *Radio Science*, **33**(3), pp. 211–222, 1988.

Themens D.R. and Jayachandran P.T., "Solar Activity Variability in the IRI at high latitudes: Comparisons with GPS Total Electron Content", *Journal of Geophysical Research*, **121**, pp. 3793–3807, doi: 10.1002/2016ja022664, 2016.

Themens D.R., Jayachandran P.T., Nicolls M.J. and MacDougall J.W., "A top to bottom evaluation of IRI 2007 within the polar cap", *Journal of Geophysical Research*, **119**, pp. 6689–6703, doi:10.1002/2014JA020052, 2014.

Thrane E.V., Jodalen V., Stewart F., Saleem D. and Katan J., "Study of measured and predicted reliability of the ionospheric HF communication channel at high latitudes", *Radio Science*, **29**(5), pp. 1293–1309, 1994.

Titheridge J.E., "Ionogram analysis: least-squares fitting of a Chapman layer peak", *Radio Science*, **20**(2), pp. 247–256, 1985.

Titheridge J.E., "The real height analysis of ionograms: a generalized formulation", *Radio Science*, **23**(5), pp. 831–849, 1988.

Tobiska W.K., Cameron G., Davenport G., Goodman J., Hand G., Papitashvili V. and Pi X., "Improved polar HF propagation using nowcast and forecast space weather parameters", J.M. Goodman, editor, *10th International ionospheric Effects Symposium*, pp. 364–371, 2002.

Tshisaphungo M., McKinnell L., Magnus L. and Habarulema J.B., "An attempt to validate HF propagation prediction conditions over SubSaharan Africa", *SPACE WEATHER*, **9**(S08001), doi:10.1029/2010SW000643, 2011.

Voiculescu M., Virtanen I. and Nygren T., "The F-region trough: seasonal morphology and relation to interplanetary magnetic field", *Annales Geophysicae*, **24**, pp. 173–185, 2006.

Warrington E.M., Bourdillon A., Benito E., Bianchi C., Monilie J.P., Muriuki M., Pietrella M., Rannou V., Rothkaehl H., Saillant S., Sari O., Stocker A.J., Tulunay E., Tulunay Y. and Zaalov N.Y., "Aspects of HF radio propagation", *Annals of Geophysics*, **52**(3/4), 2009.

Warrington E.M., Rogers N.C. and Jones T.B., "Large HF bearing errors

for propagation paths contained within the polar cap", *IEE Proceedings Microwaves Antennas Propagation*, volume 144, pp. 241–249, 1997.

Warrington E.M., Zaalov N.Y., Naylor J.S. and Stocker A.J., "HF propagation modeling within the polar ionosphere", *Radio Science*, **47**, doi: doi:10.1029/2011RS004909, 2012.

Watson C., *GPS Total Electron Content Techniques for Observing the Structure and Dynamics of the High Latitude Ionosphere*, Ph.D. thesis, University of New Brunswick, 2015.

Whitehead J.D., "Recent work on mid-latitude and equatorial sporadic E", *Atmospheric and Terrestrial Physics*, **51**, pp. 401–424, 1989.

Whitteker H., Shepherd G.G., Anger C.D., Burrows J.R., Wallis D.D., Klumper D.M., Klumpar J.K. and Walker J.K., "The Winter Polar Ionosphere", *Journal of Geophysical Research*, **83**(A4), pp. 1503–1518, 1978.

Wilkinson P.J., "Ionospheric variability and the international reference ionosphere", *Advances in Space Research*, **34**, pp. 1853–1859, 2004.

Williscroft L.A. and Poole A.W.V., "Neural networks, foF2, sunspot and magnetic activity", *Geophysical Research Letters*, **23**, pp. 3659–3662, 1996.

Xenos T.D., "Neural-network-based prediction techniques for single station modelling and regional mapping of the foF2 and M(3000)F2 ionospheric characteristics", *Nonlinear Processes in Geophysics*, **9**, pp. 477–486, 2002.

Yue X., Wan W., Liu L., Ning B. and Zhao B., "Applying artificial neural network to derive long-term foF2 trends in the Asia/Pacific sector from ionosonde observations", *Journal of Geophysical Research*, **111**(A10303), 2006.

Zaalov N.Y., Warrington E.M. and Stocker A.J., "Simulation of off-great circle HF propagation effects due to the presence of patches and arcs of enhanced electron density within the polar cap ionosphere", *Radio Science*, **38**(1052), doi:10.1029/2002RS002798, 2003.

Zaalov N.Y., Warrington E.M. and Stocker A.J., "A ray-tracing model to account for off–great circle HF propagation over northerly paths", *Radio Science*, **40**(RS4006), doi:10.1029/2004RS003183, 2005.

Zhang M., Liu C., Wan W., Liu L. and Ning B., "Evaluation of global modeling of M(3000)F2 and hmF2 based on alternative empirical orthogonal function expansions", *Advances in Space Research*, **46**, pp. 1024–1031, 2010.

Zhao X., Ning B., Liu L. and Song G., "A prediction model of short-term ionospheric foF2 based on AdaBoost", *Advances in Space Research*, **53**, pp. 387–394, 2014.

Zheng Q., ZhiGang Y., Feng Q., ShiYong H., HaiMeng L., HuiMin L., Ming L. and DeDong W., "Statistical characteristics of the polar ionospheric scale height around the peak height of F2 layer with observations

of the ESR radar: Quiet days", *Science China Technological Sciences*, doi: 10.1007/s11431-014-5729-4, 2014.

Zolesi B., Fontana G., Perrone L., Pietrella M., Romano V., Tutone G., Belehaki A., Tsagouri I., Kouris S.S., Vallianatos F., Makris J.P. and Anglinge M.J., "A new campaign for oblique-incidence ionospheric sounding over Europe and its data application", *Journal of Atmospheric and Solar-Terrestrial Physics*, **70**, pp. 854–865, 2008.

Vita

Candidate's full name: Racheal Athieno

Universities attended:

Rhodes University, Master of Science, 2011

University of Cape Town, BSc (Hons) Astrophysics and Space Science, 2009

Mbarara University of Science and Technology, BSc (Hons) with Education in Physics & Maths, 2007

Publications:

Athieno R., Jayachandran P.T. and Themens D.R., A Neural Network based foF2 model for a single station in the polar cap, submitted to the Journal of Radio Science.

Athieno R. and Jayachandran P.T., MUF variability in the Arctic region: A statistical comparison with the ITU-R variability factors, Radio Science, 51, doi: 10.1002/2016RS006096, 2016.

Athieno R., Jayachandran P.T., Themens D.R. and Danskin D.W., Comparison of observed and predicted MUF (3000)F2 in the polar cap region, Radio Science, 299 50(6), pp. 509517, doi:10.1002/2015RS005725, 2015.

Chum, J., **Athieno, R.** Bae, D. Bureov, F. Hruka, L. A. Mckinnell, and T.

indelrov (2011), Statistical investigation of horizontal propagation of gravity waves in the ionosphere over Europe and South Africa, 117, A03312, doi: 10.1029/2011JA017161.

Sindelarova, T., Z. Mosna, D. Buresova, J. Chum, L.A. McKinnell, and **R. Athieno** (2012), Observations of wave activity in the ionosphere over South Africa in geomagnetically quiet and disturbed periods, Adv. Space Rese., 50(2), 182195.

Adewale, A. O., E. O. Oyeyemi, A. B. Adeloye, C. M. Ngwira, and **R. Athieno**. "Responses of equatorial F region to different geomagnetic storms observed by GPS in the African sector."Journal of Geophysical Research: Space Physics116, no. A12 (2011).

Conference Presentations:

R. Athieno, P. T Jayachandran and David R. Themens, A Neural Network foF2 model for a single station in the polar cap, Oral presentation at the Canadian Association of Physicists congress, June 13 17, 2016, University of Ottawa, Ottawa, ON, Canada.

R. Athieno and P. T. Jayachandran, A Statistical Analysis of the Performance of High Frequency (HF) Propagation Prediction Models in the Arctic Region, Oral presentation at the 2015 IEEE International Symposium on Antennas and Propagation and North American Radio Science Meeting, July 19 24, 2015, Vancouver, BC, Canada.

R. Athieno and P. T. Jayachandran, Validation of High Frequency (HF) Propagation Prediction Models in the Arctic region, Oral presentation at the American Geophysical Union (AGU) Fall Meeting, December 14 19, 2014, San Francisco, CA, USA.

R. Athieno and P. T. Jayachandran, Empirical model in the characterization of High Frequency propagation in the Arctic region, Oral presentation at the Division of Atmospheric and Space Physics (DASP) conference, February 19 - 21, 2014, University of New Brunswick, Fredericton, NB, Canada.

R. Athieno and L. A. Mckinnell, Co-located radar observations of wave-like

structures over South Africa, Oral presentation at the International Reference Ionosphere (IRI) Workshop, October 10 14, 2011, Hermanus, South Africa. Received an award for the best MSc student oral presentation.

R. Athieno and L.-A. Mckinnell, Investigating the effect of atmospheric dynamics on HF propagation, Poster presentation at the 56th Annual Conference of the South African Institute of Physics (SAIP), July 12 15, 2011, Pretoria, South Africa. Received an award for the best MSc (Astronomy and space physics) student poster presentation.

R. Athieno and L.-A. Mckinnell, , Investigating the effect of atmospheric dynamics on HF propagation, Poster presentation at the 4th IUPAP International Conference in Physics (ICWIP), April 06 08, 2011, Stellenbosch, South Africa.